

ANALYSIS OF FINITE ELEMENT METHOD SOLUTION OF SINUSOIDAL
BUCKLING BEHAVIOUR OF DRILL STRING IN VERTICAL, DIRECTIONAL,
AND HORIZONTAL WELLBORES AND COMPARISON WITH ANALYTICAL
SOLUTIONS

A THESIS SUBMITTED TO
THE GRADUATE SCHOOL OF NATURAL AND APPLIED SCIENCES
OF
MIDDLE EAST TECHNICAL UNIVERSITY

BY

MEHMET CEBECİ

IN PARTIAL FULFILLMENT OF THE REQUIREMENTS
FOR
THE DEGREE OF MASTER OF SCIENCE
IN
PETROLEUM AND NATURAL GAS ENGINEERING

DECEMBER 2017

Approval of the thesis:

**ANALYSIS OF FINITE ELEMENT METHOD SOLUTION OF SINUSOIDAL
BUCKLING BEHAVIOUR OF DRILL STRING IN VERTICAL,
DIRECTIONAL, AND HORIZONTAL WELLBORES AND COMPARISON
WITH ANALYTICAL SOLUTIONS**

submitted by **MEHMET CEBECİ** in partial fulfillment of the requirements for the degree of **Master of Science in Petroleum and Natural Gas Engineering Department, Middle East Technical University** by,

Prof. Dr. Gülbin Dural Ünver _____
Dean, Graduate School of **Natural and Applied Sciences, METU**

Prof. Dr. Serhat Akın _____
Head of Department, **Petroleum and Natural Gas Engineering Dept., METU**

Prof. Dr. Mustafa Verşan Kök _____
Supervisor, **Petroleum and Natural Gas Engineering Dept., METU**

Assoc. Prof. Dr. İ. Hakkı Gücüyener _____
Co-Supervisor, **GEOS Energy Inc.**

Examining Committee Members:

Prof. Dr. Serhat Akın _____
Petroleum and Natural Gas Engineering Dept., METU

Prof. Dr. Mustafa Verşan Kök _____
Petroleum and Natural Gas Engineering Dept., METU

Assoc. Prof. Dr. Çağlar Sınayuç _____
Petroleum and Natural Gas Engineering Dept., METU

Assoc. Prof. Dr. İsmail Durgut _____
Petroleum and Natural Gas Engineering Dept., METU

Assist. Prof. Dr. Tuna Eren _____
Petroleum and Natural Gas Engineering Dept., BU

Date: 08.12.2017

I hereby declare that all information in this document has been obtained and presented in accordance with academic rules and ethical conduct. I also declare that, as required by these rules and conduct, I have fully cited and referenced all material and results that are not original to this work.

Name, Last Name: Mehmet Cebeci

Signature :

ABSTRACT

ANALYSIS OF FINITE ELEMENT METHOD SOLUTION OF SINUSOIDAL BUCKLING BEHAVIOUR OF DRILL STRING IN VERTICAL, DIRECTIONAL, AND HORIZONTAL WELLBORES AND COMPARISON WITH ANALYTICAL SOLUTIONS

Cebeci, Mehmet

M.S., Department of Petroleum and Natural Gas Engineering

Supervisor : Prof. Dr. Mustafa Verşan K k

Co-Supervisor: Assoc. Prof. Dr.  . Hakkı G c yener

December 2017, 104 pages

The buckling of drill string in oil, gas and geothermal wells is a critical problem that has been of interest to many researchers in the industry. Prevention of buckling of drill string is important since it may negatively affect the drilling operations. When buckling of drill string occurs, it may cause deviation control problems while drilling, inefficient load transfer to the bit, excessive torque values, even pipe failures due to fatigue.

The first rigorous treatment of stability of drill strings for vertical wellbores was presented by Lubinski in 1950 and his equation is till most widely used in the industry. Since, he used power series to solve differential equation governing the stability problem, the terms of power series become very large for long drill strings,

therefore, after a certain length, the calculations may lead to inaccurate results. Even if analytical solution for infinite-length drill string is used for deep vertical wells, the results are still under discussion. The subject studied in this thesis is of great importance in designing the bottom hole assemblies in deep and ultra-deep vertical wells to eliminate problems associated with instability of drill strings. The study includes Finite Element Method (FEM) solution of critical sinusoidal buckling force for 5 different pipes with 21 different lengths starting from 1000 ft. up to 25000 ft. The study shows effect of length on critical sinusoidal buckling force in vertical wells by FEM and to compare the results with the analytical solutions. To prepare finite element simulations, Integrated Dynamic Engineering Analysis Software (IDEAS™) is used. In summary, it is showed that critical buckling force decreases as the depth of the well increases according to FEM solutions, although, analytical solution gives only a fixed critical buckling force for a specific pipe independent from the length.

Keywords: Drilling, Buckling, Finite Element Method, Elastic Stability

ÖZ

DİK, YÖNLÜ VE YATAY KUYULARDA SİNÜZOİDAL BURKULMANIN SONLU ELEMANLAR METODU KULLANILARAK ANALİZİ VE ANALİTİK SONUÇLARLA KARŞILAŞTIRILMASI

Cebeci, Mehmet

Yüksek Lisans, Petrol ve Doğalgaz Mühendisliği Bölümü

Tez Yöneticisi : Prof. Dr. Mustafa Verşan Kök

Ortak Tez Yöneticisi : Doç. Dr. İ. Hakkı Gücüyener

Aralık 2017, 104 sayfa

Petrol, doğalgaz ve jeotermal kuyularında sondaj dizisinin burkulması ciddi bir problem olup sektördeki birçok araştırmacının ilgi konusu olmuştur. Sondaj dizisinde burkulmanın önlenmesi önemlidir, aksi takdirde sondaj operasyonlarını olumsuz yönde etkileyebilir. Operasyon esnasında sondaj dizisinin burkulması, kuyuda yönlenme problemlerine yol açabilir, matkaba verilen ağırlığın azalmasına neden olabilir, yüksek tork değerlerinin görülmesine neden olabilir hatta sondaj borularının metal yorulmasından dolayı kopmasına neden olabilir.

Dik kuyularda sondaj dizisi stabilitesinin ilk detaylı çalışması 1950 yılında Lubinski tarafından yapılmıştır ve bulunduğu denklem hala sektörde yaygın bir şekilde kullanılmaktadır. Lubinski'nin stabilite problemi için önerdiği diferansiyel denklemin çözümünde kuvvet serilerini kullanmış olması ve uzun sondaj dizileri için kuvvet serisi terimlerinin çok fazlalaşması, belirli bir uzunluktan sonra denklemin yanlış sonuçlar vermesine neden olabilmektedir. Derin dik kuyularda sonsuz uzunluktaki dizi çözümü kullanılsa da sonuçlar hala tartışılmaktadır. Burada çalışılan

konu, derin ve çok derin dik kuyularda sondaj dizisi instabilitesi nedeniyle meydana gelebilecek olan problemlerin giderilmesinde büyük önem taşımaktadır. Bu çalışma, 5 farklı sondaj borusunun 1000 feet boyundan 25000 feet boyuna kadar 21 farklı derinlikte, Sonlu Elemanlar Metodu (SEM) kullanılarak, sinüs eğrisi şeklindeki kritik burkulma kuvvetlerinin hesaplanmasını içermektedir. Bu çalışmanın amacı; uzunluk değişkeninin, dik kuyularda kritik burkulma kuvvetine olan etkisinin SEM ile gösterilmesi ve sonuçlarının analitik sonuçlarla karşılaştırılmasıdır. SEM'nun simülasyonlarının hazırlanmasında Bütünleşmiş Dinamik Mühendislik Analiz Yazılımı (IDEAS™) kullanılmıştır. Sonuç olarak, analitik sonucun belirli bir sondaj boru tipine göre uzunluktan bağımsız bir şekilde verdiği sabit değere rağmen, SEM ile belirli bir sondaj boru tipine göre kritik burkulma kuvvetinin değerinin kuyu derinliği arttıkça azaldığı gösterilmiştir.

Anahtar Kelimeler: Sondaj, Burkulma, Sonlu Elemanlar Metodu, Elastik Kararlılık

To my lovely family,
To my beautiful fiancée,

ACKNOWLEDGEMENTS

First of all, I would like to thank my supervisor Prof. Dr. Mustafa Verşan K k for his guidance, support, perspective, and criticism throughout this thesis study. I would like to thank Assoc. Prof. İ. Hakkı G c yener for his kindly advices and being my co-advisor and valuable helps when everything got messed up.

I sincerely thank Dr. Geng Yun for his valuable support, comments and suggestions during preparation of the simulations.

I would also like to express my appreciation to my company Schlumberger for allowing me to use IDEASTM software for my thesis.

I am also grateful to Tufan Akba for his advice and always sharing ideas with me. This work would not have been possible without his support. I would like also thank him for his invaluable assistance in times of need during my undergraduate study of Mechanical Engineering.

Finally, I would like to thank my family for their endless support and encouragement during my life so far.

TABLE OF CONTENTS

ABSTRACT	v
ÖZ	vii
ACKNOWLEDGEMENTS	x
TABLE OF CONTENTS	xi
LIST OF TABLES	xiv
LIST OF FIGURES	xv
LIST OF SYMBOLS AND ABBREVIATIONS	xix
CHAPTERS	
1. INTRODUCTION	1
1.1. Fundamentals of Rotary Drilling	1
1.2. Stability of Drill Strings	3
2. CLASSICAL BUCKLING OF COLUMNS.....	5
2.1. Mathematical Formulation of Euler Buckling Force	7
3. SPECIAL FEATURES FOR PIPE BUCKLING IN OIL WELLS	11
4. REVIEW OF CURRENT LITERATURE.....	15
4.1. Sinusoidal Buckling of Pipes in Vertical Wellbores.....	15
4.2. Sinusoidal Buckling of Pipes in Inclined and Horizontal Wellbores.....	17
4.3. Helical Buckling of Pipes in Vertical Wellbores	19
4.4. Helical Buckling of Pipes in Deviated and Horizontal Wells.....	19
4.5. Numerical Studies on Drill String Buckling Phenomena	21
5. SCOPE OF WORK.....	23

5.1.	Thesis Overview.....	23
5.2.	Thesis Objectives	23
5.3.	Thesis Scope.....	24
5.4.	Thesis Organization.....	24
6.	FINITE ELEMENT METHOD	25
6.1.	Basics of Finite Element Method	25
6.2.	Finite Element Method vs. Finite Difference Method	26
6.3.	General Steps of the Finite Element Method	27
6.4.	IDEAS TM – Finite Element Analysis Software	32
6.5.	Mathematical Description of the Finite Element Model.....	36
6.5.1.	Three-Dimensional Beam Element for Finite Element Analysis... 36	
6.5.2.	Transformation of Local Coordinates to Global Coordinates.....	41
6.5.3.	Solution of the Differential Equation of Motion.....	41
7.	MODEL VERIFICATION FOR IDEAS TM SOFTWARE.....	43
7.1.	Sinusoidal Buckling Validation for Deviated and Horizontal Wells	43
7.1.1.	Case-1: An Inclined Well with $\theta=30^0$	45
7.1.2.	Case-2: An Inclined Well with $\theta=90^0$	51
7.2.	Helical Buckling Validation for Deviated and Horizontal Wells	54
7.2.1.	Case-1: An Inclined Well with $\theta=30^0$	55
7.2.2.	Case-2: An Inclined Well with $\theta=90^0$	62
8.	SIMULATION RESULTS.....	69
8.1.	Analytical Solutions	69
8.2.	Simulation Results.....	71
8.2.1.	Discretization of the Finite Element Model	71
8.2.2.	Type of the Elements.....	72
8.2.3.	Size of the Elements	72
8.2.4.	Simulations for 4.75 in. Drill Collars (Type I).....	75
8.2.5.	Simulations for 6.25 in. Drill Collars (Type II)	76
8.2.6.	Simulations for 7 in. Drill Collars (Type III)	77
8.2.7.	Simulations for 8.25 in. Drill Collars (Type IV).....	78

8.2.8. Simulations for 9.5 in. Drill Collars (Type V).....	79
8- CONCLUSION & DISCUSSION	81
REFERENCES.....	83
APPENDIX.....	89
1. A-VARIABLE COEFFICIENT CURVES	89
2. B-ANALYTICAL SOLUTIONS OF THE EQUATIONS	95
Lubinski`s Solution:	95
Wu`s Solution:	103
Wang`s Solution:.....	104

LIST OF TABLES

Table 4-1 Coefficients for Different Researches.....	20
Table 7-1 Parameters for Drill String for IDEAS™ Simulation.....	44
Table 7-2 Verification Summary for Sinusoidal Buckling Case.....	67
Table 7-3 Verification Summary for Helical Buckling Case.....	67
Table 8-1 The Properties of Drill Collars and the Analytical Solutions for Critical Buckling Forces.....	71
Table 8-2 Number of Beam Elements Created for Different Lengths	73
Table 8-3 Simulation Results for Five Different Drill Collars with Different Depths	74
Table 8-4 Simulation Results Comparison Chart.....	80

LIST OF FIGURES

Figure 1-1 Essential Components of Rotary Drilling Rig [1].	2
Figure 1-2 (a) Sinusoidal Buckling, (b) Helical Buckling [2].	4
Figure 2-1 (a) Initial Form of Column, (b) Stable Form of Column, (c) Unstable Form of Column [4].	5
Figure 2-2 Euler Buckling Factors for Different End Conditions [4].	7
Figure 2-3 End Pinned Column under Bending [5].	8
Figure 3-1 Sinusoidal Buckling of Pipe in Horizontal Wellbore [4].	12
Figure 3-2 Helical Buckling of Pipes in Wellbores [4].	13
Figure 4-1 Designation of External Forces Acting upon Drill String [4].	15
Figure 4-2 Buckling Model of Paslay and Bogy for Pipes in Inclined Wellbores [4].	17
Figure 6-1 FEM Approach Methods	28
Figure 6-2 Two Main Different Direct Methods.	28
Figure 6-3 Various Types of Finite Elements [31].	31
Figure 6-4 Vibration Types Simulated in IDEAS™ Software [32].	32
Figure 6-5 IDEAS™ Model of a PDC Bit Cutting Structure in 3-D [32].	34
Figure 6-6 IDEAS™ Model of PDC Bit with Full Details with Body and Gage [32].	35

Figure 6-7 Three-Dimensional Beam Element with Forces and Displacements [33].	36
Figure 7-1 BHA of IDEAS™ Simulation for Sinusoidal Buckling in Deviated Wells	45
Figure 7-2 Initial Status of Drill String Lying on Lower Side of Wellbore.....	46
Figure 7-3 2-D View of Deflection along y- and z-Direction under 10 <i>klb</i> WOB ...	47
Figure 7-4 3-D View of Drill String under 10 <i>klb</i> WOB	48
Figure 7-5 2-D View of Deflection along y- and z-Direction under 12 <i>klb</i> WOB ...	49
Figure 7-6 3-D View of Drill String under 12 <i>klb</i> WOB	49
Figure 7-7 Axial compressive load under 12 <i>klb</i> WOB.....	50
Figure 7-8 2-D View of Deflection along y- and z-Direction under 16 <i>klb</i> WOB ...	51
Figure 7-9 3-D View of Drill String under 16 <i>klb</i> WOB	52
Figure 7-10 2-D View of Deflection along y- and z-Direction under 17.5 <i>klb</i> WOB	53
Figure 7-11 3-D View of Drill String under 17.5 <i>klb</i> WOB	53
Figure 7-12 2-D View of Deflection along y- and z-Direction under 17 <i>klb</i> WOB ..	57
Figure 7-13 3-D View of Drill String under 17 <i>klb</i> WOB	57
Figure 7-14 2-D View of Deflection along y- and z-Direction under 20 <i>klb</i> WOB ..	58
Figure 7-15 3-D View of Drill String under 20 <i>klb</i> WOB	58
Figure 7-16 2-D View of Deflection along y- and z-Direction under 20.8 <i>klb</i> WOB	59
Figure 7-17 3-D View of Drill String under 20.8 <i>klb</i> WOB	59

Figure 7-18 2-D View of Deflection along y- and z-Direction under 24 <i>klb</i> WOB .	60
Figure 7-19 3-D View of Drill String under 24 <i>klb</i> WOB	60
Figure 7-20 2-D View of Deflection along y- and z-Direction under 28 <i>klb</i> WOB .	61
Figure 7-21 3-D View of Drill String under 28 <i>klb</i> WOB	61
Figure 7-22 2-D View of Deflection along y- and z-Direction under 24 <i>klb</i> WOB .	63
Figure 7-23 3-D View of Drill String under 24 <i>klb</i> WOB	63
Figure 7-24 2-D View of Deflection along y and z Direction under 28.3 <i>klb</i> WOB	64
Figure 7-25 3-D View of Drill String under 28.3 <i>klb</i> WOB	64
Figure 7-26 2-D View of Deflection along y and z Direction under 28.4 <i>klb</i> WOB	65
Figure 7-27 3-D View of Drill String under 28.4 <i>klb</i> WOB	65
Figure 7-28 2-D View of Deflection along y- and z-Direction under 60 <i>klb</i> WOB .	66
Figure 7-29 3-D View of Drill String under 28.4 <i>klb</i> WOB	66
Figure 8-1 Critical Buckling Force vs Depth Curve for 4.75 in. Drill Collar.....	75
Figure 8-2 Critical Buckling Force vs Depth Curve for 6.25 in. Drill Collar.....	76
Figure 8-3 Critical Buckling Force vs Depth Curve for 7 in. Drill Collar.....	77
Figure 8-4 Critical Buckling Force vs Depth Curve for 8.25 in. Drill Collar.....	78
Figure 8-5 Critical Buckling Force vs Depth Curve for 9.5 in. Drill Collar.....	79
Figure A-1 Variable Coefficient for 4.75 in. Drill Collar	89
Figure A-2 Variable Coefficient for 6.25 in. Drill Collar	90
Figure A-3 Variable Coefficient for 7 in. Drill Collar	91

Figure A-4 Variable Coefficient for 8.25 in. Drill Collar	92
Figure A-5 Variable Coefficient for 9.5 in. Drill Collar	93

LIST OF SYMBOLS AND ABBREVIATIONS

a	Coefficient for Helical-Buckling Equation
a_n	General Terms of Series Solutions
A	Integration Constant
A	Cross sectional Area [in^2]
A_i	Airy Function
B	Integration Constant
B_i	Airy Function
C_1	Integration Constant
C_2	Integration Constant
E	Modulus of Elasticity in Compression [Pa]
F	Axial Compressive Force [lb]
F_1	Reaction of Elevators on the Drill String [lb]
F_2	Horizontal Component of the Reaction of the Bottom Hole on Bit [lb]
F_{cri}	Critical Buckling Force [lb]
$F_{cri_hel}^{dev}$	Critical Helical Buckling Load for Deviated Wells [lb]
$F_{cri_sin}^{ver}$	Critical Sinusoidal Buckling Load for Vertical Wells [lb]
$F_{cri_sin}^{dev}$	Critical Sinusoidal Buckling Load for Deviated Wells [lb]
F_e	Externally Applied Load Causing Helical Buckling [lb]
F_t	External Forces Applied to the Joints [lb]
G	Shear Modulus [psi].
I	Moment of Inertia of Area [in^4]
I_m	Polar Mass Moment of Inertia per Unit Length [in^3]
J	Polar Moment of Inertia [m^4]
k	Constants for Euler`s Buckling Force for Different End Conditions
k_B	Buoyancy Ratio
MN	Cross-Section of the Drill String

$M'N'$	Cross-Section of the Drill String
L	Length of the Bar [ft]
N_1	Reaction of Bushings on the Drill String [lb]
N_2	Horizontal Component of the Reaction on Drill String at Bottom [lb]
m	Length of One Dimensionless Unit [ft]
\bar{m}	Distributed Mass of the Beam [lb]
$M(x)$	Bending Moment [$ft - lb$]
n	Number of Half-Sine Wave
p	Pitch for Helical Buckling [ft]
p	Weight in Mud per Unit Length [lb/ft]
P_1	Static Forces Applied on Node on Beam Element [N]
P_2	Static Forces Applied on Node on Beam Element [N]
P_3	Static Forces Applied on Node on Beam Element [N]
P_4	Moments Applied on Node on Beam Element [Nm]
P_5	Moments Applied on Node on Beam Element [Nm]
P_6	Moments Applied on Node on Beam Element [Nm]
P_7	Static Forces Applied on Node on Beam Element [N]
P_8	Static Forces Applied on Node on Beam Element [N]
P_9	Static Forces Applied on Node on Beam Element [N]
P_{10}	Moments Applied on Node on Beam Element [Nm]
P_{11}	Moments Applied on Node on Beam Element [Nm]
P_{12}	Moments Applied on Node on Beam Element [Nm]
T_1	Applied Torque on Node on Beam Element [Nm]
T_2	Applied Torque on Node on Beam Element [Nm]
r	Radial Clearance between Pipe and Hole [$inch$]
u	System Displacement [m]
\dot{u}	System Velocity [m/s]
\ddot{u}	System Acceleration [m/s^2]
v	Lateral displacement due to bending [m]

X	Direction of the axes
Y	Direction of the axes
w	Unit Weight of the Drill String [lb/ft]
w_e	Effective Unit Weight of the Drill String [lb/ft]
W_1	Reaction of Elevators on the Drill String [lb]
W_2	Vertical Component of the Reaction on Drill String at Bottom [lb]

ABBREVIATIONS

2-D	2-Dimensional
3-D	3-Dimensional
4-D	4-Dimensional
BHA	Bottom Hole Assembly
FEM	Finite Element Method
ID	Inner Diameter [$inch$]
IDEAS	Integrated Dynamic Engineering Analysis Software
LWD	Logging-While-Drilling
MWD	Measurement-While-Drilling
OD	Outer Diameter [$inch$]
PDM	Positive Displacement Motor
RSS	Rotary Steerable Tools
WOB	Weight on Bit

GREEK SYMBOLS

$\alpha(z)$	Position Angle of the Buckled Pipe [°]
θ	Well Deviation from Vertical [°]
γ	Sinusoidal Wave Length [<i>ft</i>]
\emptyset	Perturbed Angle [°]
δ	Pipe Shortening During the Helical Buckling Process [<i>in</i>]
δ_1	Linear Displacements on Node on Beam Element [<i>m</i>]
δ_2	Linear Displacements on Node on Beam Element [<i>m</i>]
δ_3	Linear Displacements on Node on Beam Element [<i>m</i>]
δ_4	Angular Displacements on Node on Beam Element [<i>rad</i>]
δ_5	Angular Displacements on Node on Beam Element [<i>rad</i>]
δ_6	Angular Displacements on Node on Beam Element [<i>rad</i>]
δ_7	Linear Displacements on Node on Beam Element [<i>m</i>]
δ_8	Linear Displacements on Node on Beam Element [<i>m</i>]
δ_9	Linear Displacements on Node on Beam Element [<i>m</i>]
δ_{10}	Angular Displacements on Node on Beam Element [<i>rad</i>]
δ_{11}	Angular Displacements on Node on Beam Element [<i>rad</i>]
δ_{12}	Angular Displacements on Node on Beam Element [<i>rad</i>]
$\dot{\delta}$	Unit Velocity of the Beam Element [<i>m/s</i>]
$\ddot{\delta}$	Unit Acceleration of the Beam Element [<i>m/s²</i>]

CHAPTER 1

INTRODUCTION

1.1. Fundamentals of Rotary Drilling

The aim of drilling a vertical, directional or horizontal well is to reach oil, gas and geothermal resources beneath the earth and create a pathway through surface. There are several steps required to drill a well successfully as stated below:

- A downward force acting on a drilling bit,
- Giving rotation to the drilling bit,
- Drilling fluid circulation down to the drill string, through drilling bit, and back to surface from the annular space.

In other words, two different transport flows are required to drill a well: Energy transport from surface to the bit, and material transport from drill bit to the surface. This drilling technique in the industry is called rotary drilling which relies on a combination of mechanical systems and hydraulics systems for energy and material transport, as seen in Figure 1.1.

The mechanical part of the rotary drilling is composed of a rotation of the bit to create a borehole, a drill string to rotate and to apply weight on bit (WOB) to the drill bit, a rotary drive to rotate whole drill string, and a rig to support the whole drill string, the rotary drive and other equipment.

The hydraulics part consists of drilling fluid, pumps, and surface equipment. Drilling fluid is mostly consisted of water or salt water, weighting chemicals, viscosifiers and inhibitive chemicals. It helps to remove cuttings from bottom of the hole, to cool and lubricate the drill bit and downhole equipment, and to control subsurface pressures.

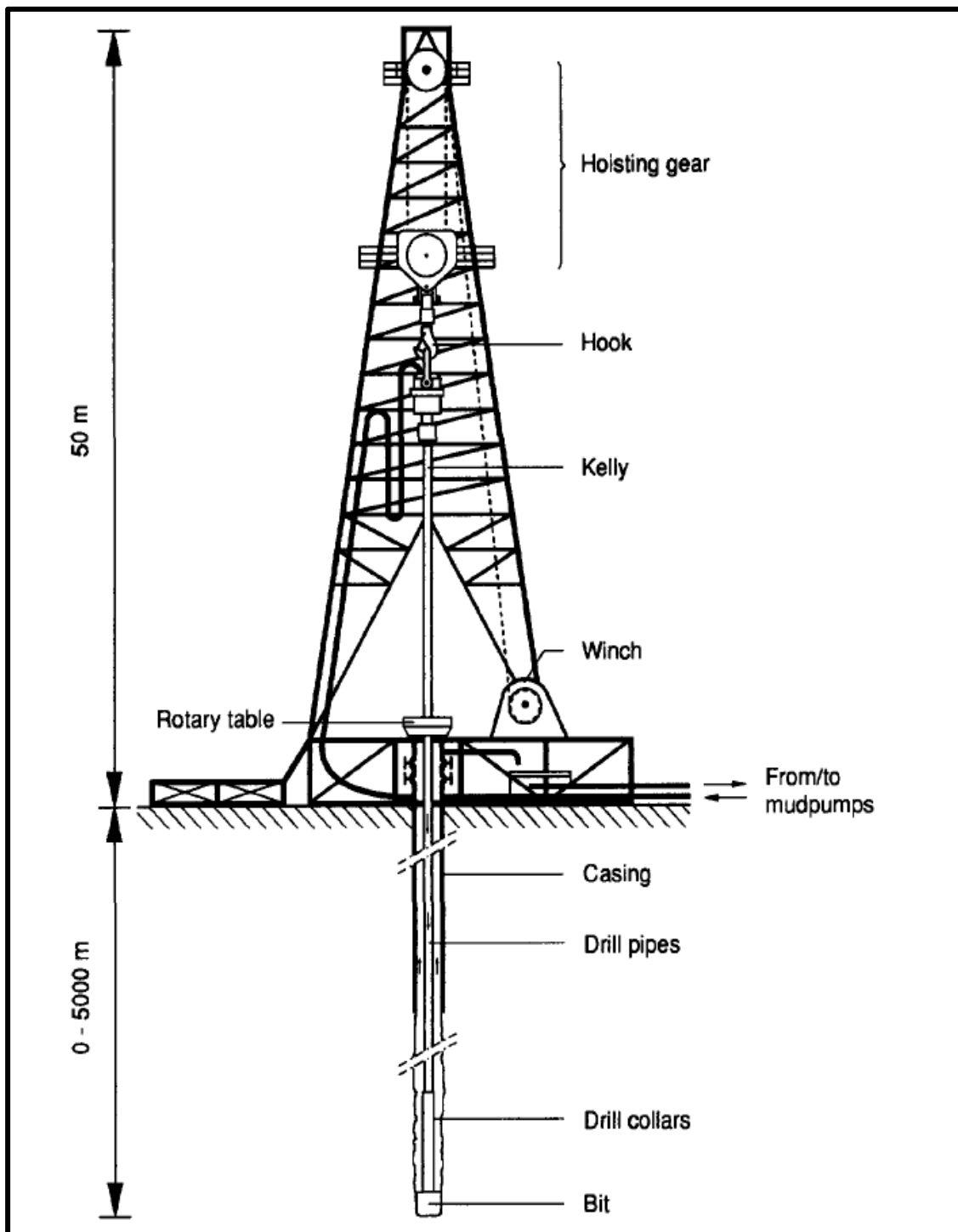


Figure 1-1 Essential Components of Rotary Drilling Rig [1].

1.2. Stability of Drill Strings

For vertical wells, without applying WOB, drill string is straight if the wellbore is straight. With a small WOB, the drill string still remains straight. When WOB is increased up to so-called first critical buckling force, the straight form of the drill string is not stable anymore. The drill string buckles and gets in contact with the wellbore. If WOB is further increased up to so-called second critical buckling force, the drill string buckles second time and it is called buckling of second order. With higher WOB values, the buckling of third and higher order occurs.

A slight increase in WOB from first critical buckling force may result in the drill string to buckle into a snaking or sinusoidal shape (2-Dimensional) at the lower end of the drill string as shown in Figure 1.2a. As WOB is increased further, the degree of the sinusoidal buckling increases and drill string starts to rise from bottom of the hole in helical shape (3 Dimensional) as shown in Figure 1.2b. That indicates that WOB is reached to another critical value at which drill string has a form of helix with total surface contact with wellbore. The drill string is defined as helically buckled.

The buckling phenomena during drilling operations for oil, gas and geothermal energy is a major problem that has been interest to many researchers in the industry for decades. Buckling may adversely affect the normal engineering operations on the field, therefore, knowledge of buckling behavior of pipes is important to eliminate buckling related problems.

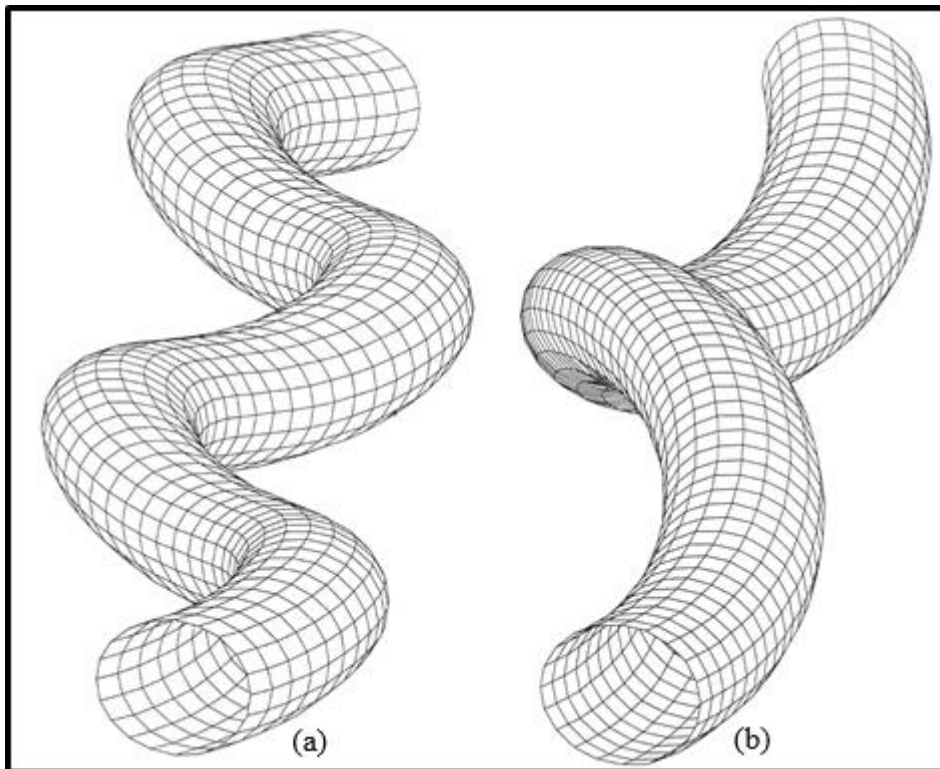


Figure 1-2 (a) Sinusoidal Buckling, (b) Helical Buckling [2].

When buckling of drill string occurs, the buckling may change the bit angle and may result in direction control problems. The buckling may also cause early failure of drill string due to fatigue. Continuous rotation of buckled drill string (when bending loads are applied) undergoes both tension and compression for every rotation of the drill string. This kind of loading on drill string produces stresses that are called fluctuating stresses. These fluctuating stresses decrease the life of the drill string significantly and cause early fatigue failure. Moreover, since buckled drill string gets in contact with wellbore, it may result in insufficient bit weight due to excessive frictional drag between drill string and wellbore. In helically buckled shape of drill string, the contact area increases significantly. After increasing WOB further, the contact force and resultant drag will be so large that any further increase of WOB, no longer felt at the bit. This situation is called as lock-up.

CHAPTER 2

CLASSICAL BUCKLING OF COLUMNS

The classical buckling of columns was first investigated by Euler in 1744 [3]. When a column undergoes a displacement transverse to the subjected compression load, the column is said to be buckled.

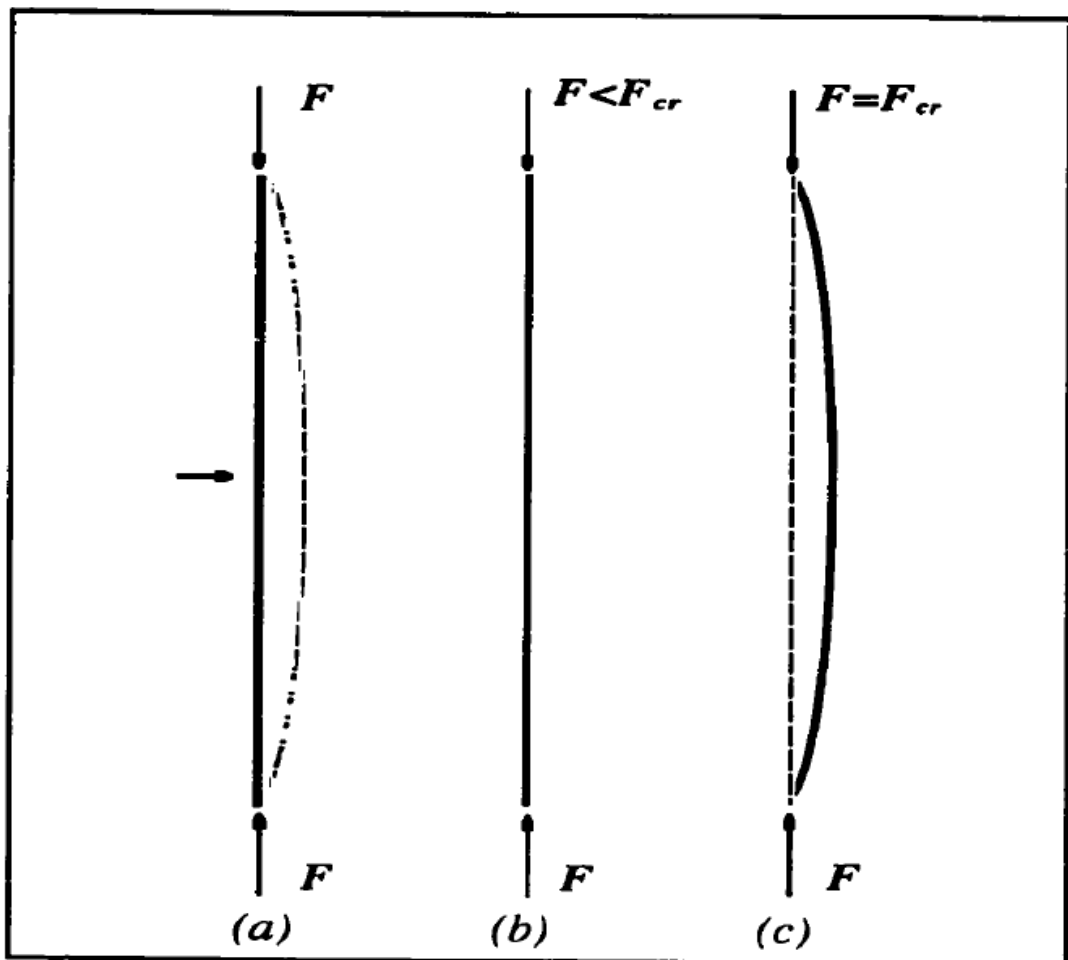


Figure 2-1 (a) Initial Form of Column, (b) Stable Form of Column, (c) Unstable Form of Column [4].

During the derivation of the equation, the column is assumed to be slender, ideal column placed in vertical direction, free from the upper end and applied an axial force, F , as shown in Figure 2-1a. Additional assumptions are: column is perfectly elastic, and stresses do not exceed the yield strength of the material. If applied load, F , is lower than the critical compression load, the column stays in straight and responses only axial compression. For that case, when a lateral force is applied to the middle of the column and a small deflection is created, the deflection vanishes when this lateral force is removed and the column returns back to its original vertical shape. This condition is called that “the straight form of elastic equilibrium of the column is stable”, as shown in Figure 2-1b. If F is gradually increased up to critical level and a lateral force is applied, deflection caused by the lateral force will not disappear even if lateral force is removed as shown in Figure 2-1c. This condition is called that “the straight form of elastic equilibrium of column is unstable”. This critical load (or Euler load) is defined as minimum force that keeps the column in a stable form.

Euler [3] showed that, the critical buckling load for columns is calculated as:

$$F_{cri} = \frac{k\pi^2 EI}{L^2} \tag{2.1}$$

wherein,

k is a numerical parameter depending on different end conditions as shown in Figure 2-2,

E is the Young Modulus for steel, pounds per square foot.

I is the moment of inertia of the pipe cross section, ft⁴.

L is the length of the bar, ft.

According to Euler critical buckling equation, the critical force depends on material, cross-section geometry, length and end conditions.

Bending and buckling are similar phenomena in which both of them include bending moments. In bending, these moments are independent of the resultant deflection, while in buckling, the bending and deflections are mutually interdependent [5].

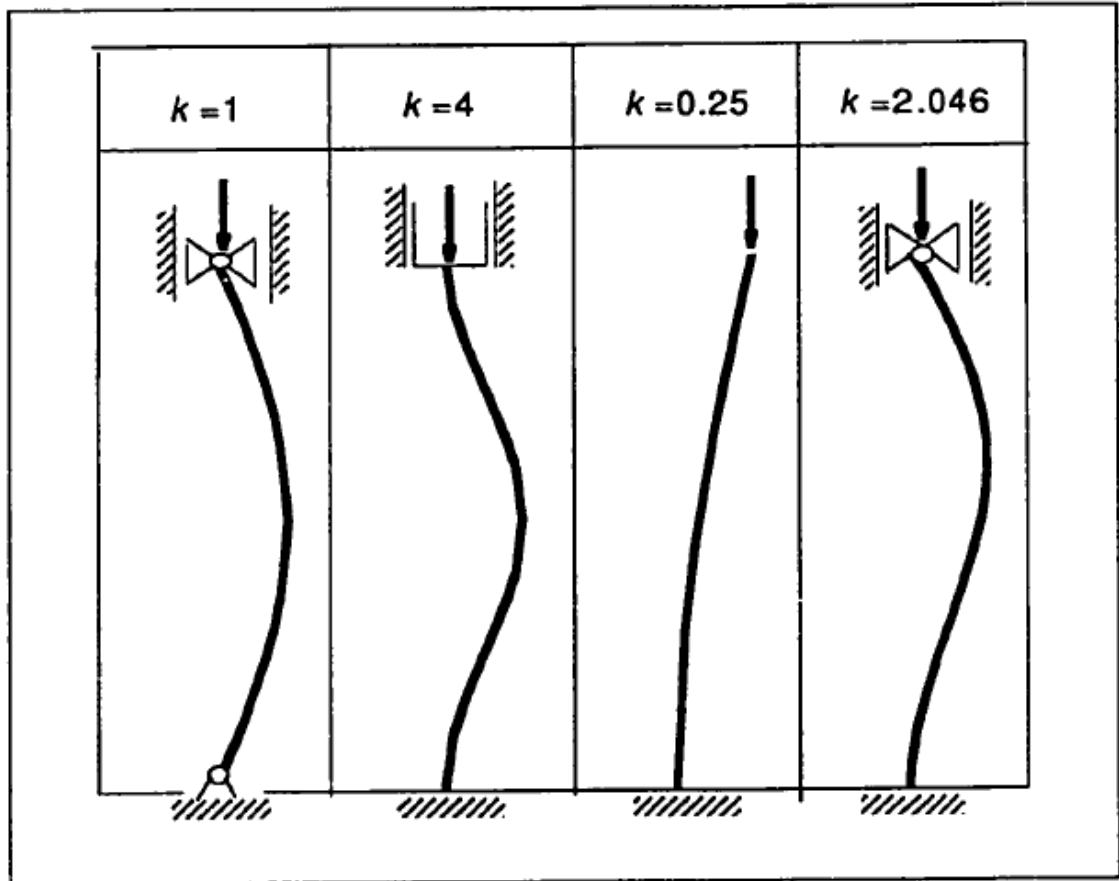


Figure 2-2 Euler Buckling Factors for Different End Conditions [4].

2.1. Mathematical Formulation of Euler Buckling Force

Let's assume a light, straight, slender, uniform, pin-ended column of a length L , with moment of inertia, I , and modulus of elasticity, E , as shown in Figure 2-3. The axial compressive load, F , is gradually increased up to critical buckling load. Upper free body diagram shows the external forces on the system. Below figure shows internal forces and bending moment in the cross section caused by buckling of the column.

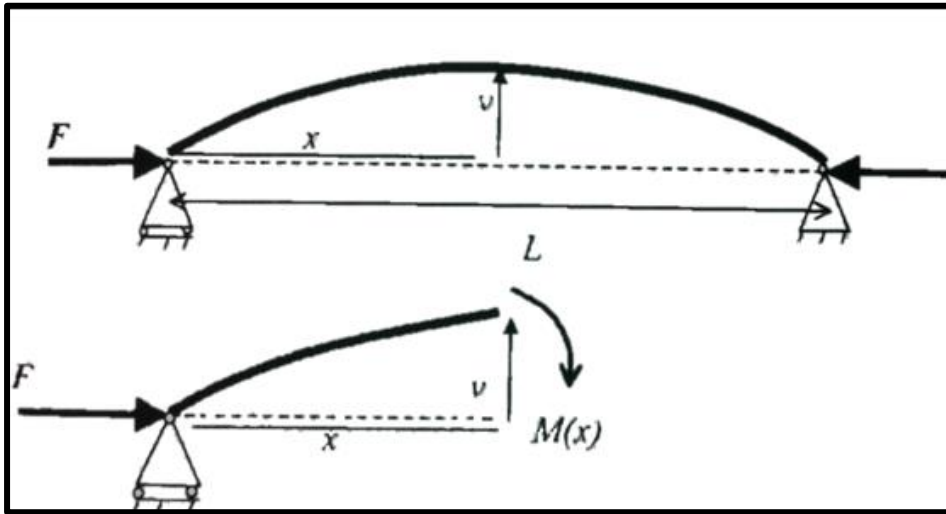


Figure 2-3 End Pinned Column under Bending [5].

By using moment equilibrium for lower free body diagram, internal bending moment, M can be calculated as:

$$M(x) = Fv \quad 2.2$$

The relations between the moment, M and the displacement, v from Beam Column Theory [6] can be written as:

$$M(x) = -EI \frac{d^2v}{dx^2} \quad 2.3$$

Combining Eq. 2.2 and Eq. 2.3:

$$EI \frac{d^2v}{dx^2} + Fv = 0 \quad 2.4$$

Eq. 2.4 is a second order homogeneous ordinary differential equation with constant coefficients. The solution is:

$$v(x) = A \sin\left(\sqrt{\frac{F}{EI}}x\right) + B \cos\left(\sqrt{\frac{F}{EI}}x\right) \quad 2.5$$

The coefficients A and B can be determined by two boundary conditions:

$$v(0) = 0 \quad 2.6$$

$$v(L) = 0 \quad 2.7$$

which yield:

$$B = 0, v(0) = 0 \quad 2.8$$

or,

$$v(x) = A \sin\left(\sqrt{\frac{F}{EI}}x\right) \quad 2.9$$

This shows that the buckling mode is a sine curve. If coefficient, A is nonzero then the column can be buckled. The resultant values are called eigenvalues. According to

Eq. 2.9, the values of $\sqrt{\frac{F}{EI}}$ should be in the form of $\sqrt{\frac{F}{EI}} = \frac{n\pi}{L}$, then

$$F = \frac{n^2\pi^2 EI}{L^2} \quad 2.10$$

Eq. 2.10 defines the buckling loads of a column. The lowest Euler buckling load is called critical load and it is found by using $n = 1$:

$$F = \frac{\pi^2 EI}{L^2} \quad 2.11$$

CHAPTER 3

SPECIAL FEATURES FOR PIPE BUCKLING IN OIL WELLS

The buckling of drill string needs to be analyzed further because there are a lot of parameters for drill string buckling those are different from Euler`s classical buckling of columns. Therefore, Euler`s buckling of columns results cannot be directly applied to drill string buckling in wellbores, but, approaches in the studies of classical buckling of columns can still be used.

Boundary conditions for drill string buckling in wellbores are quite different from the studies of Euler`s buckling of columns. First of all, there is no lateral constraint considered during derivation of the Euler`s equation which means that classical buckling of columns occurs only in a 2D plane. However, this is not the case for drill string buckling in vertical, directional and horizontal wellbores. The wellbore cylindrical surface creates a cylindrical constraint around the drill string that causes the drill string rise-up around the wellbore wall that creates 3D buckling phenomena. Moreover, in non-vertical wellbores (directional or horizontal wells) the drill string lies down to the lower side of the wellbore, and pipe buckling occurs on the cylindrical surface of the wellbore. When WOB passes the critical sinusoidal buckling force for a horizontal wellbore case, the pipe is raised up around the wellbore wall and shape of the buckling will be sinusoidal if it is observed from top side of the wellbore, as seen in Figure 3-1. End view of the buckling can be observed like a sine curve when viewed from axial direction of the wellbore as seen in Figure 3-1.

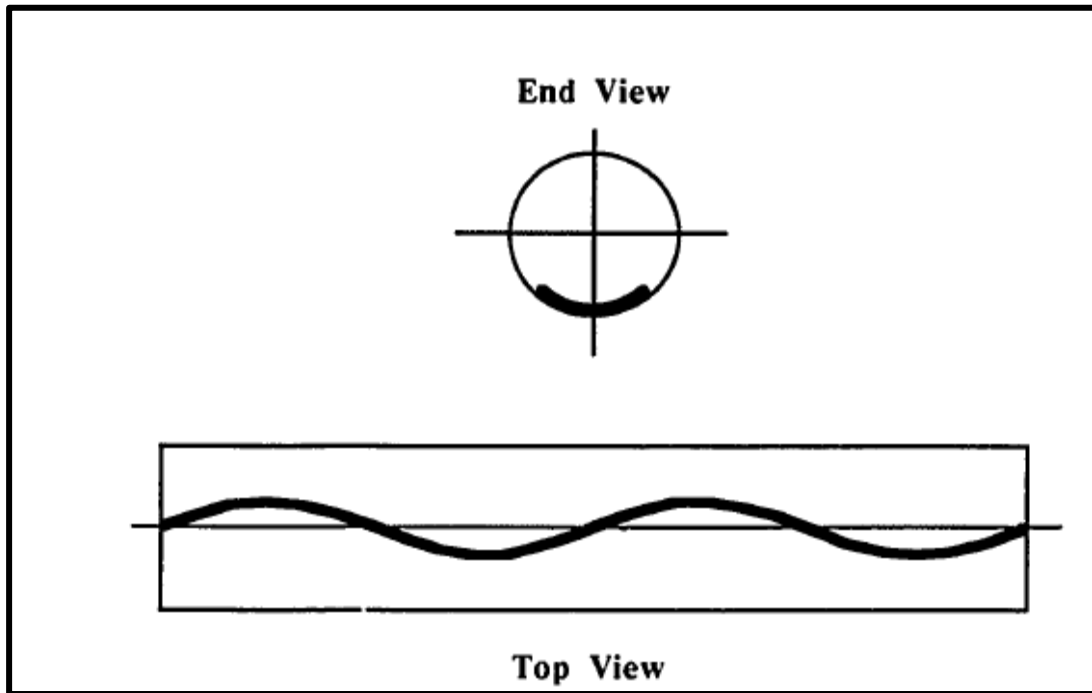


Figure 3-1 Sinusoidal Buckling of Pipe in Horizontal Wellbore [4].

Secondly, Euler's buckling of columns always occurs in the first order of buckling. However, buckling of pipes in wellbores may occur in higher orders. The difference is due to no disturbing resistance force is considered in the classical buckling study, while a disturbing lateral resistance force is applied by wellbore for pipe buckling. This results in buckling of pipes in wellbores in a sinusoidal shape with a higher order (more than one half sine waves) of buckling for long pipes.

Thirdly, there will be no change in type of buckling for Euler's model since the deflection of column may increase until the column fails due to excessive bending stress while axial load is increased further. However, sinusoidal buckling of pipes is observed to some degree, and then buckling shape will change to helical buckling. That means pipe will be in helix shape and will be in contact with the cylindrical wall of wellbore. The reason for this type change is the cylindrical wall of wellbore constrains the sinusoidal buckling development and helix takes on the post-buckling shape due to the minimum total potential energy theory. The helix is formed by

rising up every other half-sine wave form from sinusoidal buckling shape to top side of the wellbore and keeping the other half-sine waves on the bottom side of the wellbore, as seen in Figure 3-2.

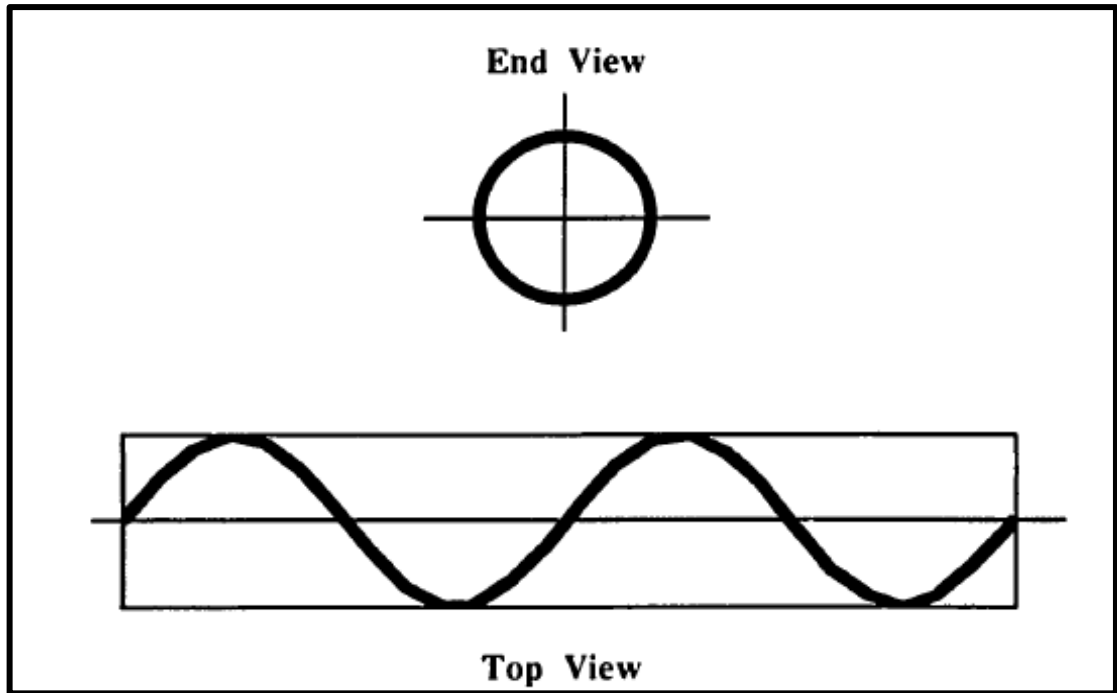


Figure 3-2 Helical Buckling of Pipes in Wellbores [4].

CHAPTER 4

REVIEW OF CURRENT LITERATURE

4.1. Sinusoidal Buckling of Pipes in Vertical Wellbores

Buckling of drill strings for vertical wells was studied in detail in 1950 by Lubinski [7] to prevent unexpected drill string failures due to fatigue and undesirable hole deviation problem from vertical. The mechanical model of Lubinski is shown in Figure 4-1 and it has the following assumptions:

1. Long drill string with no tool joint.
2. Drill string is centered completely to the wellbore.
3. Two ends of the drill string are hinged connections.
4. There is no rotation on drill string, and loading is “static loading”.

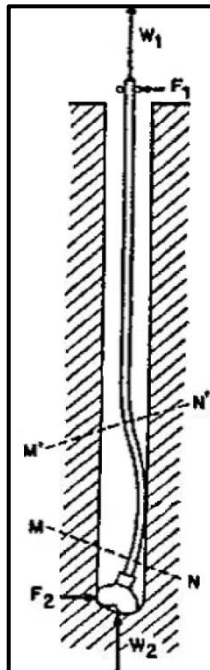


Figure 4-1 Designation of External Forces Acting upon Drill String [4].

The differential equation was derived by using shear force balance and the equation was solved by using the Bessel functions. The solution is:

$$F = 1.94(EI)^{1/3}w^{2/3} \quad 4.1$$

wherein,

E is the Young Modulus for steel, psi.

I is the moment of inertia of the pipe cross section, in⁴.

w is the unit weight of the pipe, lb/in.

Lubinski used power series to solve differential equation for the instability problem. Lubinski's method gives good results in the form of power series. Nevertheless, the power series terms get very large for long drill strings, and after a certain length, the results may be incorrect [8].

Then, in 1986, Wang [9] proposed the exact coefficient for infinite pipe length in a vertical well as 1.018793 for Lubinski's equation. The equation found is:

$$F = 1.018793(EI)^{1/3}w^{2/3} \quad 4.2$$

Wu [4] analyzed critical buckling force for vertical wells by using energy method in 1992. The equation derived is:

$$F = 2.55(EI)^{1/3}w^{2/3} \quad 4.3$$

Miska [10] stated that for deep vertical wells, the coefficient of Eqn. 4.1 should be replaced by 1.018, which is actually Eqn. 4.2.

Salies et al. [11] performed experiments for vertical buckling to verify Eqn. 4.1 on a stainless pipe having outer diameter, inner diameter, and length of 0.25 in., 0.21 in., and 643 in., respectively. A 2 in. ID tube was used to simulate the wellbore in the test

set-up. A significant difference was noticed between calculated and measured values. The difference is explained by the imperfections present in the test pipe.

Salies et al. [11] also found that Eqn. 4.1 is the solution for a drill string with a length equivalent to 7.94 dimensionless units, which is equivalent to around 400 meter length. They also showed that for drill strings with length greater than 7.94 dimensionless units, the critical buckling force is less than predicted by Eqn. 4.1.

4.2. Sinusoidal Buckling of Pipes in Inclined and Horizontal Wellbores

In 1964, Paslay and Bogy [12] studied pipe buckling in inclined wellbores by using a complicated energy method. They used the model of a circular bar which is laterally constrained to be in contact with an inclined circular cylinder surface at the low side. They proposed a position angle, $\alpha(z)$, that describes the buckled pipe as a sine function along the wellbore as shown in Figure 4-2.

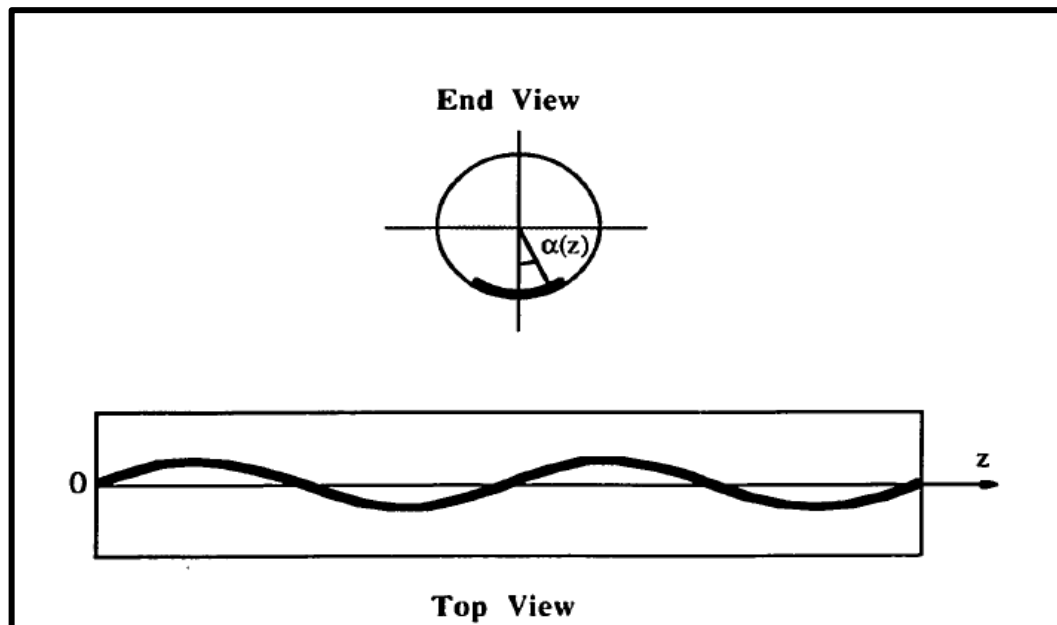


Figure 4-2 Buckling Model of Paslay and Bogy for Pipes in Inclined Wellbores [4].

In 1984, Dawson and Paslay [13] found an explicit expression of sinusoidal buckling for drill pipes in inclined wellbores. The most widely known equation is:

$$F = 2 \sqrt{\frac{EIw \sin \theta}{r}} \quad 4.4$$

wherein,

r is the radial clearance between the pipe and the hole, in.

θ is the wellbore deviation from vertical, deg.

The writers also proved that drill string become more resistance to buckling in highly deviated wells due to support by the wellbore wall.

Dellinger et al. [14] derived their equation for both directional and horizontal wells as shown below:

$$F = 2.93(EI)^{0.479}(w)^{0.522}\left(\frac{\sin \theta}{r}\right)^{0.436} \quad 4.5$$

Woods and Lubinski [13] fit an equation to their experimental data collected in 1953 but never published. The equation is:

$$F = 2.85(EI)^{0.504}(w)^{0.496}\left(\frac{\sin \theta}{r}\right)^{0.511} \quad 4.6$$

Chen et al. [15] derived an equation for sinusoidal buckling of pipes in horizontal wellbores. Their solution is similar with Dawson and Paslay`s [13] when well inclination is taken as 90^0 in their equation.

$$F = 2 \sqrt{\frac{EIw}{r}} \quad 4.7$$

4.3. Helical Buckling of Pipes in Vertical Wellbores

Helical buckling of pipes in wellbores was first studied theoretically by Lubinski, Althouse and Logan [16] in 1962. In this pioneering work, the relationship between critical helical buckling load and helical pitch, p , is derived as:

$$F = \frac{8\pi^2 EI}{p^2} \quad 4.8$$

The main assumptions made by Lubinski are:

- 1- The system is totally frictionless.
- 2- The pipe has no weight.

Because of the assumptions, the helical pitch length is constant through the wellbore.

Kwon [17] developed a new equation for helical buckling in vertical wells that includes the weight of the drill string by using beam-column theory. The derived fourth-order nonlinear differential equation was solved by a series solution approximation.

Wu [4] derived an equation to calculate helical buckling load corresponding to the complete formation of helix in vertical wellbores with the effects of pipe weights. The equation is:

$$F = 5.55(EI)^{1/3}w^{2/3} \quad 4.9$$

4.4. Helical Buckling of Pipes in Deviated and Horizontal Wells

Lubinski [16] derived critical helical buckling load for deviated and horizontal wells as follow:

$$F = 2\sqrt{2} \sqrt{\frac{EIw \sin \theta}{r}} \quad 4.10$$

However, Wu [18] showed that the so-called helical buckling load that appears in the current literature is only the average axial load in the helical buckling development process. Instead of Eqn. 4.10, they obtained a new critical helical buckling load for deviated and horizontal wells:

$$F = 2(2\sqrt{2} - 1) \sqrt{\frac{EIw \sin \theta}{r}} \tag{4.11}$$

Other researchers proposed different coefficients for the formulations to predict the helical buckling load in Table 4-1. Cunha [8] stated that these researchers used different load history assumptions such as constant load assumption or ramp load assumption, during the derivation of the equations.

Table 4-1 Coefficients for Different Researches

References	Coefficients
Chen et al. (1990) [15]	2.83
Lubinski and Woods (1953) [19]	2.85
Wu and Juvkam-Wold (1995) [20]	4.65
He and Kylingstad (1995) [21]	2.83
Qui et al. (1998a) [22]	5.66
Qui et al. (1998b) [23]	3.75

4.5. Numerical Studies on Drill String Buckling Phenomena

Aslaksen et al. [24] used four-dimensional time-based finite element simulations by using IDEASTM software to create a holistic approach to drilling system optimization which is used to study of relevant forces, accelerations, and bending moments all the way from cutting structure of the bits to the rotary table or top drive by using virtual prototyping.

Till et al. [25] used finite element method for evaluating helical buckling behavior and post-buckling behavior of the coil tubing in directional wellbores. The authors proved that finite element modeling have benefits to model exact wellbore geometry and coil tubing, and to determine of lock-up conditions by modeling post-buckling behavior of the tubing, to calculate plastic deformation and the inclusion of plastic strain of the coil tubing.

Hajianmaleki et al. [26] used explicit finite element method to simulate buckling behavior of drill strings for vertical and curved wellbores. The authors showed that the results are quite similar for simulation results and analytical results. However, there are differences in the numerical simulation results and experimental results and these differences are explained due to model and experimental uncertainties and imperfections present in the experiments. The authors worked on the effect of inclination angle, length, formation stiffness, and effective weight of the drill string on buckling in detail.

Menand et al. [27] made a comparison of an advanced model of drill string mechanics with an experimental set-up. From the experimental results, it is shown that dog-legs has a strong effect on the buckling of drill string in deviated wells. Also, finite element simulations showed that rotation of drill string significantly reduces the critical buckling force for helical buckling.

Salies et al. [28] created three different experimental set-up(vertical set-up, horizontal set-up, and variable inclination set-up) to analyze effect of well deviation of helical buckling. The authors found that measured critical helical buckling forces

are lower than the results reported in the literature. Moreover, they also found that friction increases the critical buckling forces of both sinusoidal and helical buckling and produces a hysteresis effect in the load versus axial displacement graph. They also showed that finite element method can be used to model the buckling process including friction effect.

CHAPTER 5

SCOPE OF WORK

5.1. Thesis Overview

The main weakness of the analytical solutions of the buckling problem in vertical wellbores is their inability to calculate critical buckling forces for different length of drill strings. The reason is derivations of the equations are done either for a short length of drill string or for an infinite length of drill string. Although infinite drill string length solution is being used for deep vertical wells, there are still missing points in the literature about the variation of critical buckling forces as the length of the drill string increases.

5.2. Thesis Objectives

The main purpose of this study is to develop a finite element model to analyze elastic stability of five different drill collars for deep vertical wellbores by length sensitivity. The main objectives of the thesis are listed as follows:

- To see the difference between post-buckling behavior of slender-dominated long hanging drill strings with stiffness-dominated short hanging drill strings in vertical wellbores.
- To investigate the effect of flexural rigidity of drill collars on decrease of the critical buckling forces as the length of the drill string increases,
- To see the behavior and amount of decrease in the critical buckling forces as the length of the drill string increases,
- To compare the simulation results with different analytical solutions (short length solutions and infinite length solution) to see the validity of numerical finite element model.

5.3. Thesis Scope

The present work focuses on the stability of long drill strings in vertical wellbores. Since the main purpose of this study is to simulate stability of drill strings in five different configurations by length sensitivity, various complexities are simplified in bottom hole assembly (BHA) to make the simulation results comparable with analytical solutions.

However, the work can also be adapted to other instability problems of drill strings with different kind of parameters, including torque, rotation effect, friction, wellbore deviation, tapered drill strings, tool joint effects, and effect of special tools in the BHA, etc., when their special characteristics are included in the model.

5.4. Thesis Organization

In this thesis, firstly, fundamental review of classical Euler`s buckling of columns is introduced. Then, differences between classical Euler`s buckling of columns and drill string buckling in wellbores are compared. Unlike Euler`s buckling of columns, the lateral deflection of buckled drill string in wells is limited by the outer constraint of the wellbore. A review of current literature about sinusoidal and helical buckling for vertical, directional and horizontal wellbores is also presented. Next, the theory of FEM and the model created for buckling simulations are explained in detail. Finally, the simulation results are compared with analytical solution, then advantages and disadvantages of the model are discussed, and possible ways for improving the model are given. Suggestions for prospected researchers are also advised in this section.

CHAPTER 6

FINITE ELEMENT METHOD

6.1. Basics of Finite Element Method

The finite element analysis is a numerical method that is being used to obtain solutions of different types of engineering problems including solid mechanics, heat and mass transfer, electromagnetic problems, and fluid mechanics [29]. The main idea of the finite element method is to find a simpler approximate solution to a complicated problem. The existing mathematical tools may not be enough to find the analytical solution of the most of the real problems. Therefore, in the absence of any analytical solution of a given problem, the finite element method is the most preferred numerical method to obtain approximate solutions. In addition, finite element method solution can be improved or refined the approximate solution by spending more computational time and effort [30].

Theoretically, engineering problems are mathematical modeling of physical phenomena. Mathematical modeling of engineering problems is mostly differential equations with different corresponding boundary and/or initial conditions applied. These differential equations are found by using fundamental of nature to a system. These laws are mass balance, momentum balance, and energy balance equations. Analytical solutions of these problems have two different parts, which are homogenous part and particular part. Design parameters of a given problem affect the system behavior. Therefore, there are some parameters that give some information of the natural tendency of a given system. These parameters include material and geometric properties of the system such as modulus of elasticity, thermal conductivity of the material, viscosity, second moment of area. However, there are some parameters that produce disturbances in the system such as external

forces, moments, temperature difference in the medium, and pressure difference in fluid flow. The parameters that show the natural behavior of the system always appear in homogenous solution part, in contrast, the parameters that create disturbance always appear in particular solution part.

It is critical to know the role of these parameters in FEM for calculation of the stiffness matrices and load matrices. The system characteristics will always appear in stiffness matrix, although the disturbance parameters will always appear in the load matrix [29].

6.2. Finite Element Method vs. Finite Difference Method

There are lots of engineering problems that don't have exact solutions. The reason to not being able to obtain exact solution is either because of the complexities in the nature of the problem or difficulties that may come from boundary and/or initial conditions. Rather than using analytical solutions those gives exact solution of a system at any point, numerical results approximate exact solutions at discrete points, those are called as nodes. The most widely used numerical methods are finite difference method and finite element method.

In finite difference method, the differential equation is written for each node, and the derivatives of the parameters are calculated by finite difference equations. This method gives a set of linear equations to be solved. Although finite difference methods are easy to apply and interpret in simple cases, the method becomes complicated to apply to complex problems with difficult boundary conditions.

On the other hand, the finite element analysis uses integral forms of equation to create a set of algebraic equations to be solved. Furthermore, an approximate continuous function is assumed to the solution for each element as representations. The full solution is found by assembling of all individual results which allows for total continuity of the solution from the elements connectivity [29].

6.3. General Steps of the Finite Element Method

This section explains general steps in a finite element analysis to an engineering problem. Typically, for structural stress-analysis problems, the aim is to determine displacements and/or stresses for whole structure. For most of the structures, it is nearly impossible to find the exact values of the distribution of the deformation and stresses by using analytical methods due to complexities of the geometry, materials, and boundary conditions, therefore, the numerical methods analysis is needed such as finite element method, finite difference method, etc.

In general, there are several approaches to formulate finite element problems as shown in Figure 6.1.

For structural stress-analysis problems, direct method is the most suitable approach for a basic element in finite element analysis [31]. This method is most easily adaptable to line or one-dimensional element systems. There are two different direct methods for structural problems as shown in Figure 6.2.

Force method uses internal forces as unknowns of the problem. To obtain the equations, equilibrium equations are used initially. Next, additional equations are obtained by applying compatibility equations if necessary. The result is a set of algebraic equations to find unknown forces in the system.

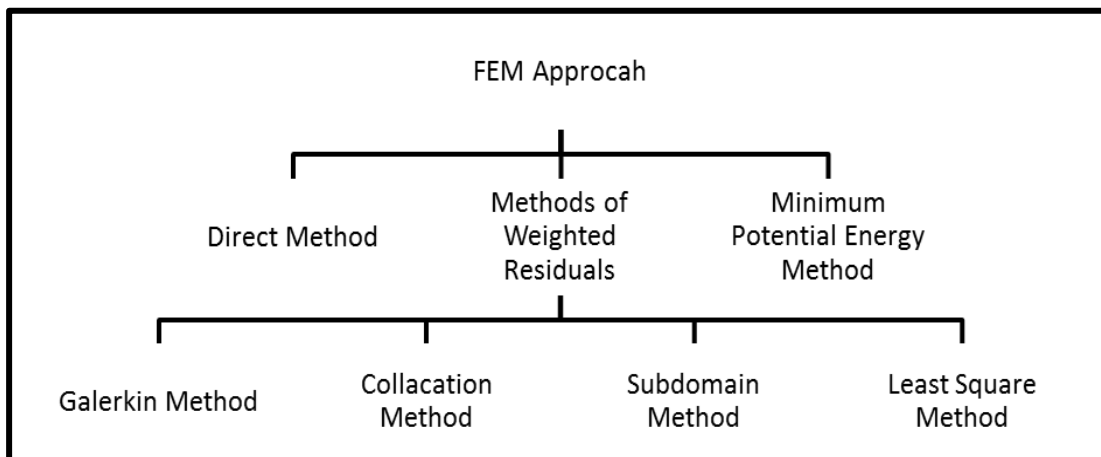


Figure 6-1 FEM Approach Methods

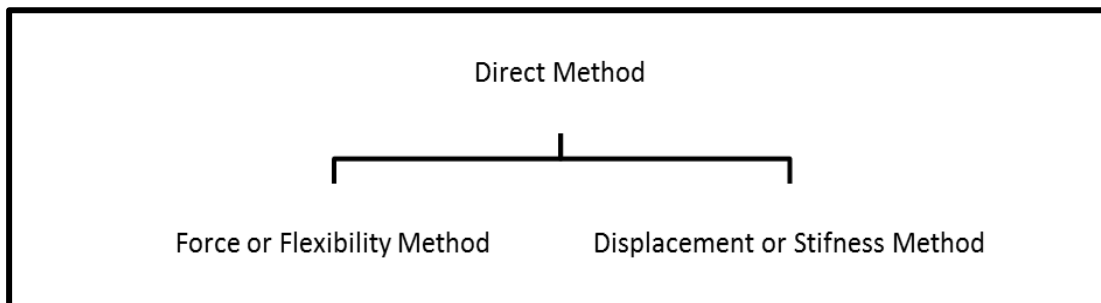


Figure 6-2 Two Main Different Direct Methods.

Displacement method uses displacements of the nodes as unknowns of the problem. Next, governing equations are expressed in terms of nodal displacements by using the equations of equilibrium and/or a related law to find the relationship between forces and displacements.

Since, these two different direct approaches result in different unknowns (forces and displacements) in the analysis, different matrices (flexibilities and stiffnesses) with their formulations are required to be solved. For computational process and computing time, displacement method is recommended due to simplicity of its formulation.

The methods of weighted residuals are useful for developing the element equations; particularly the most popular is Galerkin's method. These methods yield the same results as the energy methods wherever the energy methods are applicable. They are especially useful when a functional such as potential energy is not readily available. The weighted residual methods allow the finite element method to be applied directly to any differential equation.

For minimum potential energy theorem, developing stiffness matrix and equations for two- and three-dimensional elements, it is easier to apply a work or energy method whenever potential energy data is available [31]. The principle of virtual work, the principle of minimum potential energy, and Castigliano's theorem are frequently used methods for derivation of element equations.

The general steps followed in finite element formulation are presented below as described in "A First Course in the Finite Element Method by Daryl L. Logan" [31].

a. Discretize and Select the Element Types:

First step involves dividing the body into an equivalent system of finite elements with associated nodes and choosing the most appropriate element type to model most closely the actual physical behavior. The total number of elements used and their variation in size and type within a given body are primarily matters of engineering judgment. Elements that are commonly used in practice are shown in Figure 6.3.

b. Select a Displacement Function:

Second step involves choosing a displacement function within each element. The function is defined within the element using the nodal values of the element. Linear, quadratic, and cubic polynomials are most frequently used functions because they are simple to work with in finite element formulation.

c. Define the Strain/Displacement and Stress/Strain Relationships:

Strain/displacement and stress/strain relationships are necessary for deriving the equations for each finite element. Moreover, the stresses must be related to the strains through the stress/strain law—generally called the constitutive law. The ability to define the material behavior accurately is most important in obtaining acceptable results. The simplest of stress/strain laws, Hooke’s law, which is often used in stress analysis.

d. Derive the Element Stiffness Matrix and Equations:

The development of element stiffness matrices and element equations was based on the approaches selected on the concept of stiffness influence coefficients, which presupposes a background in structural analysis.

e. Assemble the Element Equations to Obtain the Global or Total Equations and Introduce Boundary Conditions:

In this step the individual element nodal equilibrium equations generated in step “d” are assembled into the global nodal equilibrium equations.

f. Solve for the Element Strains and Stresses:

For the structural stress-analysis problem, important secondary quantities of strain and stress (or moment and shear force) can be obtained because they can be directly expressed in terms of the displacements determined in step “e”.

g. Interpret the Results:

The final goal is to interpret and analyze the results for use in the design/analysis process. Determination of locations in the structure where large deformations and large stresses occur is generally important in making design/analysis decisions. Postprocessor computer programs help the user to interpret the results by displaying them in graphical form.

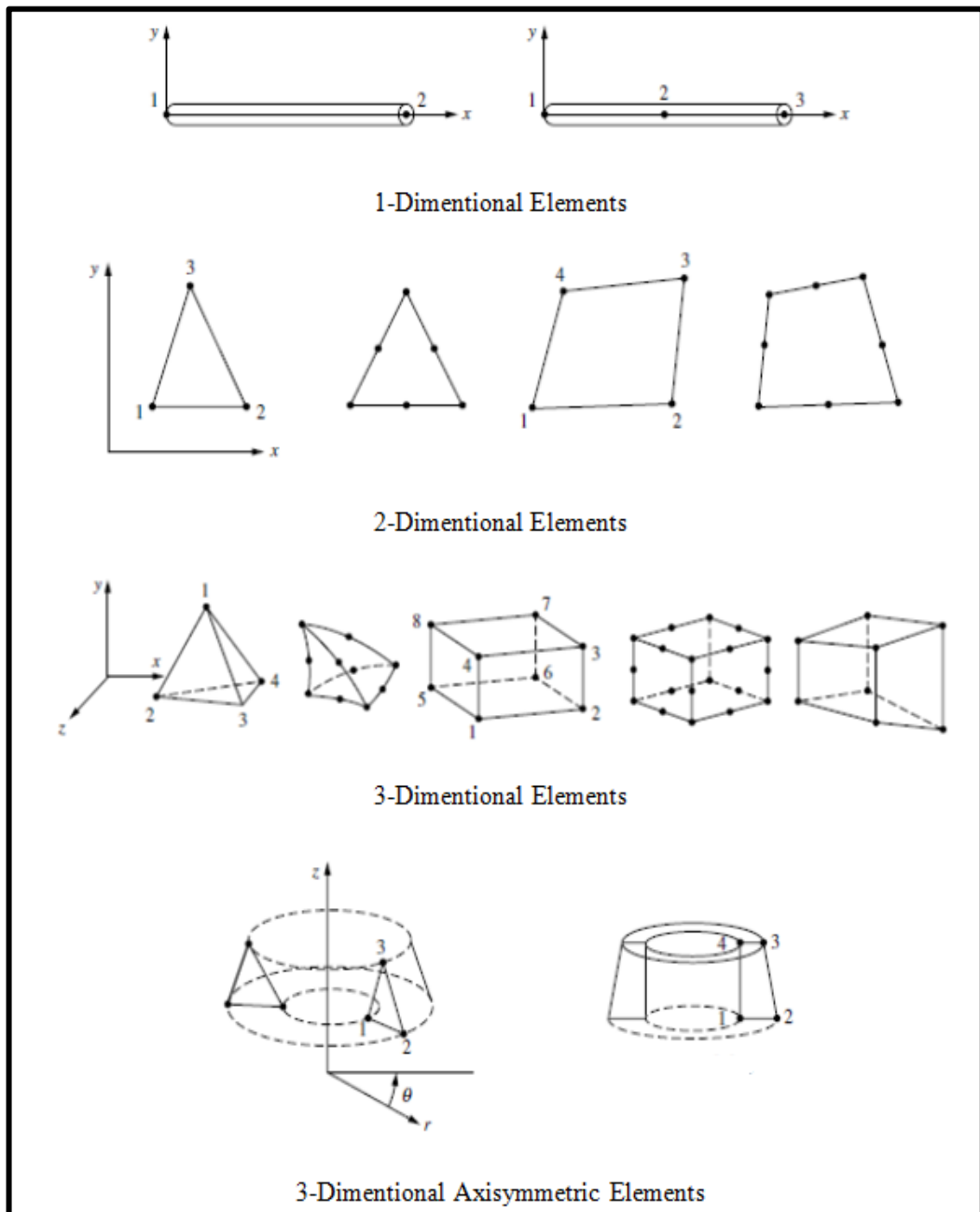


Figure 6-3 Various Types of Finite Elements [31].

6.4. IDEAS™ – Finite Element Analysis Software

IDEAS™ stands for Integrated Dynamic Engineering Analysis Software™. It was created in the 1990s in Smith Bits, a Schlumberger Company, for the purpose of designing Roller Cone Bits, gradually evolved and in 2003 became a powerful simulator of the bit and the entire drill string all the way to surface, capable of predicting vs. time the behavior of the following parameters of particular interest for bit design and selection [32]:

- Lateral Accelerations,
- Axial Acceleration,
- Torsional Oscillations,
- RPM oscillations (Stick Slip),
- ROP.

As shown in Figure 6-4.

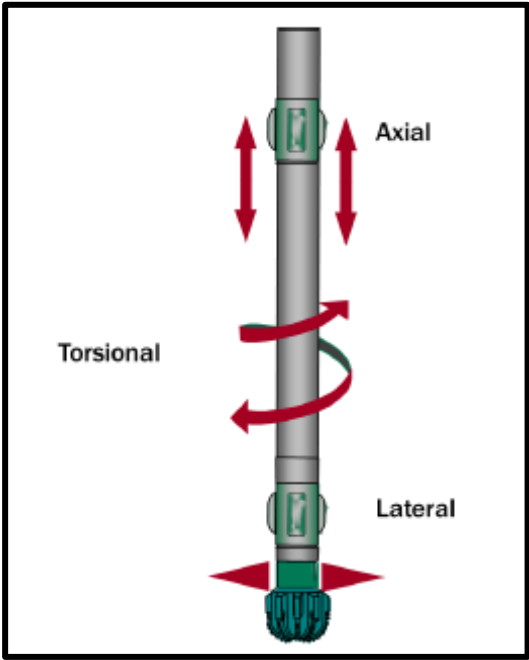


Figure 6-4 Vibration Types Simulated in IDEAS™ Software [32].

Regarding the modeling of the entire drill string, it predicts the vibrations and accelerations that have detrimental effects on directional control, tool reliability, drill string integrity, and drilling performance. The ability to pinpoint the source and effects of torsional, axial, and lateral oscillations allows engineers to qualify design changes to the drill string configuration and optimize parameters. Regarding the drill string, these are some parameters of interest [32]:

- Bending stresses,
- Buckling,
- Neutral point location,
- Side contact forces for drill pipe wear,

The modeling capabilities include but are not limited to [32]:

- Formation type and hardness,
- PDC and Roller Cone cutting structure and body geometry,
- Concentric and Eccentric hole opening devices,
- Push and point the bit Rotary Steerable Systems,
- Positive Displacement Motors,
- Vertical drilling device,
- Stabilizers,
- Jars,
- Drill Collars,
- Heavy Weight Drill Pipe,
- DP including tool joints.

IDEAS™ is composed of several sub-software packages, of which the IDEAS™ time simulation output with Requester Version.20170524 is the one used in this thesis, as seen in Figure 6-5. Other IDEAS™ software packages include: Critical Speed Analysis, Natural frequencies, bit and roller cone design modules without considering the BHA.

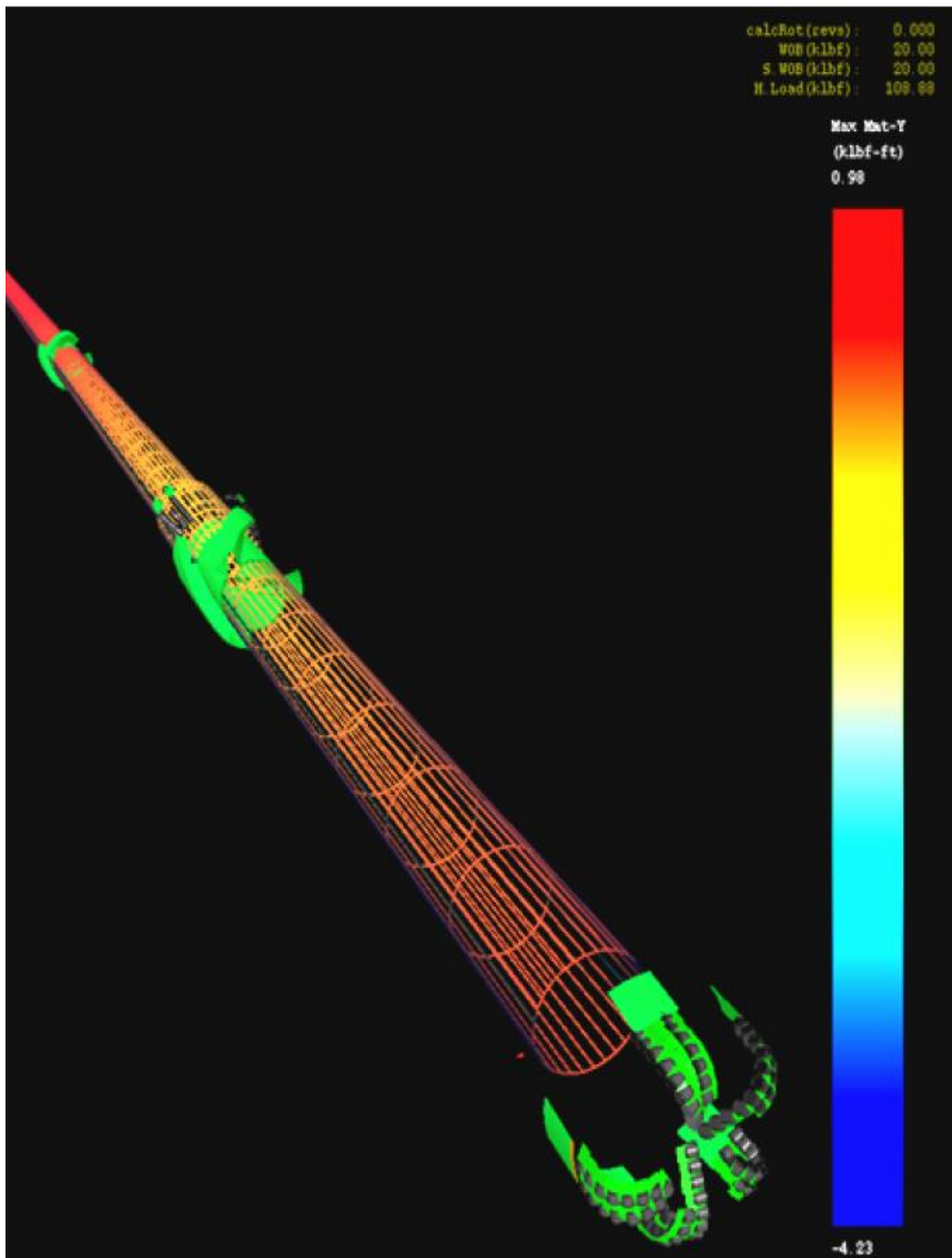


Figure 6-5 IDEAS™ Model of a PDC Bit Cutting Structure in 3-D [32].

The following are the main independent parameters considered in IDEAS™ [32]:

- **Bit Cutting Structure:** 3D description of the bit for modeling can be implemented to IDEAS™ software, as seen in Figure 6-6.
- **Formation Effects:** Dip, strike, homogeneity and anisotropy can be implemented.
- **Overbalance:** IDEAS™ indentation tests are performed at 3000, 6000 and 9000 psi confinement pressure.
- **Wellbore Trajectory:** Planned and actual surveys can be entered in IDEAS™ thus modeling the 3D trajectory of the well.
- **Hole Size:** At every survey station IDEAS™ allows the user to specify hole size, therefore washouts or under gage holes can be modeled.
- **BHA and Drive Type:** IDEAS™ has the capability to model all of the drilling tools.
- **Parameters:** WOB and RPM can be adjusted.
- **Eccentricity of Components:** Referred to as the distance between the geometric center of the tool and its center of gravity.

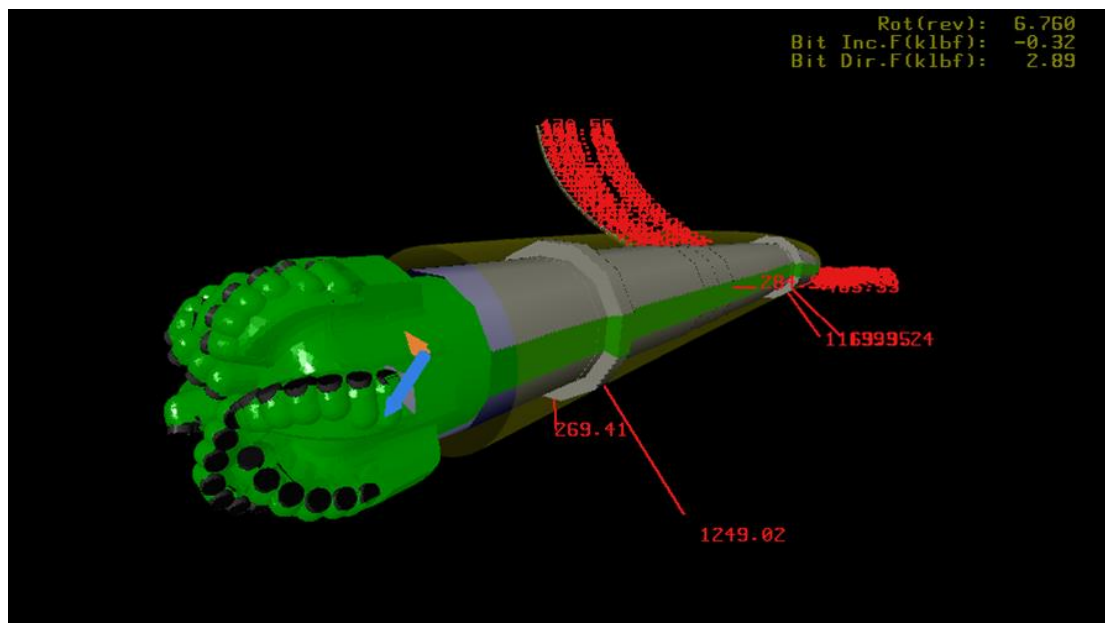


Figure 6-6 IDEAS™ Model of PDC Bit with Full Details with Body and Gage [32].

6.5. Mathematical Description of the Finite Element Model

6.5.1. Three-Dimensional Beam Element for Finite Element Analysis

To model the drill string in IDEAS™ software, three-dimensional beam elements are used in this study. Three-dimensional beam element has six nodal displacements at each unconstraint node: three translational components and three rotational components in three coordinate axes. Therefore, a three-dimensional beam element for its two joints has 12 nodal coordinates which means the resulting element matrices will be of dimension 12x12 matrices [33].

For buckling analysis, three-dimensional beam elements are suitable for implementing co-rotational formulation to handle rigid body motion. Secondly, stiffness matrix of the beam element includes geometric nonlinearity terms due to large deformation. Moreover, loading and boundary conditions can be from top drive, bit, wellbore contact, RSS pushing, gravity, etc. [34]. The Figure 6-7 shows a three-dimensional beam element with its 12 nodal coordinates below:

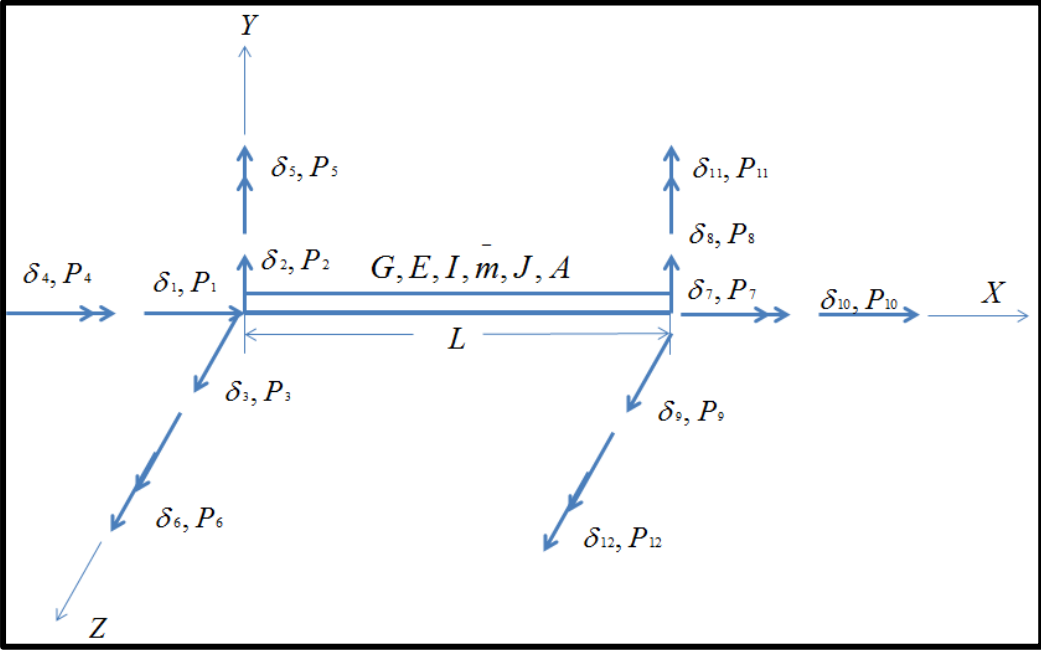


Figure 6-7 Three-Dimensional Beam Element with Forces and Displacements [33].

Where,

G is the shear modulus, Pa.

E is the modulus of elasticity, Pa

I is the moment of inertia of the bar, m^4 .

\bar{m} is the distributed mass of the beam, N.

J is the polar moment of inertia, m^4 .

A is the cross sectional area, m^2 .

P_1, P_2, P_3 and P_7, P_8, P_9 are static forces applied in each direction, N.

P_4, P_5, P_6 and P_{10}, P_{11}, P_{12} are moments applied in each direction, Nm.

$\delta_1, \delta_2, \delta_3$ and $\delta_7, \delta_8, \delta_9$ are linear displacements in each direction, m.

$\delta_4, \delta_5, \delta_6$ and $\delta_{10}, \delta_{11}, \delta_{12}$ are angular displacements in each direction, rad.

To create the differential equation of motion for a three-dimensional beam element, stiffness, mass and damping matrices are required. The stiffness matrix of a three-dimensional beam element is created by the method of superposition of the axial stiffness matrix, torsional stiffness matrix and flexural stiffness matrices.

Axial stiffness matrix of the beam is given as below [33]:

$$\begin{Bmatrix} P_1 \\ P_2 \end{Bmatrix} = \frac{AE}{L} \begin{bmatrix} 1 & -1 \\ -1 & 1 \end{bmatrix} \begin{Bmatrix} \delta_1 \\ \delta_2 \end{Bmatrix} \quad 6.1$$

Torsional stiffness matrix of the beam is given as [33]:

$$\begin{Bmatrix} T_1 \\ T_2 \end{Bmatrix} = \frac{JG}{L} \begin{bmatrix} 1 & -1 \\ -1 & 1 \end{bmatrix} \begin{Bmatrix} \delta_1 \\ \delta_2 \end{Bmatrix} \quad 6.2$$

Damping matrix for a three-dimensional beam element can be obtained by the same manner to those of the stiffness and mass matrices. However, in practice, damping is generally expressed by using damping ratios for different kind of vibration modes. Thus, if the response is needed by using superposition method, these damping ratios can directly be imported to the modal equations [33].

Direct method can be used to assemble the stiffness, mass and damping matrices for three dimensional beam elements to find the differential equation of motion. Differential equation of motion for a three-dimensional beam element with inertial, damping, elastic and external forces can be expressed as follow:

$$[M]\{\ddot{u}\} + [C]\{\dot{u}\} + [K]\{u\} = \{F(t)\} \quad 6.9$$

where,

$[M]$ is the mass matrix of an element,

$[C]$ is the damping matrix of an element,

$[K]$ is the stiffness matrix of an element,

$\{u\}$ is the system displacement vector,

$\{\dot{u}\}$ is the system velocity vector,

$\{\ddot{u}\}$ is the system acceleration vector,

$F(t)$ is the force vector including forces applied to the joints and equivalent forces for the forces not applied to the nodes of an element. Unknown parameters are system displacement vectors, velocity vectors, and acceleration vectors. Known parameters are mass matrix, stiffness matrix, damping matrix and external forces matrix.

6.5.2. Transformation of Local Coordinates to Global Coordinates

The stiffness matrix, Eqn. 6.4, and the mass matrix, Eqn. 6.8, of the beam element are calculated based on the local coordinate axes fixed on the beam element. If the coordinates of the beams are the same with the global coordinates of the structure, nodal coordinates can be added to obtain global stiffness and mass matrices. However, if it is not the case, then transformation of these local coordinates to global coordinates are necessary. Before attempting to obtain the characteristic equations of the entire system of elements, firstly, coordinate transformation should be done. Sometimes, element matrices and vectors may be calculated in local coordinates. And, local coordinates may be different for different elements. Therefore, before assembling the all element matrices, it is necessary to transform local coordinates to global coordinate system. The choice of the global coordinate system may be arbitrary. [30].

6.5.3. Solution of the Differential Equation of Motion

The integration of the differential equation of motion for a three-dimensional beam element may be calculated by several methods to obtain the response of the structures modeled as beams. The selection of the particular method of solution is mostly depends on the linearity of the Eqn. 6.9. If the differential equation of motion is linear, then the superposition method for modal analysis can be applied. If the structure has an elastoplastic behavior of material or any other nonlinearity, it is necessary to use any of numerical integration methods to solve the differential equation of motion. To solve Eqn. 6.9 numerically, there are several methods to apply. The most efficient way to solve the equation of motion is Newmark Method [34]. Newmark Method is numerical integration method specialized for nonlinear force-deformation model in structural dynamics. Details of the Newmark Method can be found in the book of Structural Dynamics written by Chopra [35].

After all coordinate transformations done, the next step is to construct system equations. The procedure to construct the system equations are the same for any kind

of problems regardless of the number and type of the elements used [30].
Assembling of the element matrices are done by using general matrix algebra rules.

CHAPTER 7

MODEL VERIFICATION FOR IDEAS™ SOFTWARE

IDEAS™ will be validated for sinusoidal and helical buckling for deviated and horizontal wells by comparing analytical solutions. After validation, IDEAS™ will be cleared to use for buckling for vertical wells. That is, IDEAS™ software will be validated for most complicated cases; then it will be used for a simpler case.

7.1. Sinusoidal Buckling Validation for Deviated and Horizontal Wells

The objective of this section is to compare sinusoidal buckling phenomena predicted by IDEAS™ against analytical equations in the literature. The most widely adopted critical compressive load inducing buckling force for deviated wells is given by Dawson and Paslay [13]. The equation is:

$$F_{cri_sin}^{dev} = 2 \sqrt{\frac{EIw \sin \theta}{r}} \quad 7.1$$

Associated with Eq. 7.1, the number of buckles is calculated as:

$$n = \left(\frac{L^4 w \sin \theta}{\pi^4 EIr} \right)^{1/4} \quad 7.2$$

If sinusoidal buckling arises due to the critical compressive load in Eq. 7.1, the relevant sinusoidal wavelength is calculated based on Eq. 7.2 as:

$$\gamma = \frac{2L}{n} \quad 7.3$$

When axial compressive load reaches critical buckling force, sinusoidal buckling is expected to arise. With increasing compressive load applied, sinusoidal buckling is transiting to helical buckling. For deviated wells, Eqn. 7.1 will be used to simulate in IDEAS™.

In the following, a developing process of buckling predicted by IDEAS™ will be shown. A 10" frictionless wellbore with $\theta = 30^\circ$ and $\theta = 90^\circ$ is considered. The parameters for drill string are given in below Table 7-1:

Table 7-1 Parameters for Drill String for IDEAS™ Simulation

Outer Diameter	3.5"
Inner Diameter	2.602"
Modulus of Elasticity	$3 \times 10^7 \text{ psi}$
Poisson's Ratio	0.286
Unit Weight of Drill Pipe	15.5 lb/ft
Length	510 ft

The mud weight is taken as 10 ppg which gives Buoyancy ratio as $k_B = 0.84733$. Figure 7-1 shows the BHA within which the bit is taken quite small (both diameter and length is 0.001").

Corresponding boundary conditions are:

- 1- At the top : Laterally Free Contact
- 2- At the bit : Laterally Free Contact

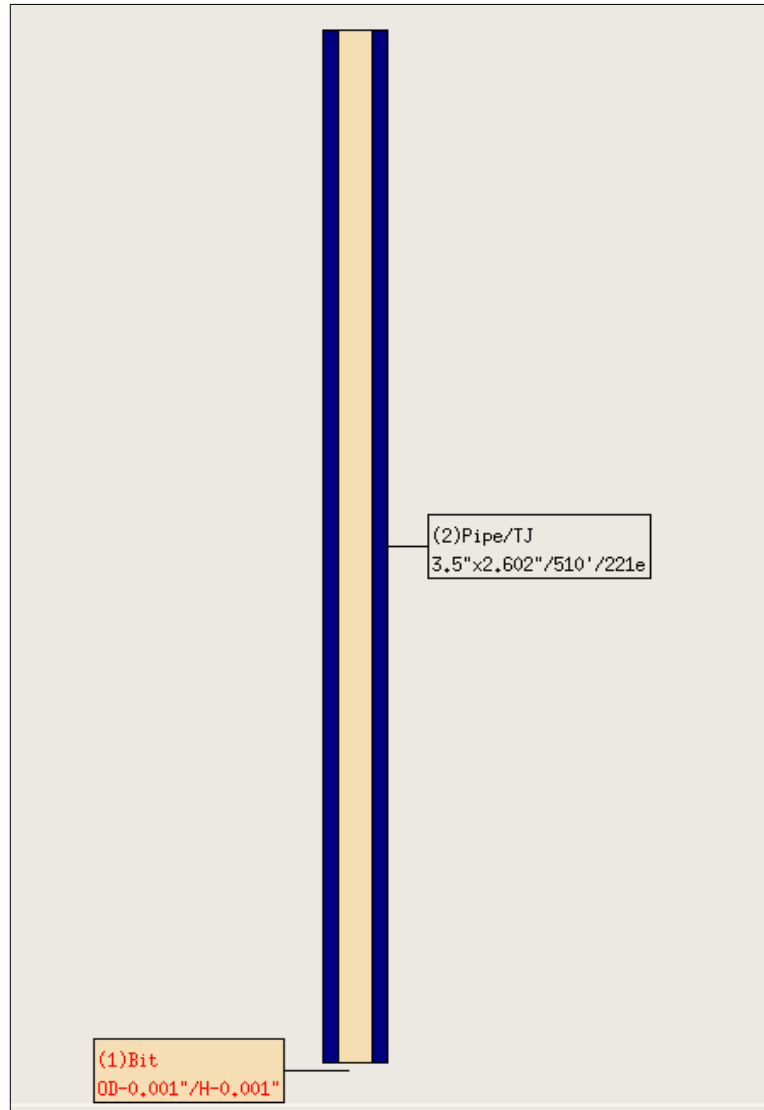


Figure 7-1 BHA of IDEAS™ Simulation for Sinusoidal Buckling in Deviated Wells

7.1.1. Case-1: An Inclined Well with $\theta=30^0$

Based on the above modeling parameters, critical buckling force when $\theta = 30^0$ is calculated by Eq. 7.1:

$$F_{cri_sin}^{dev} = 11.894 \text{ klb} \tag{7.4}$$

In order to trigger buckling when drill string is in equilibrium under compression, a small torque is applied at bit as a small perturbation to achieve this goal. However, the torque can't be too large otherwise it is not clear how much this torque contributes to buckling behaviors. Figure 7-2 shows the initial status of the drill string. It is lying on the lower side of the well bore.

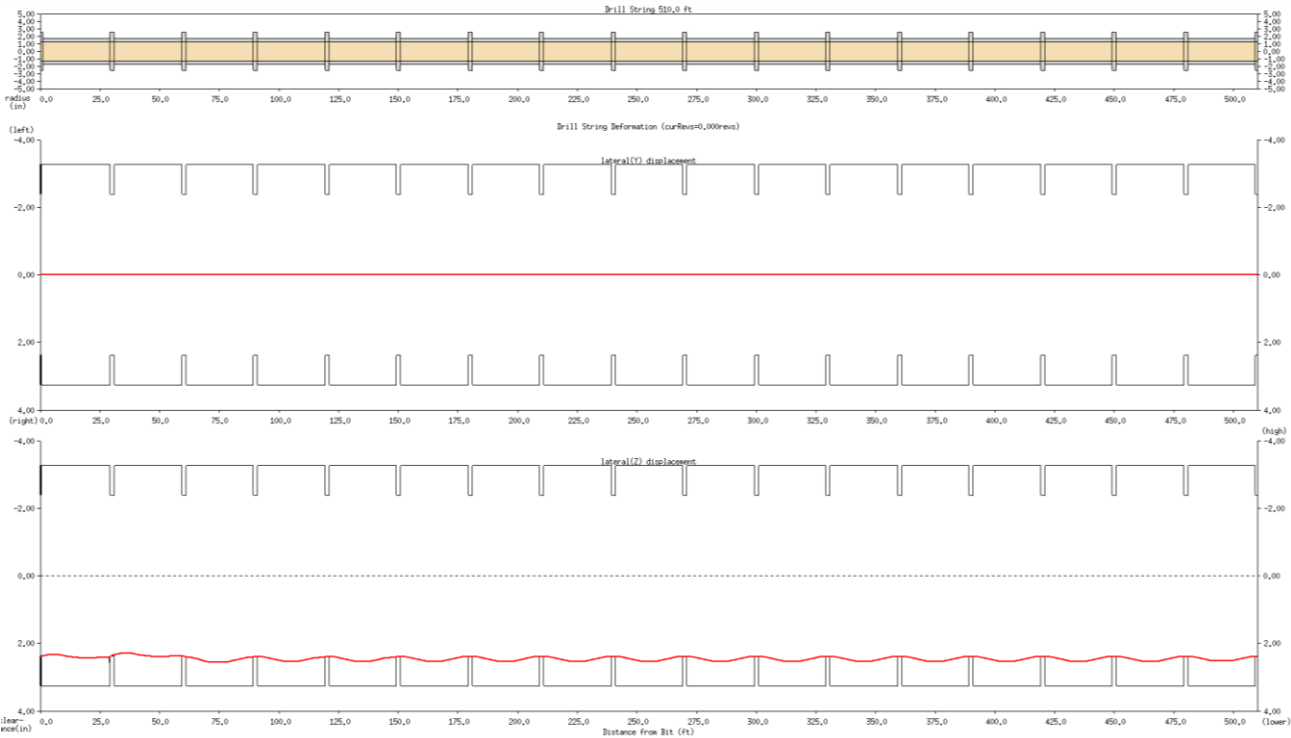


Figure 7-2 Initial Status of Drill String Lying on Lower Side of Wellbore

Figure 7-3 and Figure 7-4 correspond to a 10 *klb* WOB on drill string. It is clear that no buckling occurs. One thing has been mentioned above is that the deflection along z-direction comes from the self-weight of the drill pipe. Buckling occurs when drill string deflects along y-direction, which can be seen in Figure 7-5 later.

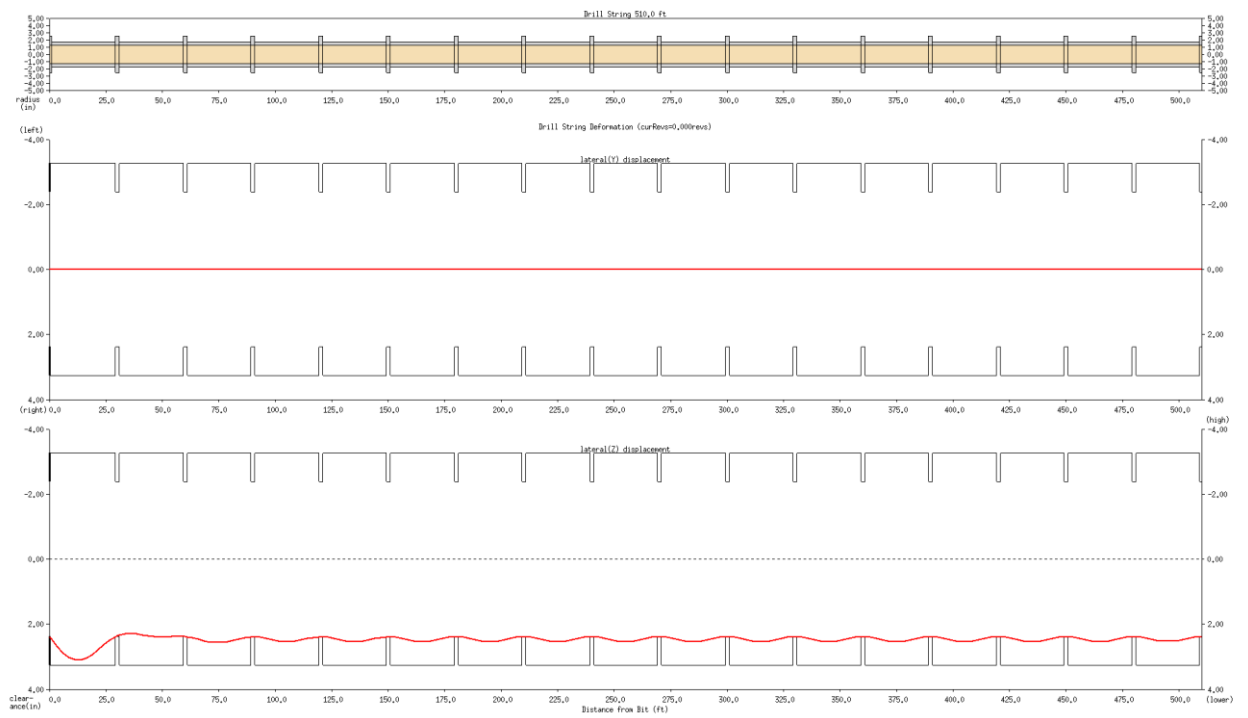


Figure 7-3 2-D View of Deflection along y- and z-Direction under 10 *klb* WOB

In Figure 7-4, 2-D view of the BHA can be seen under 10 *klb* WOB. It is clearly seen that there is no buckling occurred at this level of WOB.

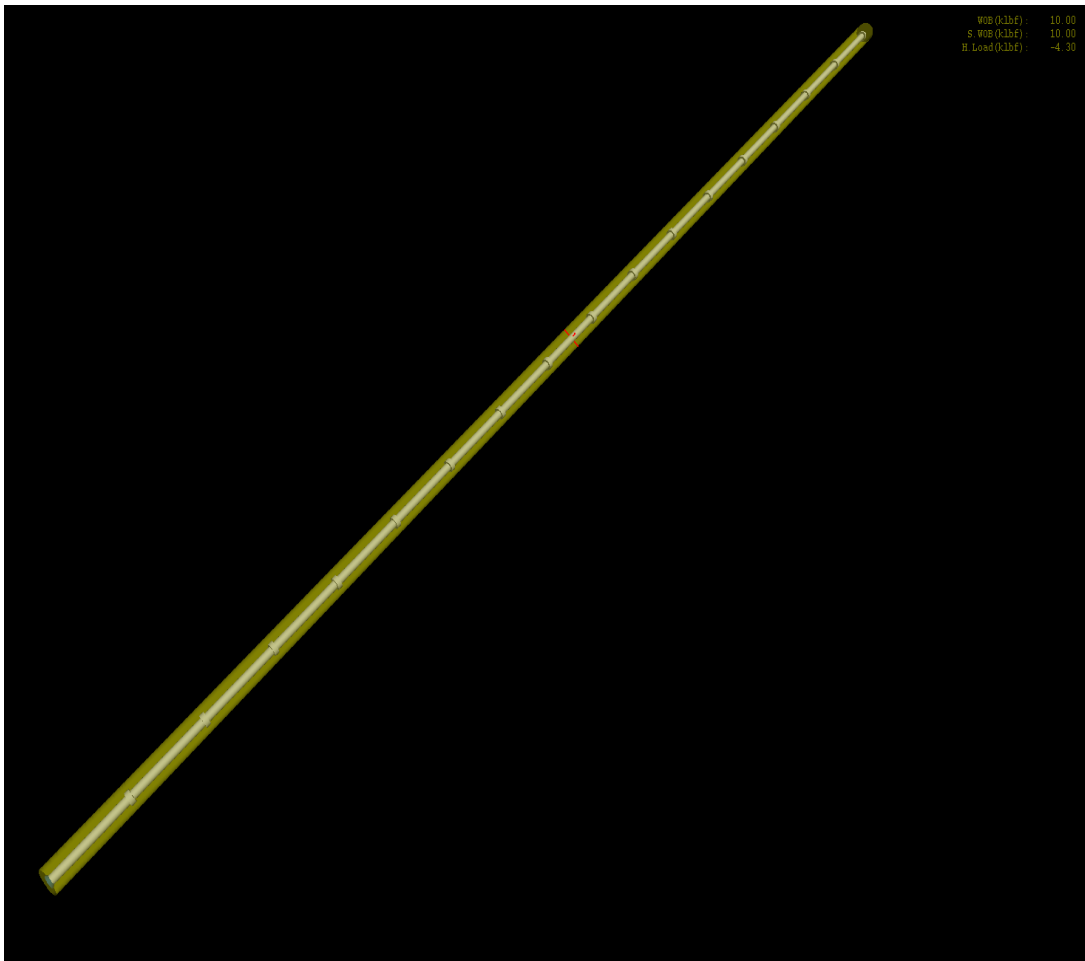


Figure 7-4 3-D View of Drill String under 10 *klb* WOB

When WOB is increased to 11.5 *klb* WOB, no buckling is observed. The figures of drill string when WOB 11.5 *klb* are not shown here since the figures are similar as when WOB is 10 *klb*. Therefore, WOB is increased to 12 *klb* and buckling is observed as shown in the Figure 7-5 and Figure 7-6. Therefore, IDEAS™ predicts the critical buckling force as 12 *klb*. The error with the analytical solution is 0.9%. Since the axial compressive load is not a constant, the maximum value occurs near the bit. As a result, the pipes away from the bit do not show buckling due to smaller axial compressive load.

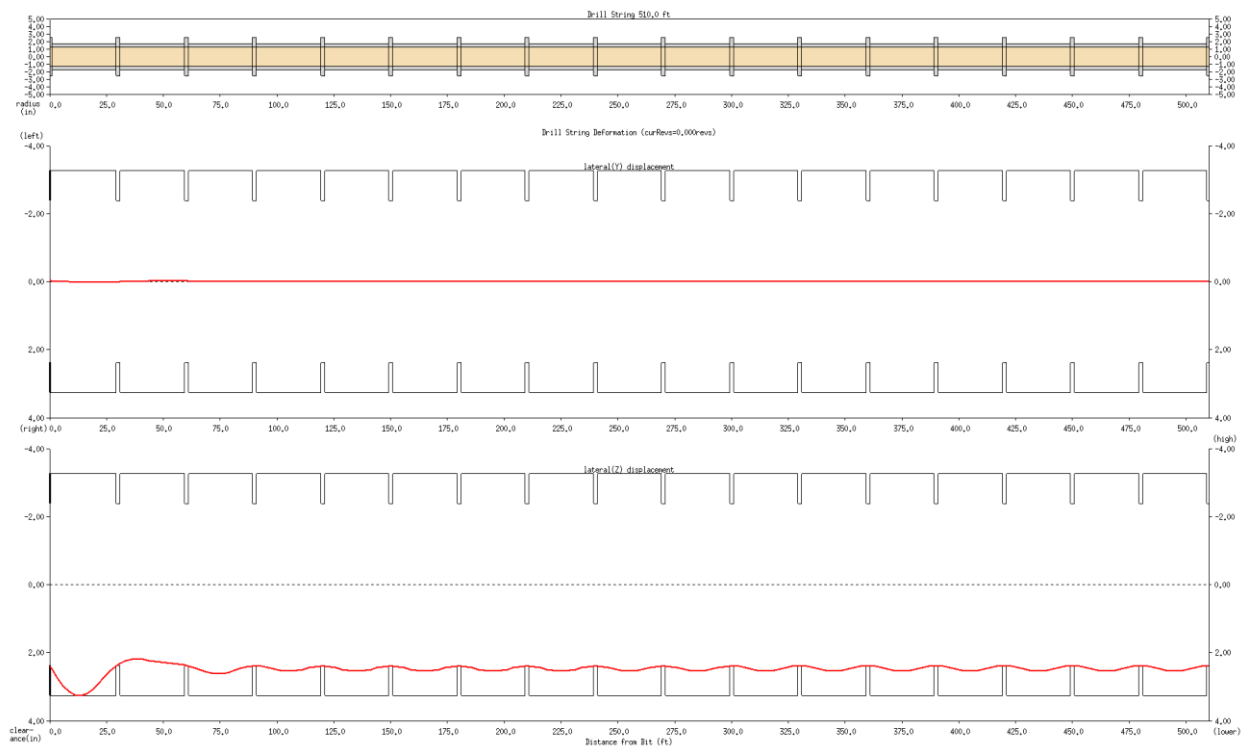


Figure 7-5 2-D View of Deflection along y- and z-Direction under 12 *klb* WOB

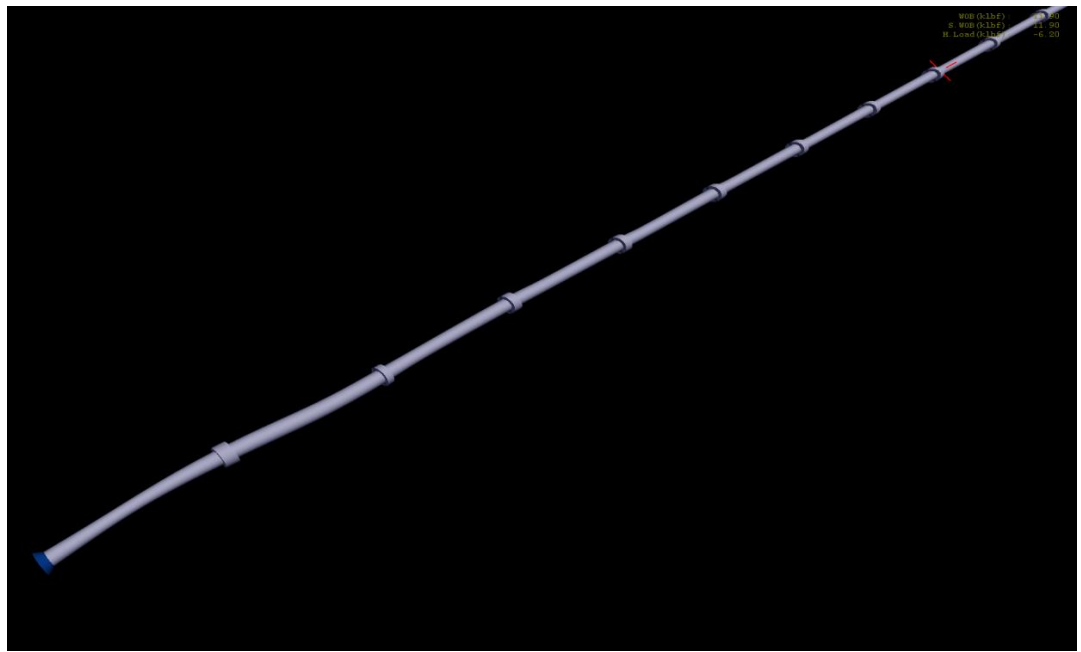


Figure 7-6 3-D View of Drill String under 12 *klb* WOB

Figure 7-7 shows the axial compressive load is almost linear instead of being a constant. Only the value near the bit is close to the critical load which leads to occurrence of sinusoidal buckling locally.

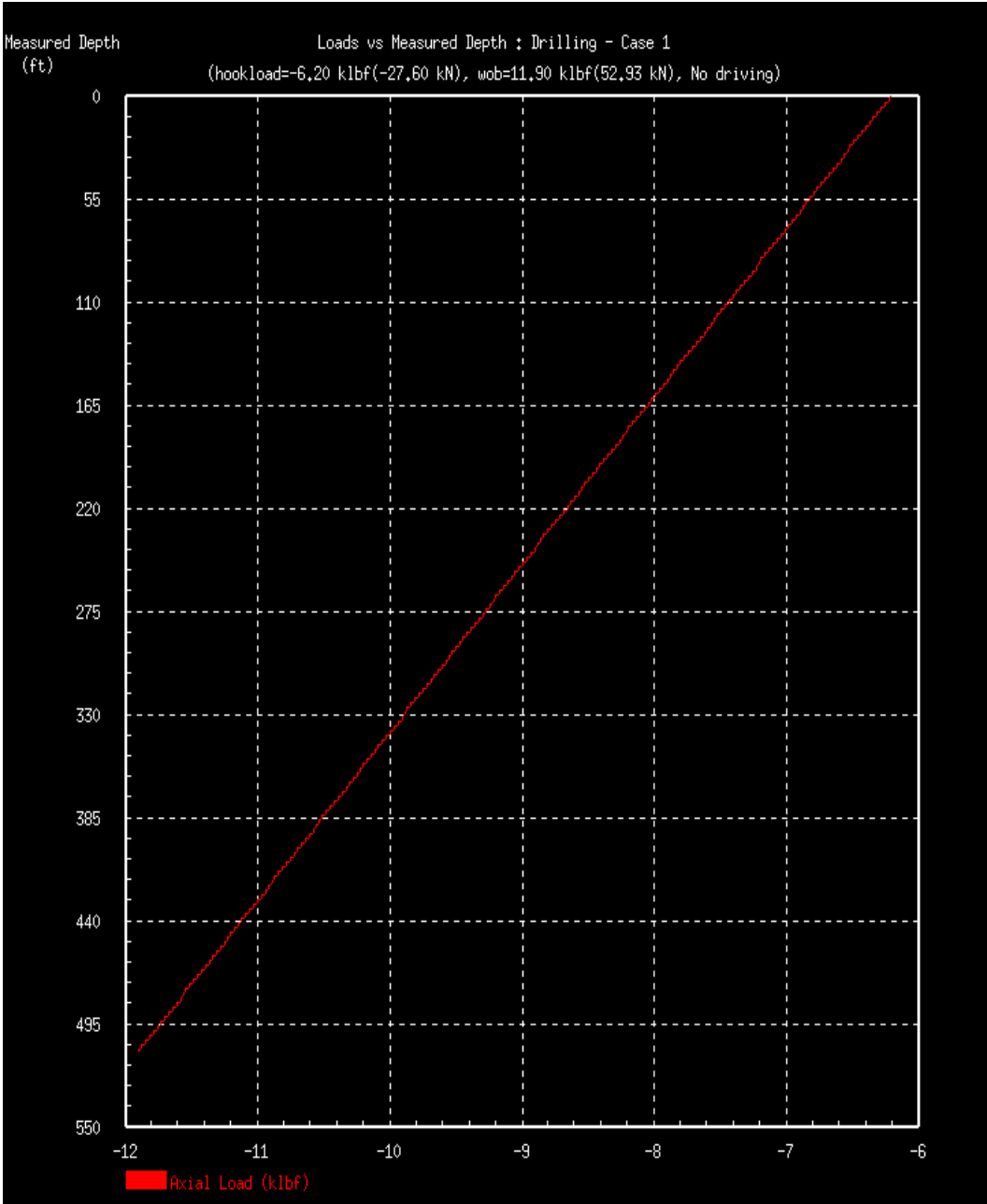


Figure 7-7 Axial compressive load under 12 klb WOB

7.1.2. Case-2: An Inclined Well with $\theta=90^0$

In this case, a horizontal well is being investigated. A horizontal well incurs some new points as compared to an inclined well (for example, a $\theta = 30^0$ well) because the former has an essentially constant axial load while the latter does not. This difference matters since it will generate different pictures of developing buckling. Based on the above parameters, critical buckling force when $\theta = 90^0$ is calculated by Eq. 7.1:

$$F_{cri_sin}^{dev} = 16.8 \text{ klb} \quad 7.5$$

As in the previous inclined well, we applied a torque at bit to trigger buckling as well. For this horizontal well, we applied a torque with a quite small amount of $0.1 \text{ lb} - \text{ft}$. Figure 7-8 and Figure 7-9 correspond to a 16 klb WOB. It is clear that no buckling occurs.

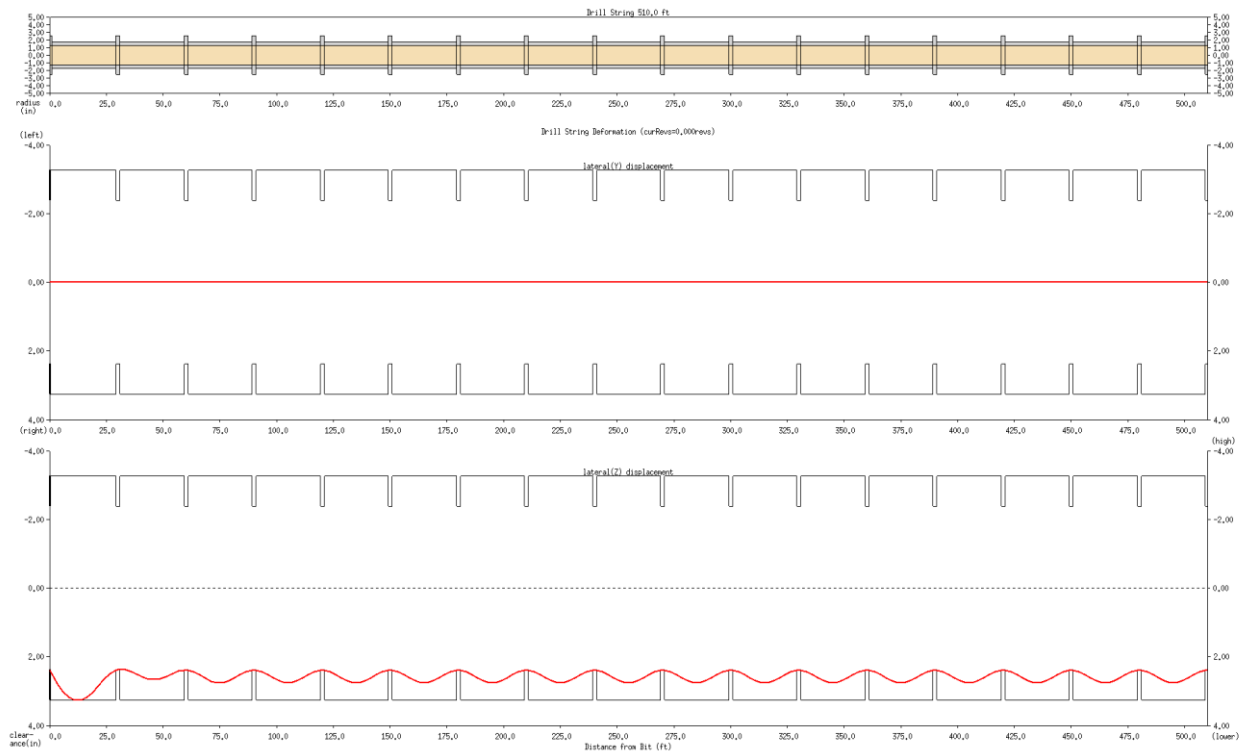


Figure 7-8 2-D View of Deflection along y- and z-Direction under 16 klb WOB



Figure 7-9 3-D View of Drill String under 16 *klb* WOB

When WOB is increased to 17.4 *klb* WOB, no buckling is observed. The figures of drill string when WOB is 17.4 *klb* are not shown here since the figures are similar as when WOB is 16 *klb*. Therefore, WOB is increased to 17.5 *klb* and buckling is observed as shown in the Figure 7-10 and Figure 7-11. Therefore, IDEAS™ predicts the critical buckling force as 17.5 *klb*. The error with the analytical solution is 4 %.

For this case, suddenly, more than one buckle was created. Buckling phenomena behaved different than when $\theta = 30^0$ case.

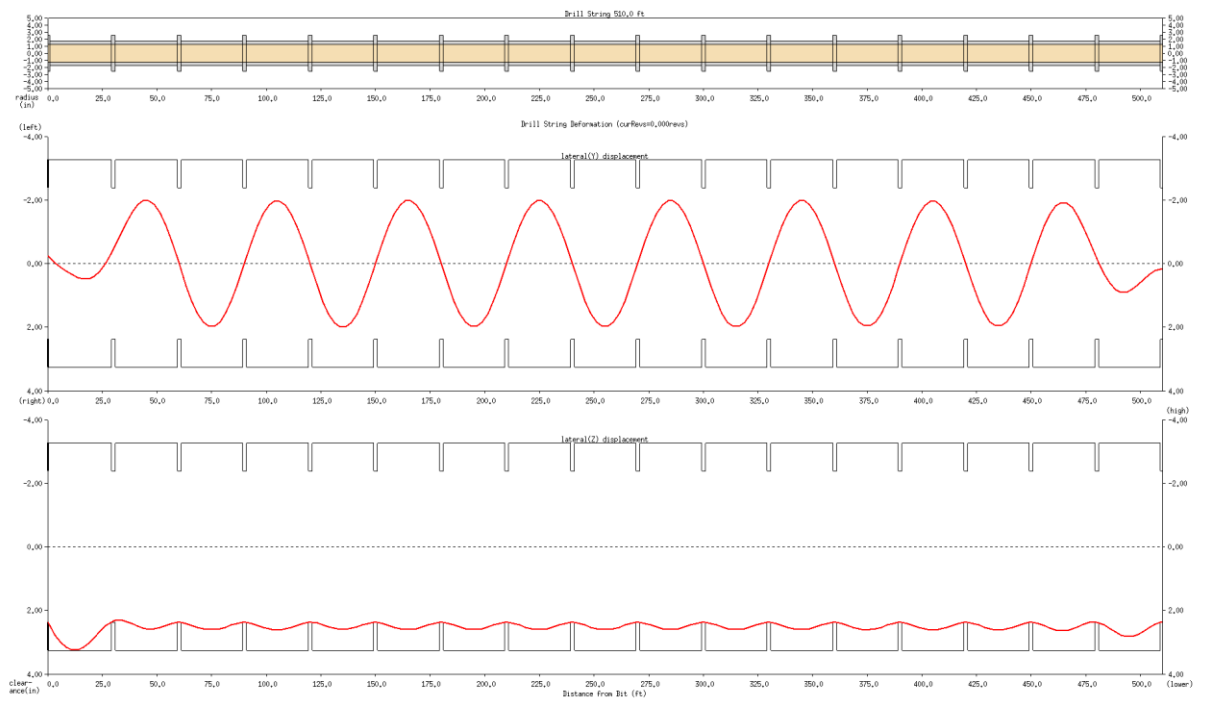


Figure 7-10 2-D View of Deflection along y- and z-Direction under 17.5 *klb* WOB



Figure 7-11 3-D View of Drill String under 17.5 *klb* WOB

7.2. Helical Buckling Validation for Deviated and Horizontal Wells

With increasing compressive load applied, sinusoidal buckling shifts to helical buckling. For a complete helix under axial compressive load F , ($F > F_{cri_hel}^{dev}$), its pitch is obtained by Lubinski et al. [16]

$$p = \pi \sqrt{\frac{8EI}{F}} \quad 7.6$$

Critical helical buckling force for deviated wells is calculated by Lubinski as [7]:

$$F_{cri_hel_Lub}^{dev} = 2.828 \sqrt{\frac{EIw \sin \theta}{r}} \quad 7.7$$

However; J. Wu et al. [18] showed that the so-called helical buckling load that appears in the current literature is only the average axial load in the helical buckling development process. Instead of Eq. 7-7, they obtained a new helical buckling critical load:

$$F_{cri_hel_Wu}^{dev} = 3.657 \sqrt{\frac{EIw \sin \theta}{r}} \quad 7.8$$

J. Wu et al. performed theoretical and experimental investigations to obtain Eq. 7.8. The essential idea in their research is that the assumption that the axial load is constant during the helical buckling process is inconsistent with the real helical buckling process due to the changing of axial load. From a sense of work average, they proved that equation of Lubinski, Eq. 7.7, is actually equal to the average load which is:

$$F_{cri_hel}^{dev} = \frac{1}{\delta} \int_0^{\delta} F dx \quad 7.9$$

Generally speaking, the load is changing during the helical buckling process. As a result, the actual helical buckling load is not given by Eq. 7.6. Based on their experiments, J. Wu et al. [18] explained that the changing axial load profile is almost a linear curve so that they introduced a linear approximation of the axial load changing profile. Therefore, Eq. 7.8 will be used as an analytical solution to calculate for critical helical buckling force for deviated wells.

Same simulation model that was used for sinusoidal buckling verification for deviated and horizontal wells will be used. That is, a 10" frictionless wellbore with $\theta = 30^\circ$ and $\theta = 90^\circ$ is considered. The parameters for drill string were given in Table 7-1 above.

7.2.1. Case-1: An Inclined Well with $\theta=30^\circ$

Using above modeling parameters, pitch length is calculated by Eq. 7.6 and critical buckling force when $\theta = 30^\circ$ is calculated by Eq. 7.8:

$$p = 58.02 \text{ ft} \quad 7.10$$

$$F_{cri_hel_Lub}^{dev} = 16.8 \text{ klb} \quad 7.11$$

$$F_{cri_hel_Wu}^{dev} = 21.747 \text{ klb} \quad 7.12$$

In order to trigger buckling when drill string is in equilibrium under compression, a small torque is applied at bit as a small perturbation to achieve this goal. However, the torque can't be too large otherwise it is not clear how much this torque contributes to buckling behaviors. Meanwhile, for sinusoidal buckling and helical buckling, the amounts of corresponding triggering torques should be different since bit torque has different effects on these two types of buckling behaviors. Based on IDEASTM simulations, it is concluded that a much smaller torque is needed to trigger helical buckling. As a result, during the developing process of sinusoidal buckling, the triggering torque applied at bit is $300 \text{ lb} - \text{ft}$, while the counterpart for helical buckling is only $2 \text{ lb} - \text{ft}$.

In fact, it is straightforward to see that a torque has a “positive” effect on helical buckling because it causes the pipe to undergo spiral movement within the well. As a result, triggering torque for helical buckling should be quite small to avoid pseudo helical buckling behavior caused by torque itself since we just want the axial compressive load to cause buckling.

The buckling is developing from sinusoidal to helical when axial load is increasing. When buckled pipe is rising up to touch the upper side of the wellbore, the helical buckling starts. According to Eq. 7.7, helical buckling should arise when the axial compressive load reaches around 16.8 *klb*. However, Figure 7-12 and Figure 7-13, corresponding to WOB, 17 *klb*, have not shown any helical buckling. The buckling is higher order of sinusoidal buckling, not helical buckling. This gave us the idea that Eq. 7.8 should be used instead of Eq. 7.7. That is, Eqn. 7.7 underestimates the critical helical buckling load for deviated wells. Therefore, to compare simulation results, Eqn. 7.8 will be used.

Similar observation, as shown in Figure 7-14 and Figure 7-15, is made when WOB reaches 20 *klb*. The buckling is higher order of sinusoidal buckling, not helical buckling. When WOB is increased gradually to 20.8 *klb*, helical buckling is observed in Figure 7-14 and Figure 7-15. Therefore, IDEAS™ calculated critical helical buckling for deviated wells as 20.8 *klb*. The error compared to analytical solution is 4.35 %. When load keeps increasing, helical buckling is also developing in higher orders. Figure 7-18 and Figure 7-19 show more helical buckling is appearing when load is 24 *klb*.

The last point for this $\theta = 30^0$ well is to check against Eq. 7.6. This was done by referring to a 28 *klb* WOB. Eq. 6.6 gave 58.02 *ft* while IDEAS™ predicted quite close result as about 60 *ft* for a 28 *klb* load. These are shown in Figure 7-20 and 7-21.

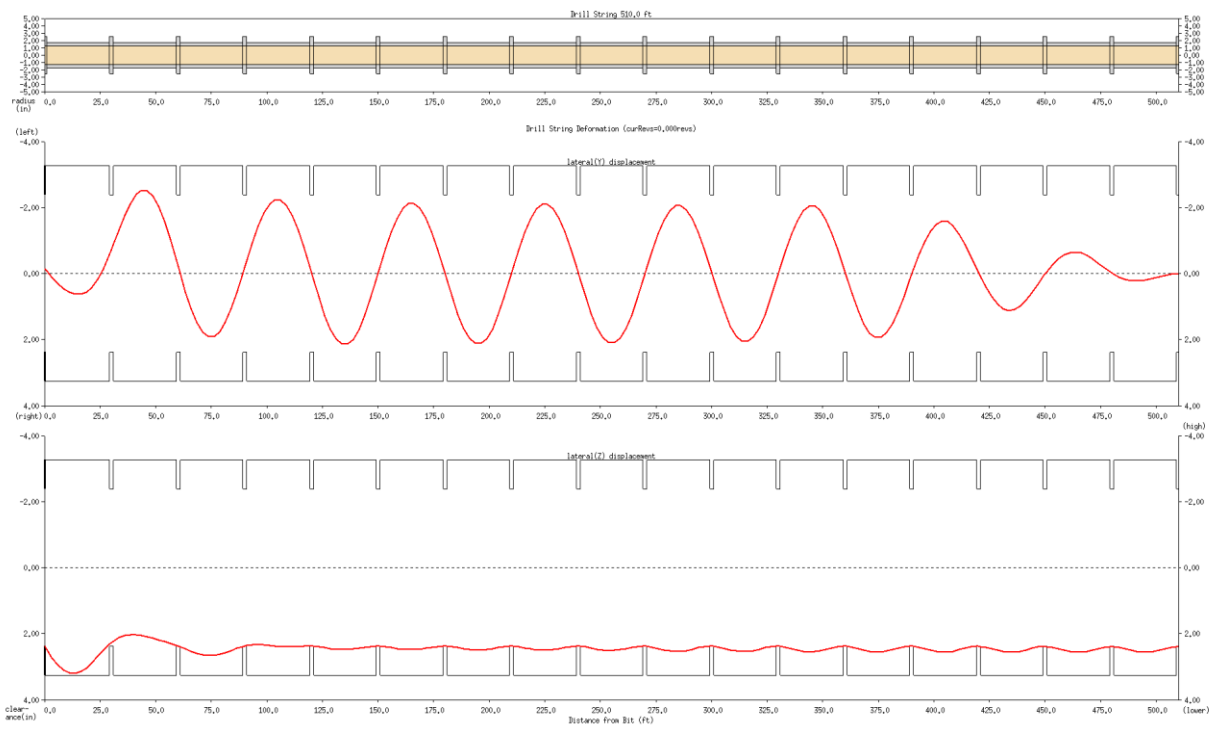


Figure 7-12 2-D View of Deflection along y- and z-Direction under 17klb WOB



Figure 7-13 3-D View of Drill String under 17 klb WOB

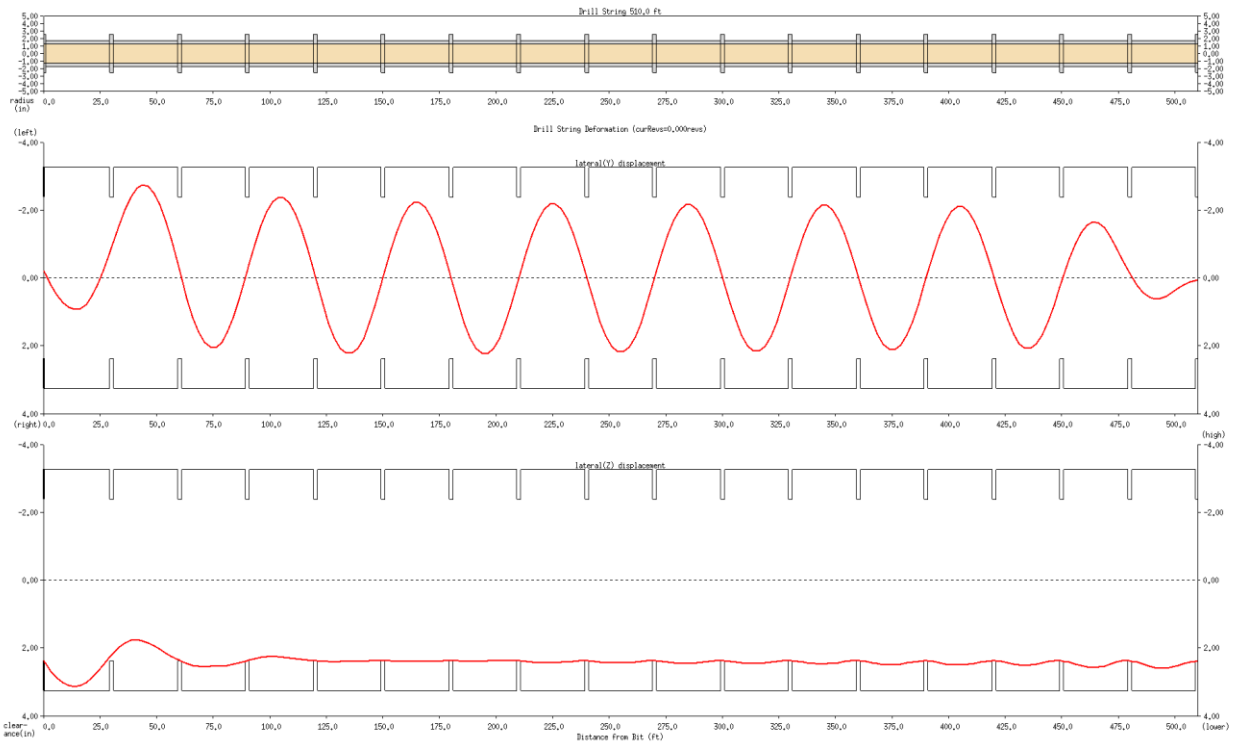


Figure 7-14 2-D View of Deflection along y- and z-Direction under 20klb WOB



Figure 7-15 3-D View of Drill String under 20 klb WOB

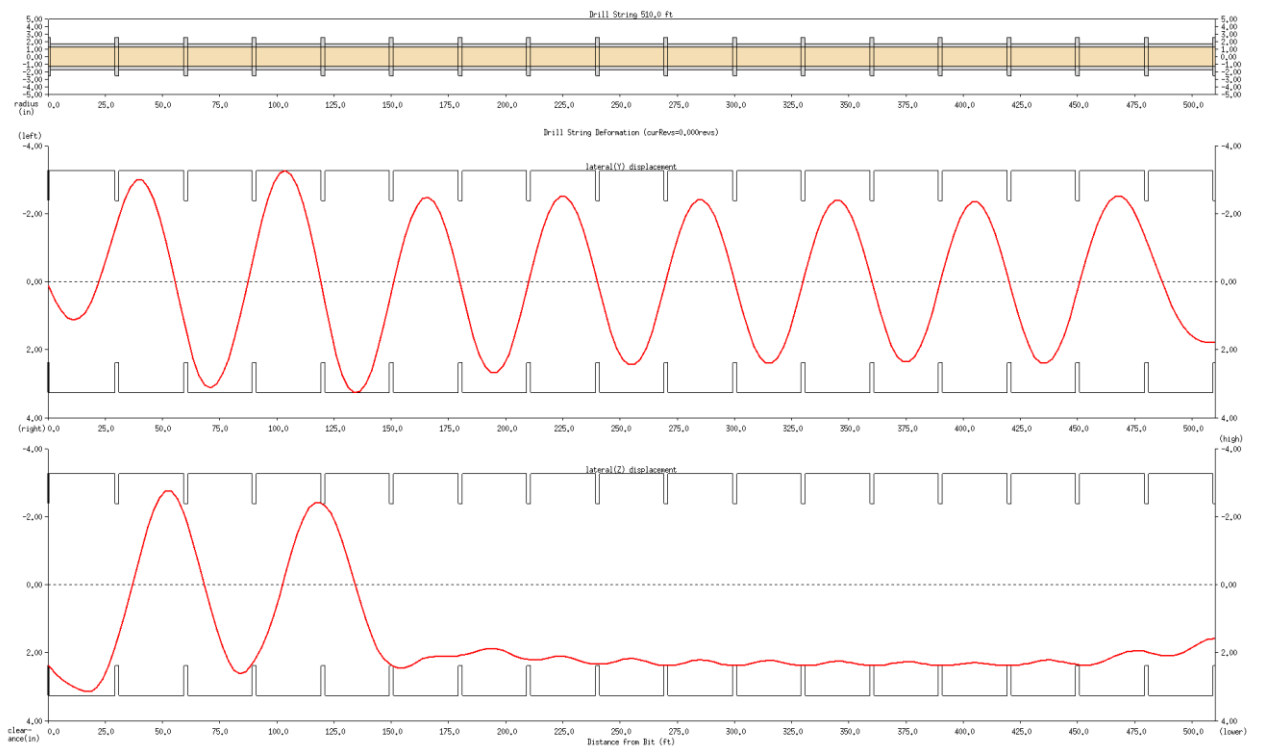


Figure 7-16 2-D View of Deflection along y- and z-Direction under 20.8klb WOB

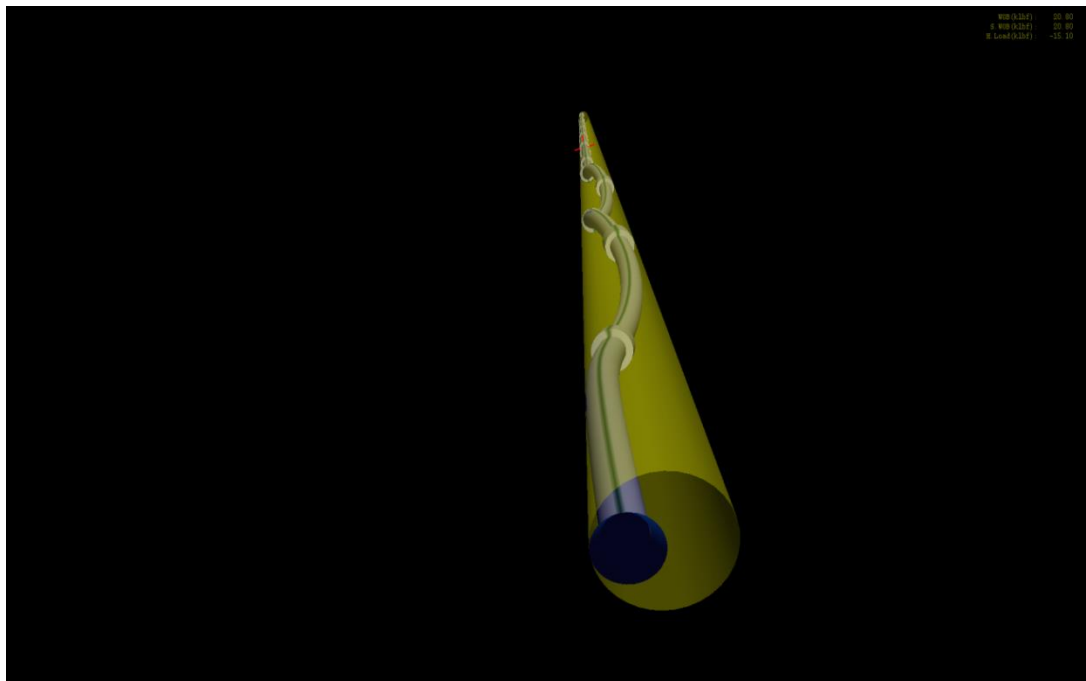


Figure 7-17 3-D View of Drill String under 20.8 klb WOB

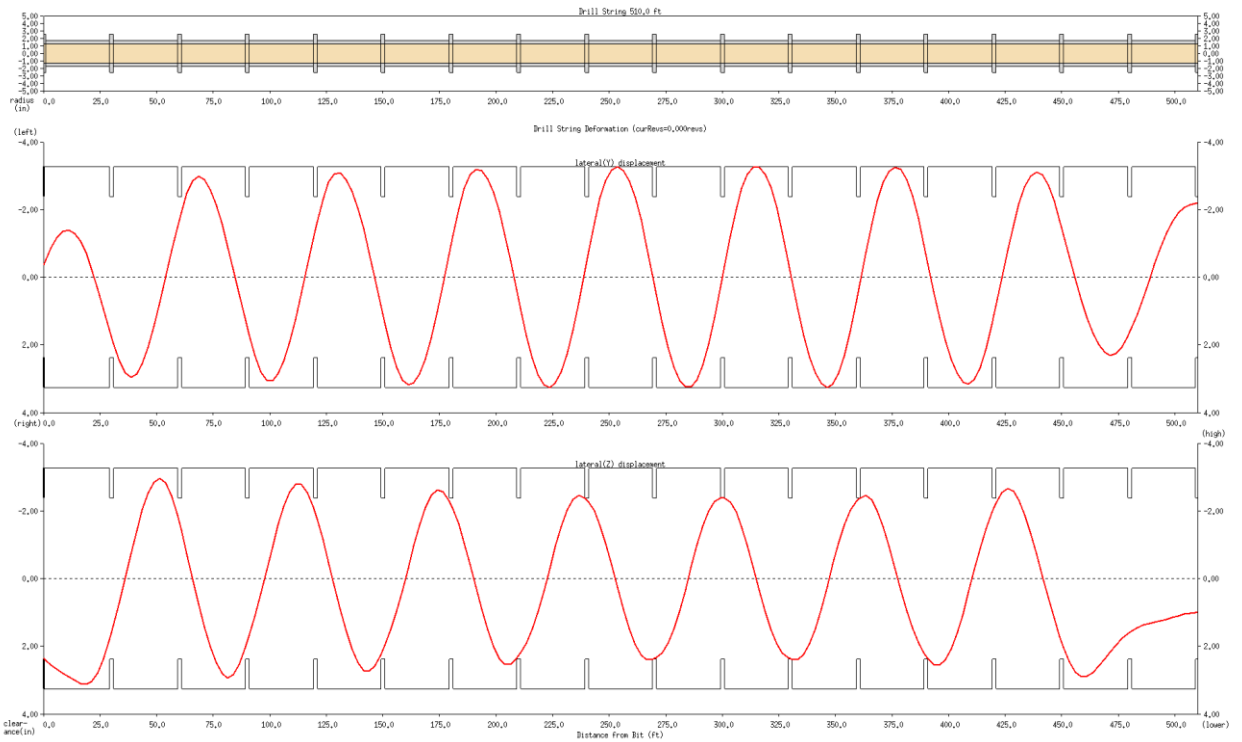


Figure 7-18 2-D View of Deflection along y- and z-Direction under 24 *klb* WOB

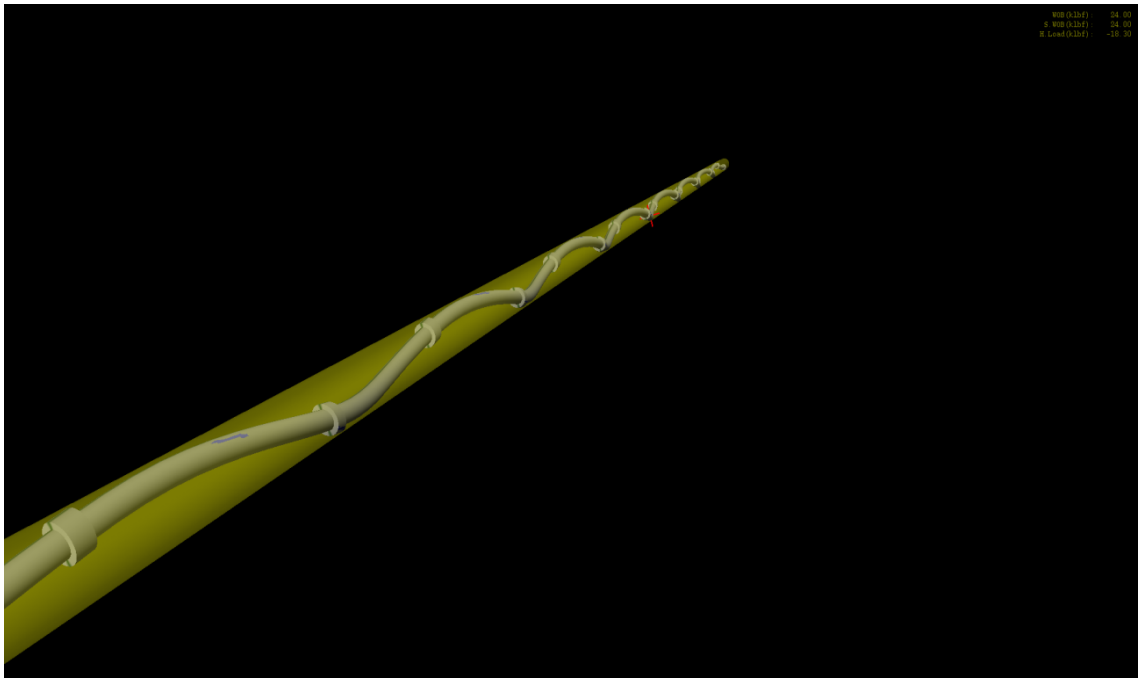


Figure 7-19 3-D View of Drill String under 24 *klb* WOB

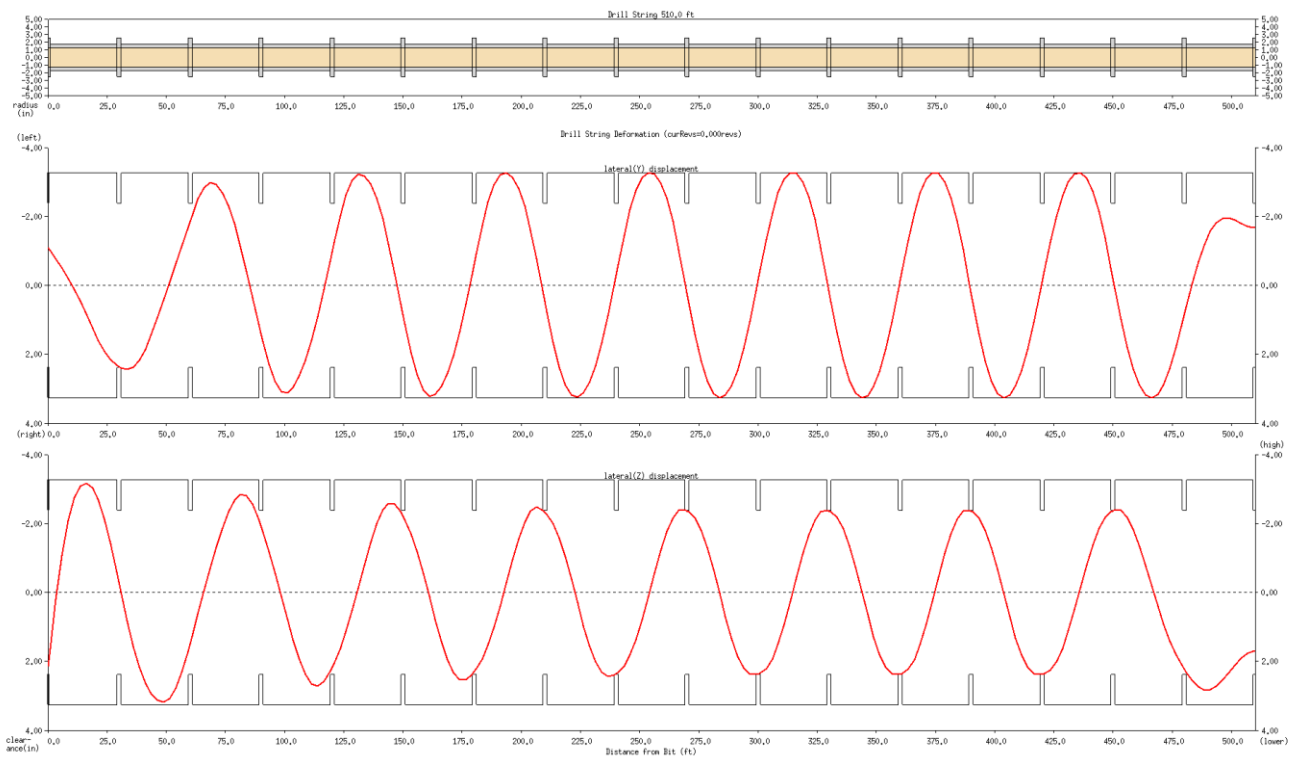


Figure 7-20 2-D View of Deflection along y- and z-Direction under 28 *klb* WOB

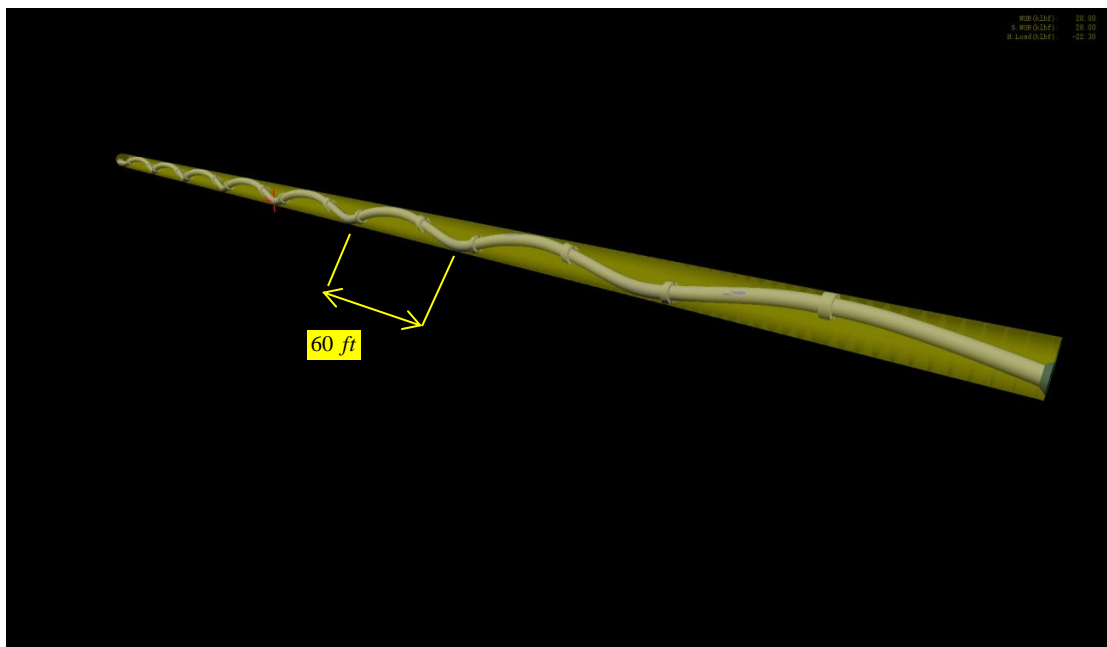


Figure 7-21 3-D View of Drill String under 28 *klb* WOB

7.2.2. Case-2: An Inclined Well with $\theta=90^0$

Using the above modeling parameters, pitch length is calculated by Eq. 7.6 and critical buckling force when $\theta = 90^0$ is calculated by Eq. 7.8:

$$p = 37.45 \text{ ft} \quad 7.13$$

$$F_{cri_hel_Lub}^{dev} = 23.78 \text{ klb} \quad 7.14$$

$$F_{cri_hel_Wu}^{dev} = 30.75 \text{ klb} \quad 7.15$$

As in the previous case, we applied a torque at bit to trigger buckling as well. For this horizontal well, we applied a torque amount of $0.1 \text{ lb} - \text{ft}$. Torque should be applied very small since torque has a positive effect on initiation of buckling in horizontal wells. As stated, sinusoidal buckling force for horizontal case is found as 17.5 klb . Seeing helical buckling for horizontal case, WOB increased gradually. When WOB is increased to 24 klb , higher order of sinusoidal buckling is observed as shown in Figure 7-22 and Figure 7-23. The difference between higher order of buckling and helical buckling is in deformation in z-direction. When higher order of sinusoidal buckling occurs, y-direction deformation is like a helix, but in z-direction deformation, it seems like a straight line. For helical buckling, both direction deformations shapes looks like a helix. When WOB is increased to 28.3 klb , still higher order of sinusoidal buckling is observed as shown in Figure 7-24 and Figure 7-25. The deformation in z-direction starts to deviate from straight line to helical shape. For this horizontal well, Eq. 7.14 predicts a critical helical load 23.78 klb which has been shown insufficient to incur helical buckling in Figure 7-22 and Figure 7-23. Figure 7-26 and Figure 7-27 show the occurrence of helical buckling when WOB reaches 28.4 klb . Eq. 7.15 predicted 30.75 klb which is much closer to 28.4 klb than Eq. 7.7, which is 23.78 klb . This comparison agrees with what is observed for the case of the inclined well. As a result, Eq. 7.15 gives a more reliable critical load for helical buckling. Figure 7-28 shows the constant axial load corresponding to WOB 28.4 klb .

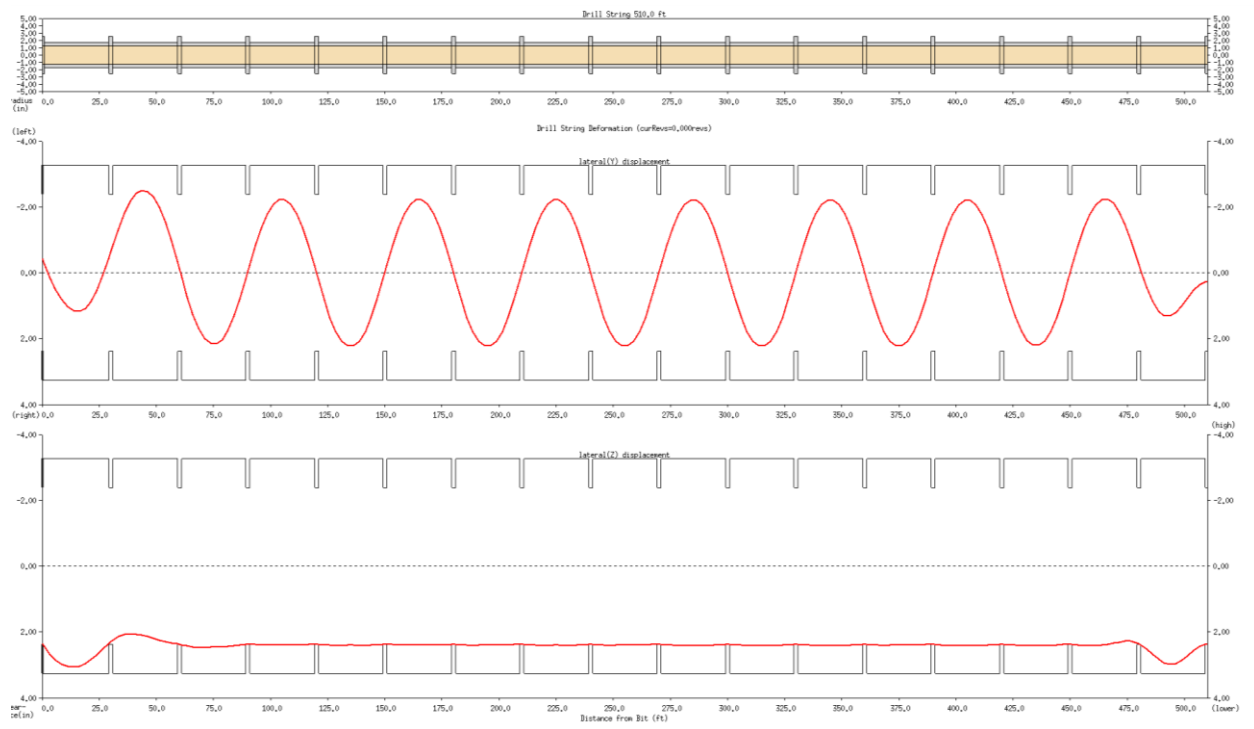


Figure 7-22 2-D View of Deflection along y- and z-Direction under 24 *klb* WOB

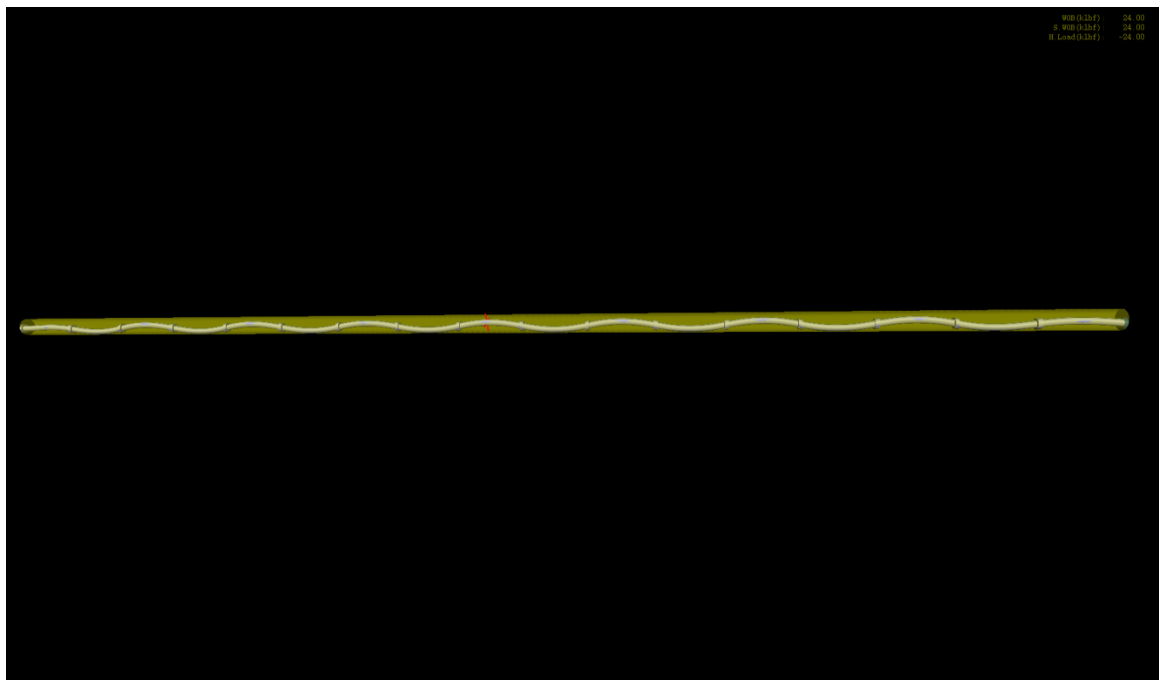


Figure 7-23 3-D View of Drill String under 24 *klb* WOB

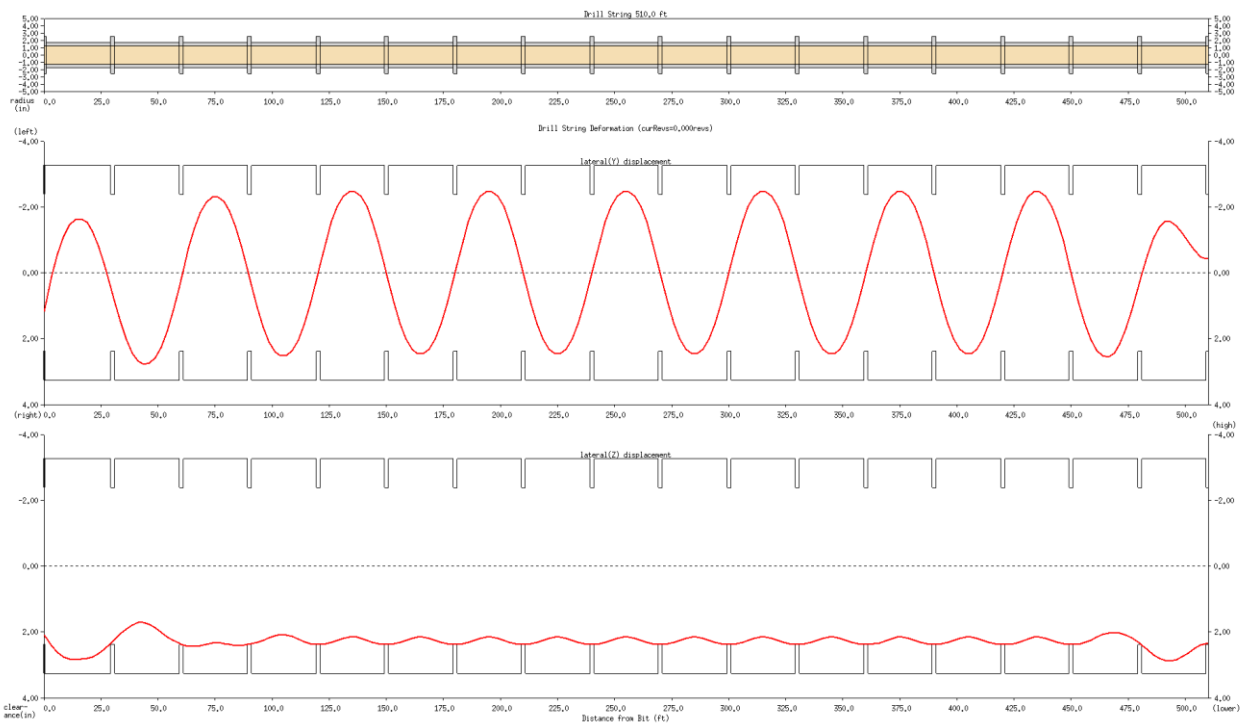


Figure 7-24 2-D View of Deflection along y and z Direction under 28.3 *klb* WOB

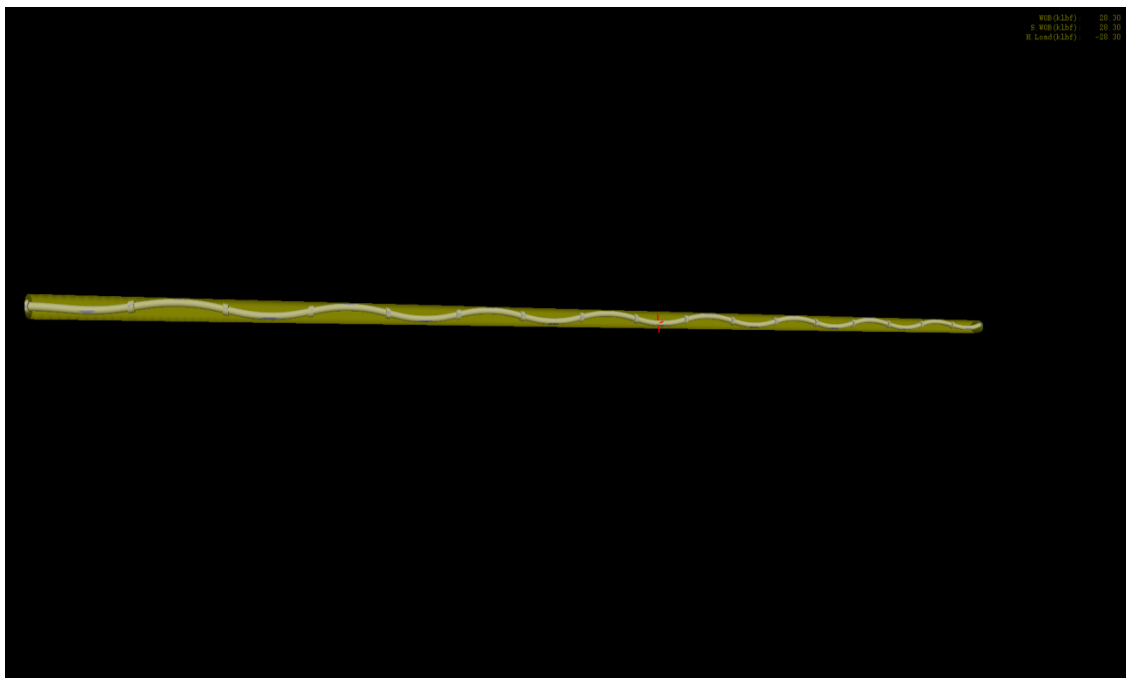


Figure 7-25 3-D View of Drill String under 28.3 *klb* WOB

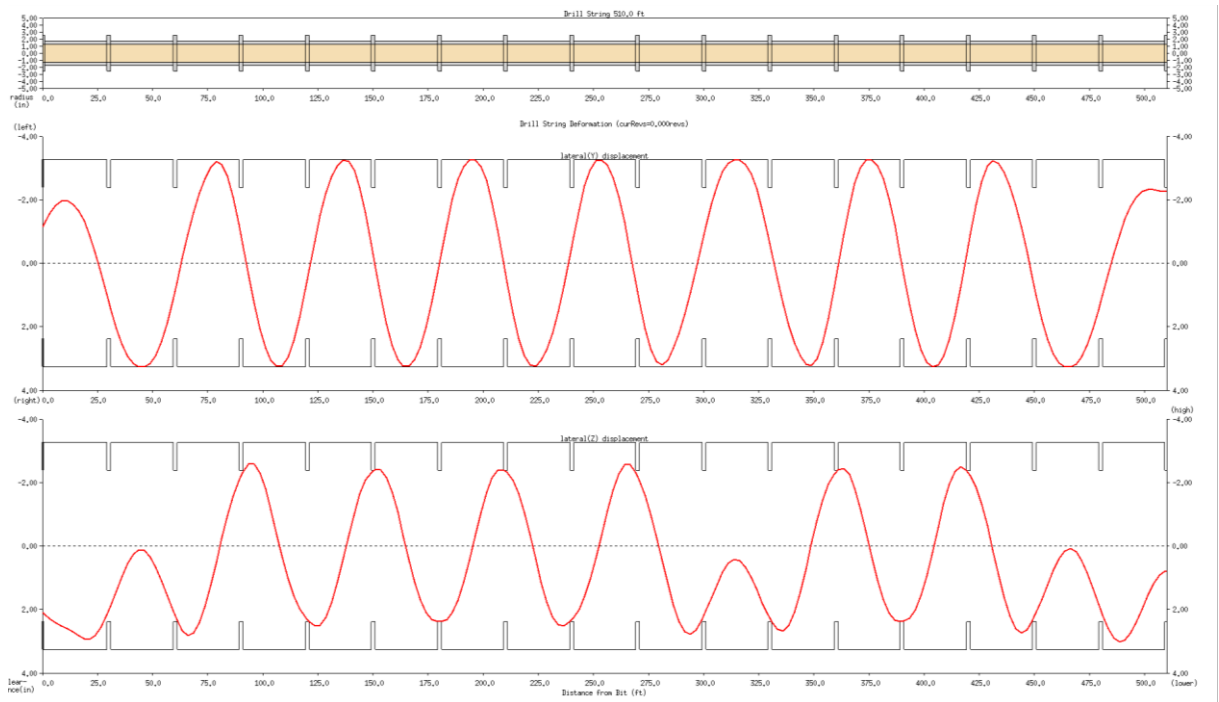


Figure 7-26 2-D View of Deflection along y and z Direction under 28.4 *klb* WOB

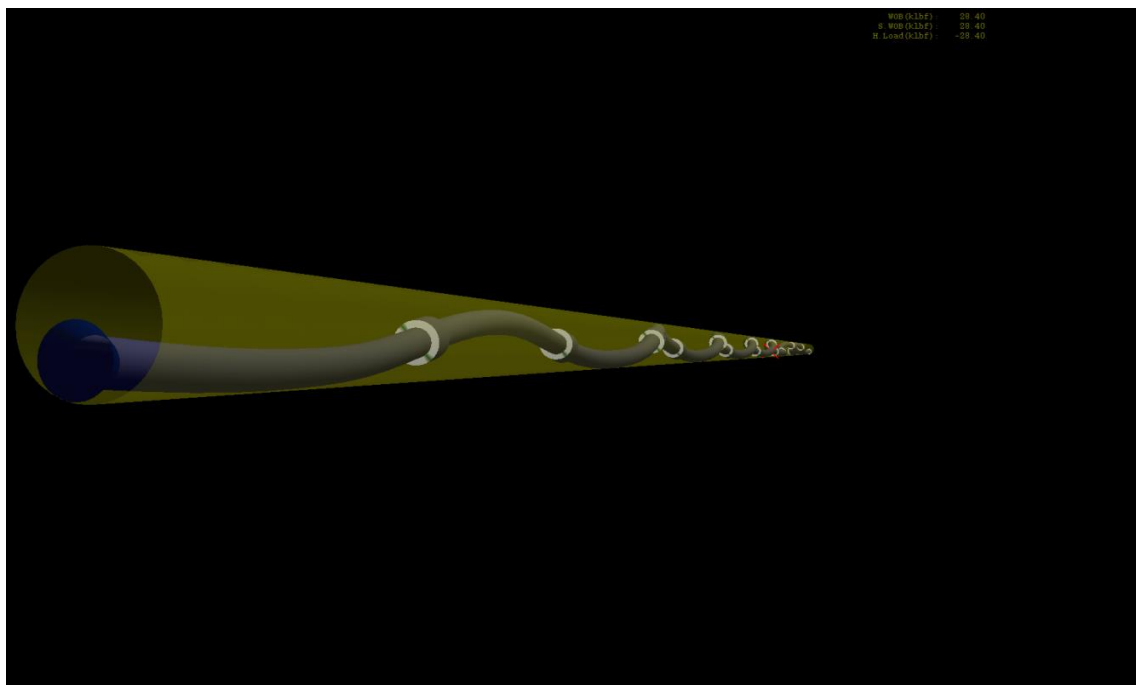


Figure 7-27 3-D View of Drill String under 28.4 *klb* WOB

WOB is increased to 60 *klb* to see full developed helical buckling to verify Eq.7.6. IDEAS™ predicted $p = 39 \text{ ft}$ while analytical solution gives 37.451 *ft* and error is 3.97 %. Pitch length predicted by IDEAS™ is shown in Figure 7-28 and Figure 7-29.

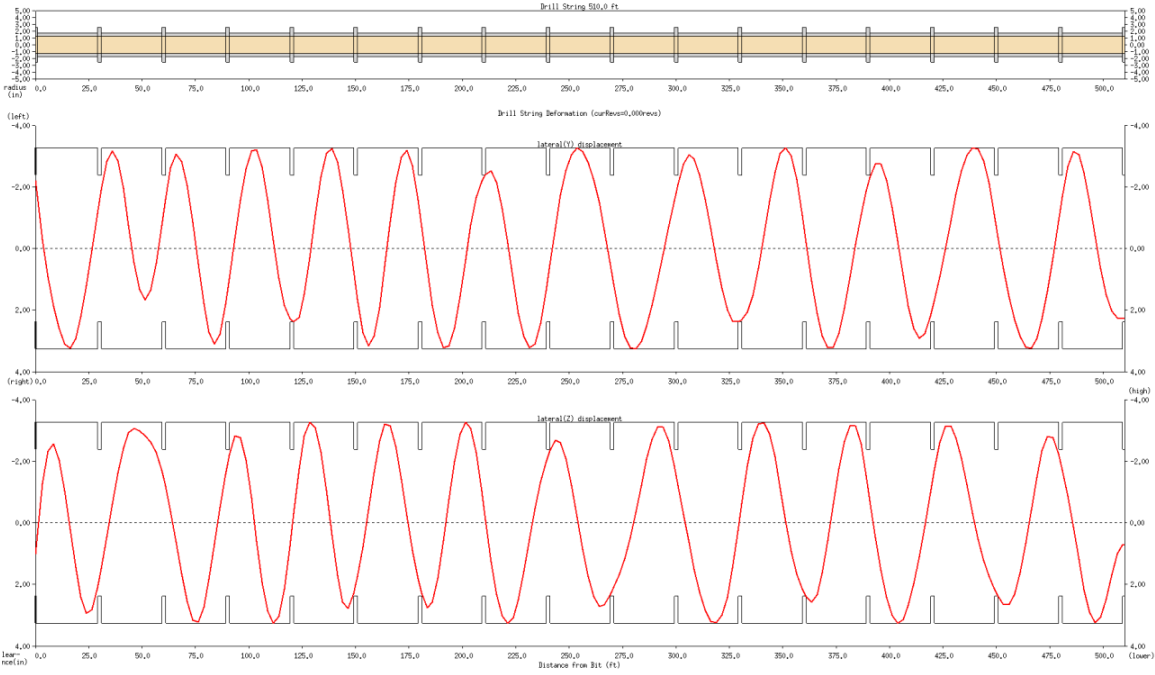


Figure 7-28 2-D View of Deflection along y- and z-Direction under 60 *klb* WOB

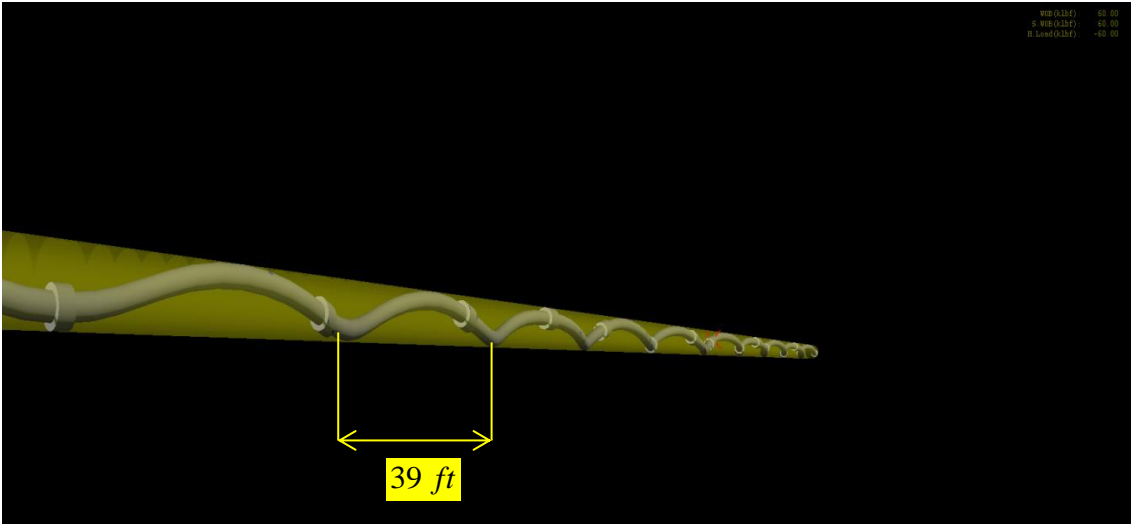


Figure 7-29 3-D View of Drill String under 28.4 *klb* WOB

In summary, after verifying the IDEAS™ simulation results with the analytical solutions for $\theta = 30^0$ deviated well and $\theta = 90^0$ horizontal well for both sinusoidal and helical buckling cases, the model is ready to use for vertical well analysis for sinusoidal buckling. Errors are less than 10% range which is quite acceptable for FEA cases. As stated before, deviated and horizontal well analysis is more complicated than vertical well analysis for buckling. And, model is verified by more complex cases, and it is ready to use for vertical case.

In the Table 7-2 and Table 7-3 below, verifications are summarized:

Table 7-2 Verification Summary for Sinusoidal Buckling Case

	Analytical Value	IDEAS™	Error
F_{cri} - Sinusoidal at 30^0 Deviated Well	11.894 klb.	12.0 klb.	0.9 %
F_{cri} - Sinusoidal at 90^0 Horizontal Well	16.800 klb.	17.5 klb.	4.0 %

Table 7-3 Verification Summary for Helical Buckling Case

	Analytical Value	IDEAS™	Error
F_{cri} - Helical at 30^0 Deviated Well	21.747 klb.	20.8 klb.	4.35 %
F_{cri} - Helical at 90^0 Horizontal Well	30.750 klb.	28.4 klb.	7.64 %
Pitch Length at 30^0 Deviated Well	58.02 ft.	60.0 ft.	3.30 %
Pitch Length at 90^0 Horizontal Well	37.45 ft.	39 ft.	3.97 %

CHAPTER 8

SIMULATION RESULTS

After verification of the FEM model in previous chapter, simulations for vertical cases can be run for five different drill collars. First of all, analytical solutions will be explained in this section to compare with simulation results. Then, technical details of the finite element used in this work will be explained. Finally, simulations results will be given.

8.1. Analytical Solutions

Lubinski [7] calculated critical buckling force in vertical wellbores for a length of 7.94 dimensionless units, which is equivalent to around 400 meter. Lubinski used power series to solve differential equation for the instability problem. Lubinski's method gives good results in the form of power series. Nevertheless, the power series terms get very large for long drill strings, and after a certain length, the results may be incorrect [8]. The equation found by Lubinski is given below:

$$F = 1.94(EI)^{1/3}w^{2/3} \quad 4.1$$

Wang [9] proposed analytical closed-form equation for critical buckling forces by using moment balance equations for infinite pipe length. He used Airy functions to find the smallest root for the stability of the infinite length strings. He also stated that the coefficient of Eqn. 4.1 is an unsatisfactory value because buckling of the long hanging string is quite different from the buckling of the stiffness-dominated short hanging strings [9]. The equation found by Wang is given below:

$$F = 1.018793(EI)^{1/3}w^{2/3} \quad 4.2$$

Wang proved that for practical purposes, one should use Eqn. 4.2 to guarantee stability since all possible alignments the buckling force under free lateral motion is the true minimum. However, using infinite length solution for real cases is unrealistic.

Wu [4] used energy method to solve the critical buckling force equation for vertical wells. He states that rather than using power series, using energy method is quite simpler and more accurate.

$$F = 2.55(EI)^{1/3}W^{2/3} \tag{4.3}$$

Analytical solutions of Eqn. 4.1, Eqn. 4.2, Eqn. 4.3 are given in Appendix-B in detail.

Lubinski calculated critical buckling forces for three different drill collars (with OD 7 in, 6.25 in, and 4.75 in) and two different drill pipes. To understand sensitivity of the length parameter in FEM solution for critical buckling force for vertical wells, additional two different drill collars (with OD 9 in and 8.25 in) are included in the analysis. The properties of drill collars and the solutions for critical buckling force by Eq. 4.1 and Eqn. 4.2 for these given drill collars are shown in Table 8-1 below.

This work is focused on buckling of drill collars; therefore, drill pipe buckling is out-of-scope. The reasons are:

- Drill pipe bodies and tool joints are manufactured to be durable in tension during drilling operation, therefore, it is not recommended to use drill pipes under compression. Even if drill pipes are used under compression, they start to buckle soon since their critical buckling force values are quite low. To illustrate, a drill string comprising 4.5 in. drill pipe only buckles at 1400 lb.; and at 3000 lb., it is already buckled twice [36].

- To eliminate lateral movement of the drill pipes because of centrifugal forces whilst the drill pipe is being rotated, in vertical or nearly vertical wellbores, maintaining the drill pipe under effective tension is vital [10].

Table 8-1 The Properties of Drill Collars and the Analytical Solutions for Critical Buckling Forces

TYPE	OD [in]	ID [in]	w [lb/ft]	I [in ⁴]	Eqn. 4. 1[lb]	Eqn. 4. 2[lb]	Eqn. 4. 3[lb]
I	4.75	1.75	52	24.53	4655	2395	6119
II	6.25	2.25	91	73.64	9753	5122	12820
III	7	3	107	113.88	12564	6598	16515
IV	8.25	2.813	161	224.32	20681	10861	27184
V	9.5	3	217	395.4	30493	16013	40081

8.2. Simulation Results

In the previous section, five different drill collar critical buckling forces are calculated by using analytical solutions. In this section, first of all, technical details of the finite element model will be given. Then, simulation results for these five different drill collars will be found.

8.2.1. Discretization of the Finite Element Model

In most engineering problems, the values of field variables such as displacement, stress, temperature, pressure, and velocity as a function of global coordinate system are needed. If the case is transient or unsteady-state problem, the variables has to be calculated as a function of not only spatial coordinates, but also time as well. The domain of the problem is mostly irregular shape. The first step of the finite element analysis is to discretize the irregular domains into smaller and regular sub-domains,

which is called finite elements [30]. The aim is to replace the original domain which has infinite number of degree of freedom to a finite number of degree of freedom.

There are different methods being used to model the domain of the problem with finite elements. Different ways of discretization of the main domain in sub-domains with finite elements require different amount of computational time and most of time may lead to different solution methods of the problem. The process of discretization is mainly an engineering judgement since selection of efficient discretization methods some experience and guidelines.

8.2.2. Type of the Elements

Most of the time, type of the element to used is easy to find from physical problem. For example, if a truss structure under given some external loads is to be analyzed, one dimensional beam or truss elements will be used for idealization, as shown in Figure 6-3. For the problems involving curved geometries and surfaces, three-dimensional finite element with curved size should be selected, as shown in Figure 6-3. This type of elements is called higher-order elements.

For this study, the drill string is modeled by using three-dimensional beam elements with rigid body motion, as shown in Figure 6-7, where mathematical modeling of this element explained in detail in Section 6.5.1. This type of element is the most suitable element to model the slender drill strings [26].

8.2.3. Size of the Elements

If the size of the element is small, the final solution is getting more accurate. On the other hand, it should be noted that the use of the smaller-sized elements will also cause more computational time. The more the computational time for each simulation spent, the more expensive the simulation is.

In this study, each element size is set as “1 inch” to increase the accuracy of the model in IDEASTM software. Therefore, in Table 8-2, total number of elements used for different lengths are shown.

Table 8-2 Number of Beam Elements Created for Different Lengths

Length of Drill String, ft.	Number of Beam Elements
1000	12000
2000	24000
3000	36000
4000	48000
5000	60000
6000	72000
7000	84000
8000	96000
9000	108000
10000	120000
11000	132000
12000	144000
13000	156000
14000	168000
15000	180000
16000	192000
17000	204000
18000	216000
19000	228000
20000	240000
25000	300000

Number of elements per each length is the same for different drill collars simulated. And, as the length of the drill string increases, simulation time is getting longer. The simulations are run with super computers in IDEAS™ in China which have more than 500 processors and have a capability to make 1 trillion processes in one second.

The simulation results for five different drill collar are given for five different drill collars as shown in Table 8-3 below:

Table 8-3 Simulation Results for Five Different Drill Collars with Different Depths

Depth, ft	Critical Buckling Force, klb				
	Type-I	Type-II	Type-III	Type-IV	Type-V
1000	6,89	14,28	18,27	29,84	43,62
2000	6,54	13,52	17,23	28,03	40,78
3000	6,41	13,16	16,75	27,19	39,47
4000	6,31	12,93	16,44	26,67	38,66
5000	6,24	12,77	16,23	26,3	38,08
6000	6,18	12,65	16,06	26,01	37,64
7000	6,14	12,55	15,93	25,78	37,29
8000	6,1	12,47	15,82	25,6	37
9000	6,07	12,4	15,73	25,44	36,76
10000	6,04	12,34	15,65	25,3	36,55
11000	6,019	12,29	15,58	25,18	36,36
12000	6	12,24	15,52	25,07	36,2
13000	5,98	12,2	15,46	24,98	36,05
14000	5,963	12,16	15,41	24,89	35,91
15000	5,948	12,13	15,36	24,81	35,79
16000	5,934	12,1	15,32	24,74	35,68
17000	5,921	12,07	15,28	24,67	35,58
18000	5,908	12,04	15,25	24,61	35,48
19000	5,897	12,02	15,21	24,55	35,39
20000	5,887	11,99	15,18	24,5	35,31
25000	5,843	11,89	15,05		

Simulations cannot be run for Type-IV and Type-V drill collars at 25000 ft. due to convergence problem in the model. Therefore, simulations are done up to 20000 ft. for Type-IV and Type-V drill collars. Simulation results will be discussed for each drill collar in detail in next sections.

8.2.4. Simulations for 4.75 in. Drill Collars (Type I)

The results for different depths for 4.75 in. drill collars are given in Table 8-3 and critical buckling force versus depth curve is given in Figure 8-1 below:

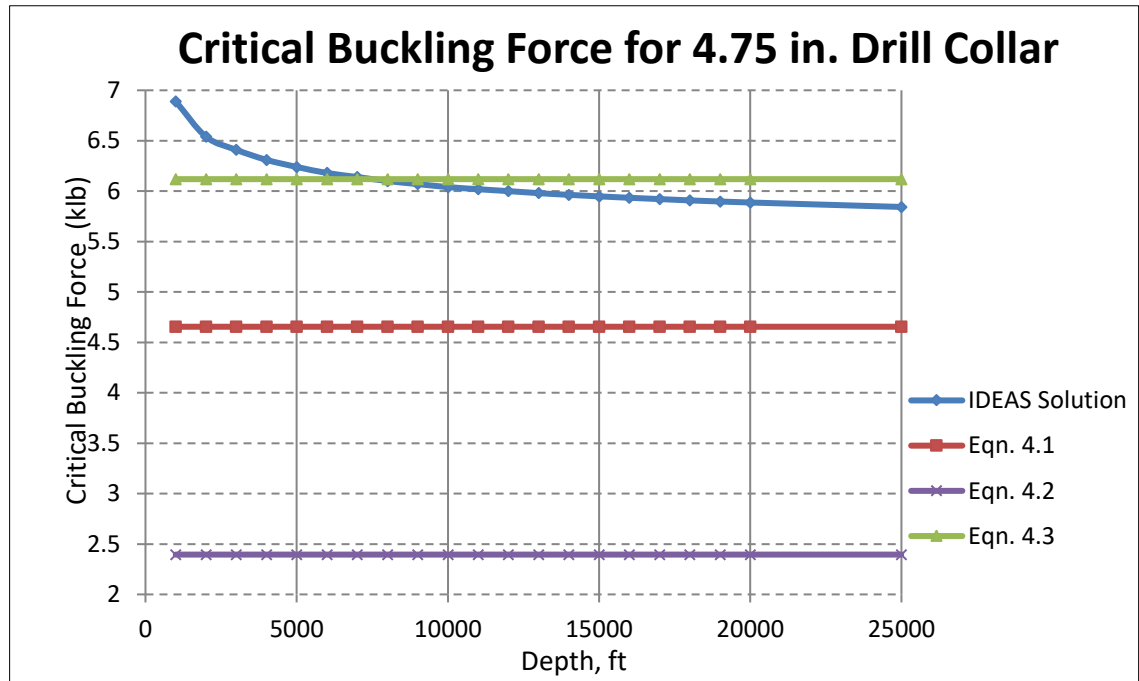


Figure 8-1 Critical Buckling Force vs Depth Curve for 4.75 in. Drill Collar.

It is shown that critical buckling force is decreasing slightly as depth is increasing. From IDEAS™ simulations, it found that at 1000 ft., the critical buckling force is 6890 lb. while at 25000 ft., critical buckling force is 5843 lb. There is a 15% reduction for critical buckling force as depth increases from 1000 ft. to 25000 ft. Eqn. 4.1 and Eqn. 4.2 give even lower results compared to simulation result at 25000 ft. although Eqn. 4.1 is the analytical solution for around 400 m. length drill string. The results of Eqn. 4.2 are shown in the figure at the bottom since the values are quite lower than Eqn. 4.1, Eqn. 4.3, and IDEAS™ results. However, the simulation result at around 7500 ft. is the same as the results of Eqn. 4.3.

8.2.5. Simulations for 6.25 in. Drill Collars (Type II)

The results for different depths for 6.25 in. drill collars are given in Table 8-3 and critical buckling force versus depth curve is given in Figure 8-2 below:

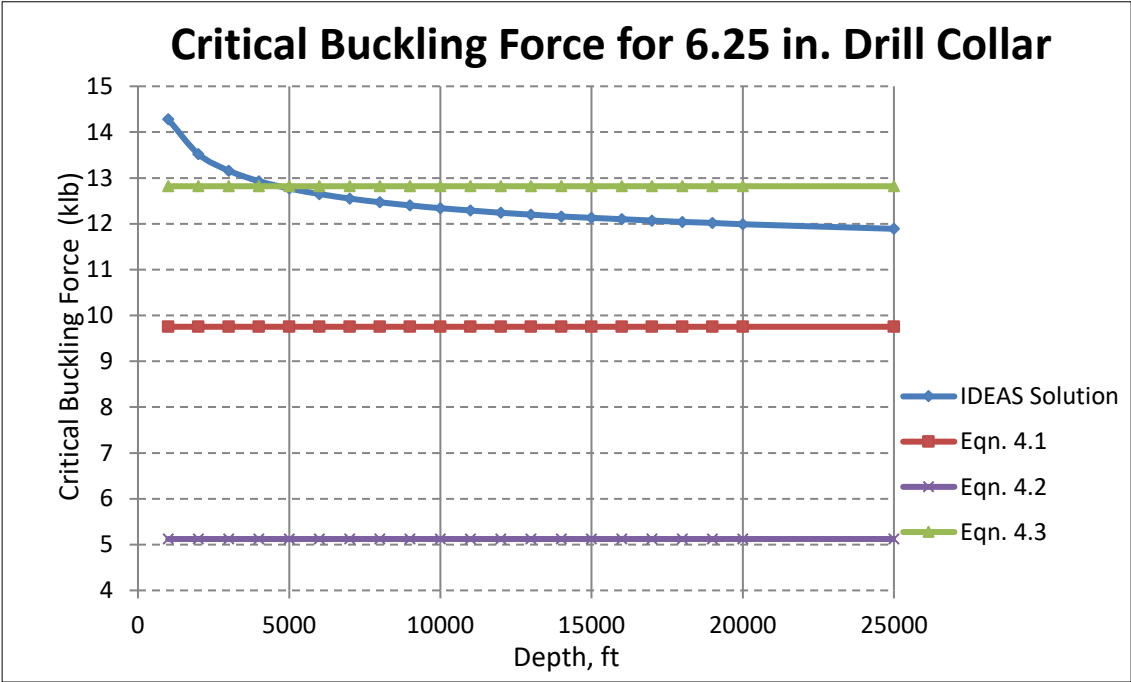


Figure 8-2 Critical Buckling Force vs Depth Curve for 6.25 in. Drill Collar.

It is shown that critical buckling force is decreasing slightly as depth is increasing. The difference between the value of critical buckling force at 1000 ft. and 25000 ft. is 2390 lb. It was 1047 lb. for 4.75 in. drill collar. At 1000 ft., the critical buckling force is 14280 lb. while at 25000 ft., critical buckling force is 11890 lb. There is a 17% reduction for critical buckling force as depth increases from 1000 ft. to 25000 ft. Eqn. 4.1 and Eqn. 4.2 give even lower results compared to simulation result at 25000 ft. although Eqn. 4.1 is the analytical solution for around 400 m. length drill string. The results of Eqn. 4.2 are shown in the figure at the bottom since the values are quite lower than Eqn. 4.1, Eqn. 4.3, and IDEAS™ results. However, the simulation result at around 5000 ft. is the same as the results of Eqn. 4.3.

8.2.6. Simulations for 7 in. Drill Collars (Type III)

The results for different depths for 7 in. drill collars are given in Table 8-3 and critical buckling force versus depth curve is given in Figure 8-3 below:

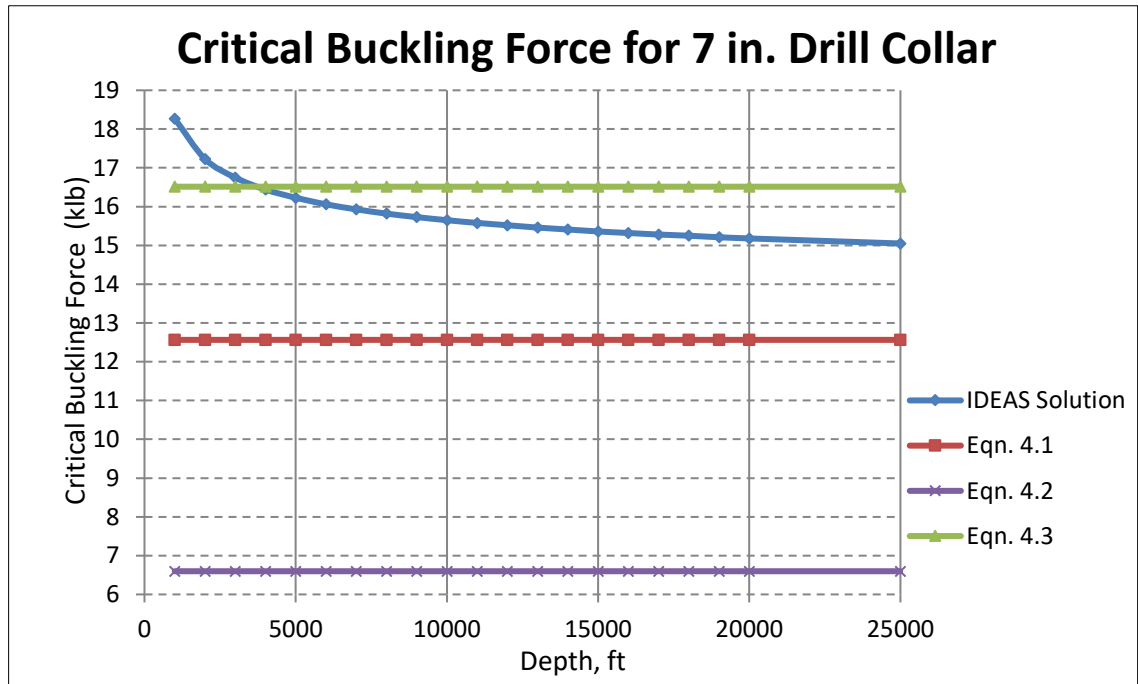


Figure 8-3 Critical Buckling Force vs Depth Curve for 7 in. Drill Collar.

It is shown that critical buckling force is decreasing as depth is increasing. The difference between the value of critical buckling force at 1000 ft. and 25000 ft. is 3220 lb. It was 2390 lb. for 6.25 in. drill collar. At 1000 ft., the critical buckling force is 18270 lb. while at 25000 ft., critical buckling force is 15050 lb. There is a 16% reduction for critical buckling force as depth increases from 1000 ft. to 25000 ft. Eqn. 4.1 and Eqn. 4.2 give even lower results compared to simulation result at 25000 ft. although Eqn. 4.1 is the analytical solution for around 400 m. length drill string. The results of Eqn. 4.2 are shown in the figure at the bottom since the values are quite lower than Eqn. 4.1, Eqn. 4.3, and IDEAS™ results. However, the simulation result at around 4500 ft. is the same as the results of Eqn. 4.3.

8.2.7. Simulations for 8.25 in. Drill Collars (Type IV)

The results for different depths for 8.25 in. drill collars are given in Table 8-3 and critical buckling force versus depth curve is given in Figure 8-4 below:

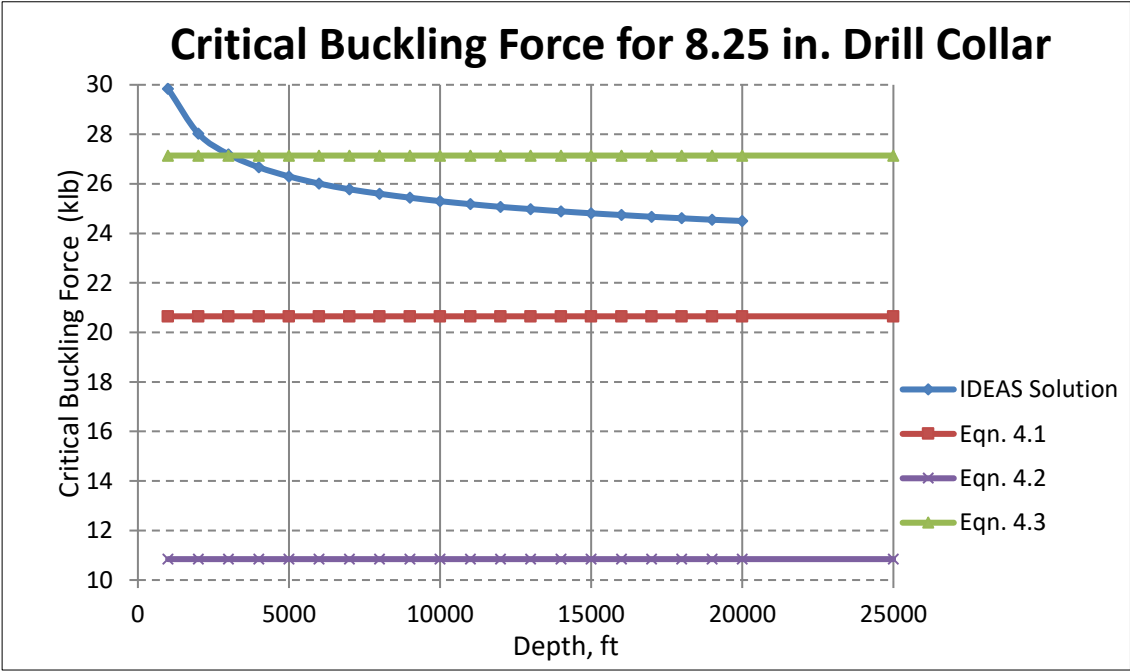


Figure 8-4 Critical Buckling Force vs Depth Curve for 8.25 in. Drill Collar.

It is shown that critical buckling force is decreasing as depth is increasing as expected. The difference between the value of critical buckling force at 1000 ft. and 20000 ft. is 5340 lb. It was 3220 lb. for 7 in. drill collar. At 1000 ft., the critical buckling force is 29840 lb. while at 20000 ft., critical buckling force is 24500 lb. There is 18% reduction for critical buckling force as depth increases from 1000 ft. to 20000 ft. Eqn. 4.1 and Eqn. 4.2 give even lower results compared to simulation result at 20000 ft. although Eqn. 4.1 is the analytical solution for around 400 m. length drill string. The results of Eqn. 4.2 are shown in the figure at the bottom since the values are quite lower than Eqn. 4.1, Eqn. 4.3, and IDEAS™ results. However, the simulation result at around 3000 ft. is the same as the results of Eqn. 4.3.

8.2.8. Simulations for 9.5 in. Drill Collars (Type V)

The results for different depths for 9 in. drill collars are given in Table 8-2 and critical buckling force versus depth curve is given in Figure 8-5 below:

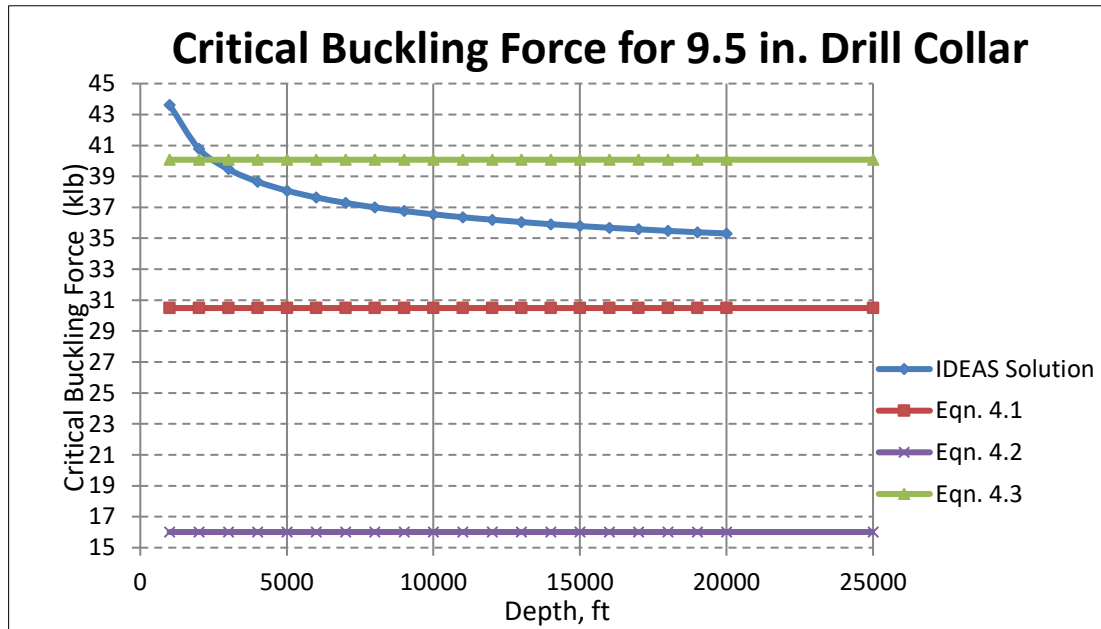


Figure 8-5 Critical Buckling Force vs Depth Curve for 9.5 in. Drill Collar

It is shown that critical buckling force is decreasing as depth is increasing as expected. The difference between the value of critical buckling force at 1000 ft. and 20000 ft. is 8310 lb. It was 5340 lb. for 8.25 in. drill collar. At 1000 ft., the critical buckling force is 43620 lb. while at 20000 ft., critical buckling force is 35310 lb. There is a 19% reduction for critical buckling force as depth increases from 1000 ft. to 20000 ft. Eqn. 4.1 and Eqn. 4.2 give even lower results compared to simulation result at 20000 ft. although Eqn. 4.1 is the analytical solution for around 400 m. length drill string. The results of Eqn. 4.2 are shown in the figure at the bottom since the values are quite lower than Eqn. 4.1, Eqn. 4.3, and IDEAS™ results. However, the simulation result at around 2000 ft. is the same as the results of Eqn. 4.3.

The results taken from the simulations are summarized in the below Table 8-4:

Table 8-4 Simulation Results Comparison Chart

Simulation Results					
Type	Drill Collar Dia., in	FEM Solution, lb.		Amount of Decrease in Critical Force, lb.	% Decrease of the Critical Force
		at 1000 ft.	at 25000 ft.		
I	4.75	6890	5843	1047	15
II	6.25	14280	11890	2390	17
III	7	18270	15050	3220	16
IV	8.25	29840	24500*	5340	18
V	9.5	43620	35310*	8310	19

*Results for 20000 ft. length.

CHAPTER 9

CONCLUSION & DISCUSSION

Results related to comparisons with analytical solutions are given below:

- It is showed that critical buckling force decreases as the depth of the well increases according to IDEASTM simulations, although, analytical solutions give only a fixed critical buckling force for a specific pipe independent from the length.
- Both Lubinski's [7] short-length solution and Wang's [9] infinite-length solution underestimate the critical buckling force for each depth from 1000 ft. to 25000 ft. for each drill collar compared to FEM solution results.
- Wu's solution curves intersect with IDEASTM simulation curves at one point (between 0 ft. and 5000 ft. except 4.5 in. drill collar) for all drill collars analyzed. Before the intersection point, Wu's equation underestimates the critical buckling force compared to IDEASTM simulations. After the intersection point, the case is the opposite. Therefore, Wu's equation gives better results for short-length drill strings to IDEASTM simulation compared to other analytical solutions.
- Moreover, Wu's [4] equation gives the closest results to IDEASTM simulation results compared to other analytical solutions for all lengths analyzed. The error is $\pm 10\%$ range. Therefore, for both shallow and deep vertical wells, Wu's equation should be used for practical cases.

Results related to flexural rigidity of the drill collars are given below:

- From these results, it can be concluded that post-buckling behavior of slender-dominated long hanging drill strings with stiffness-dominated short hanging drill strings in vertical wellbores are different. Therefore, it can be concluded that length of the drill string is also another parameter to determine the critical sinusoidal buckling force for vertical wells. Also, from IDEAS™ simulation curves, it can be seen that after a certain point, the behavior of the drill string is changing since the slope of the curve is changing dramatically which shows that stiffness domination decreases and slenderness effect increases after that point.
- For small size drill collars, IDEAS™ simulation result curves are closer to the Wu`s solution curves for each length analyzed. However, as the diameter of the drill collar increases, IDEAS™ simulation result curves starts separation from Wu`s solution curve towards the Lubinski`s solution.
- According to simulation results, for small diameter drill collars, the decrease in critical buckling force value from 1000 ft. to 25000 ft. is small, but, for larger drill collars, the amount of decrease is higher (Table 7-4).
- In simulation results, it is observed that the difference between the critical buckling force at 1000 ft. and 25000 ft.(20000 ft. for 8.25 in and 9.5 in drill collars), is increasing as the diameter of the drill collars increasing.

After it is concluded that critical buckling force decreases as the depth of the well increases according to IDEAS™ simulations, this change can be reflected as a change in the coefficient of the analytical equations since the analytical solutions are in the same format except the coefficient. In the appendix section, variable coefficient curves are prepared according to FEM solutions for these five drill collars to find an approximate coefficient of the equation for different. The curves of the variable coefficient can be found in Appendix-A.

REFERENCES

- [1] J. D. Jansen, «Nonlinear Dynamics of Oilwell Drillstrings,» Delft University Press, PhD. Dissertation, Amsterdam, 1993.
- [2] R.F. Mitchell, "Effects of Well Deviation on Helical Buckling," *SPE Drilling & Completion*, pp. 63-69, 8 March 1997.
- [3] L. Euler, *Methodus Inveniendi Lineas Curvas Maximi Minimive Proprietate Gaudentes. Appendix: De Curvis Elasticis*, 3rd ed., vol. 1, Lausanne and Geneva, 1744.
- [4] J. Wu, "Buckling Behaviour of Pipes in Directional and Horizontal Wells," Texas A&M University, Collage Station, Texas, 1992.
- [5] M. Belayneh, *A Review of Buckling in Oil Wells*, Aachen: Shaker Verlag, 2006.
- [6] S. P. Timoshenko and J. M. Gere, *Theory of Elastic Stability*, New York: Dower Publications, 2009.
- [7] S. Miska, *Developments in Petroleum Engineering Volume-1 Collected Works of Arthur Lubinski*, Houston, Texas: Gulf Publishing Company, 1987, p. 178.

- [8] J. Cunha, «Buckling of Tubulars Inside Wellbores: A Review on Recent Theoretical and Experimental Works,» *SPE Drilling & Completion*, pp. 13-19, 2004.
- [9] C. Wang, «A Critical Review of the Heavy Elastica,» *International Journal of Mechanical Science*, cilt 28, no. 8, pp. 549-559, 1986.
- [10] R. F. Mitchell and S. Z. Miska, *Fundamentals of Drilling Engineering*, Richardson, TX: SPE Textbook Series, 2011.
- [11] J. B. Salies, J. C. Cunha and J. J. Azar, «Experimental and Analytical Study of Sinusoidal Buckling in Vertical Wells,» *Society of Petroleum Engineers*, pp. 77-85, 1994.
- [12] P. Paslay and D. Bogy, "The Stability of a Circular Rod Laterally Constrained to be in Contact with an Inclined Circular Cylinder," *Journal of Applied Mechanics*, pp. 605-610, 1964.
- [13] Dawson, Rapier; P.R. Paslay, «Drillpipe Buckling in Inclined Holes,» *Journal of Petroleum Technology*, pp. 1734-1738, 1984.
- [14] B. D. Thomas, W. Gravley and J. E. Walraven, «Preventing Buckling in Drill String». United States Patent 4384483, 24 May 1983.
- [15] Y. Chen, Y. Lin and J. Cheatham, «Tubing and Casing Buckling in Horizontal Wells,» *Journal of Petroleum Technology*, pp. 140-141, 1990.

- [16] A.Lubinski; Althouse W.S.; Logan J.L., «Helical Buckling of Tubing Sealed in Packers,» *Journal of Petroleum Technology*, pp. 655-670, 1962.
- [17] Y. W. Kwon, «Analysis of Helical Buckling,» *SPE Drilling Engineering*, pp. 211-216, 1988.
- [18] J. Wu, H. Juvkam-Wold and R. Lu, «Helical Buckling of Pipes in Extended Reach and Horizontal Wells-Part 1,» *Journal of Energy Resources Technology*, no. 115, p. 190, 1993.
- [19] A. Lubinski and H. B. Woods, «Factors Affecting the Angle of Inclination and Dog-Legging in Rotary Bore Holes,» *Society of Petroleum Engineer*, pp. 222-250, 1953.
- [20] J. Wu and H. C. Juvkam-Wold, «The Effect of Wellbore Curvature on Tubular Buckling and Lockup,» *Journal of Energy Resources Technology*, cilt 117, pp. 214-218, 1995.
- [21] X. He and A. Kyllingstad, «Helical Buckling and Lock-up Conditions for Coil Tubing in Curved Wellbores,» *SPE Drilling&Completions*, pp. 10-15, 1995.
- [22] W. Qui, S. Miska and L. Volk, «Drill Pipe/Coil Tubing Buckling Analysis in a Hole of Constant Curvature,» *SPE Permian Basin Oil and Gas Recovery Conference*, Midland, TX, 1998.
- [23] W. Qui, S. Miska and L. Volk, «Analysis of Drill Pipe/Coil Tubing Buckling in a Constant-Curvature Wellbore,» *Journal of Petroleum Technology*, pp. 66-77, 1998.

- [24] H. Aslaksen, M. Annand, R. Duncan, A. Fjaere, L. Paez and U. Tran, «Integrated FEA Modeling Offers System Approach to Drillstring Optimization,» *IADC/SPE Drilling Conference*, Miami, 2006.
- [25] L. T. Till and D. V. Datye, «First-Principles Finite Element Modeling of Coiled Tubing in Directional Wellbores,» *30th International Conference on Ocean, Offshore and Arctic Engineering*, Rotterdam, The Netherlands, 2011.
- [26] M. Hajianmaleki, J. S. Daily, L. Ring and R. Gandikota, «Critical Buckling Load Assessment of Drill Strings in Different Wellbores Using Explicit Finite Element Method,» *SPE Offshore Europe Oil and Gas Conference and Exhibition*, Aberdeen, UK, 2013.
- [27] S. Menand, H. Sellami, M. Tijani and J. Akowanou, «Buckling of Tubulars in Actual Field Conditions,» *SPE Annual Technical Conference and Exhibition*, San Antonio, Texas, 2006.
- [28] J. Salies, J. J. Azar and J. R. Sorem, «Experimental and Mathematical Modeling of Helical Buckling of Tubulars in Directional Wellbores,» *SPE International Petroleum Conference and Exhibition*, Veracruz, Mexico, 1993.
- [29] S. Moaveni, *Finite Element Analysis Theory and Application with ANSYS*, New Jersey: Pearson Education, Inc., 2003.
- [30] S. S. Rao, *Finite Element Method in Engineering*, New York: Elsevier, 2011.
- [31] D. L. Logan, *A First Course in the Finite Element Method*, 4th Edition, Toronto: Thomson, 2007, pp. 7-14.

[32] "IDEAS Integrated Drillbit Design Platform," Schlumberger, 24 June 2017.
[Online].

Available:

http://www.slb.com/services/drilling/drill_bits/drillstring_design/ideas.aspx.

[Accessed 10 January 2017].

[33] M. Paz and W. Leigh, *Structural Dynamics Theory and Computation*, United States of America: Kluwer Academic Publishers, 2004.

[34] Y. Chen, *IDEAS Drillstring Finite Element Analysis Model*, Houston: Schlumberger Internal.

[35] A. K. Chopra, *Structural Dynamics*, New Jersey: Prentice-Hall In., 1995.

[36] A. Lubinski, «A Study of the Buckling of Rotary Drill Strings,» *API Drilling and Production Practice*, pp. 178-214, 1950.

APPENDIX

A-VARIABLE COEFFICIENT CURVES

In Figure A-1, variable coefficients are calculated for 4.75 in. drill collar based on simulation data.

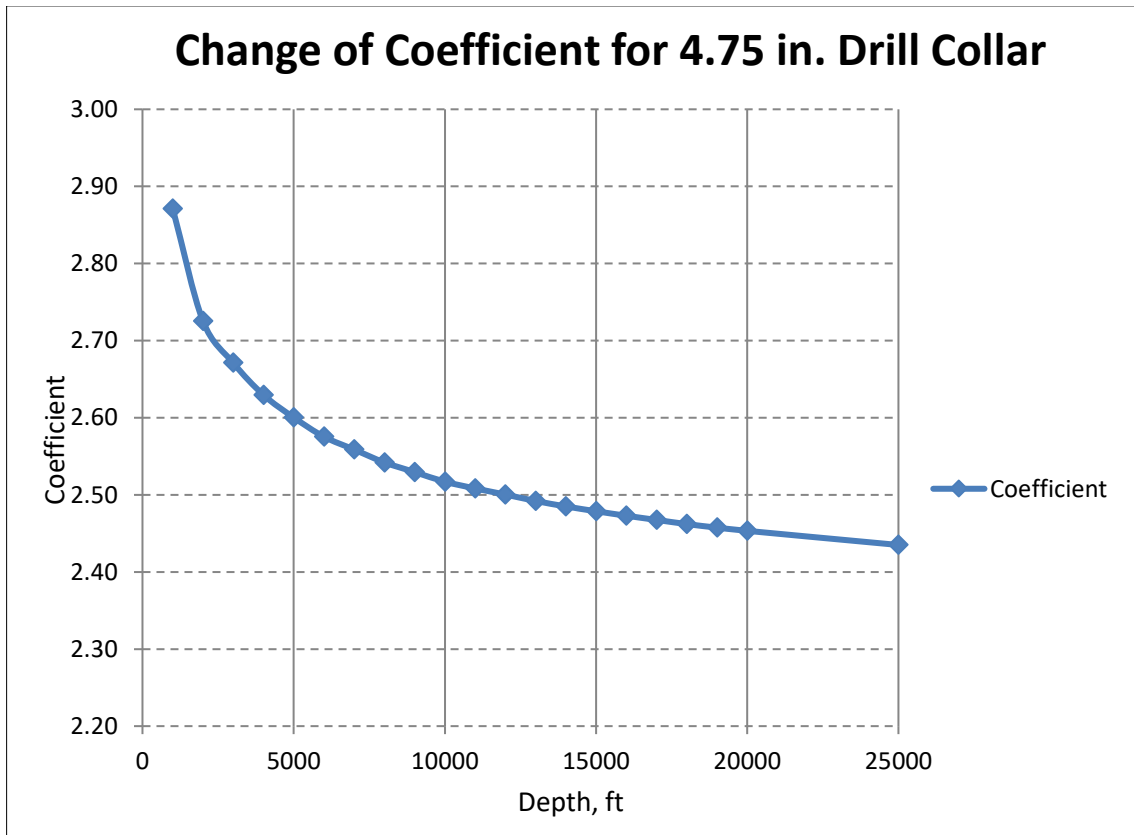


Figure A-1 Variable Coefficient for 4.75 in. Drill Collar

In Figure A-2, variable coefficients are calculated for 6.25 in. drill collar based on simulation data.

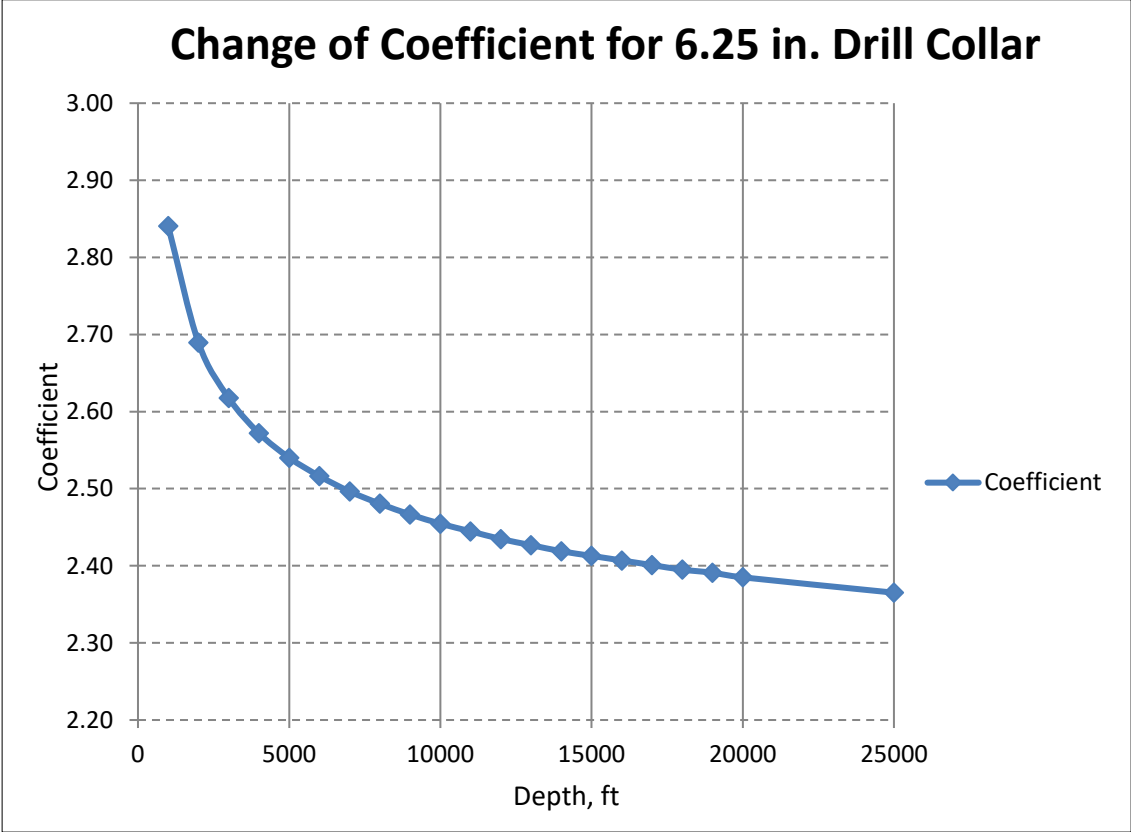


Figure A-2 Variable Coefficient for 6.25 in. Drill Collar

In Figure A-3, variable coefficients are calculated for 7 in. drill collar based on simulation data.

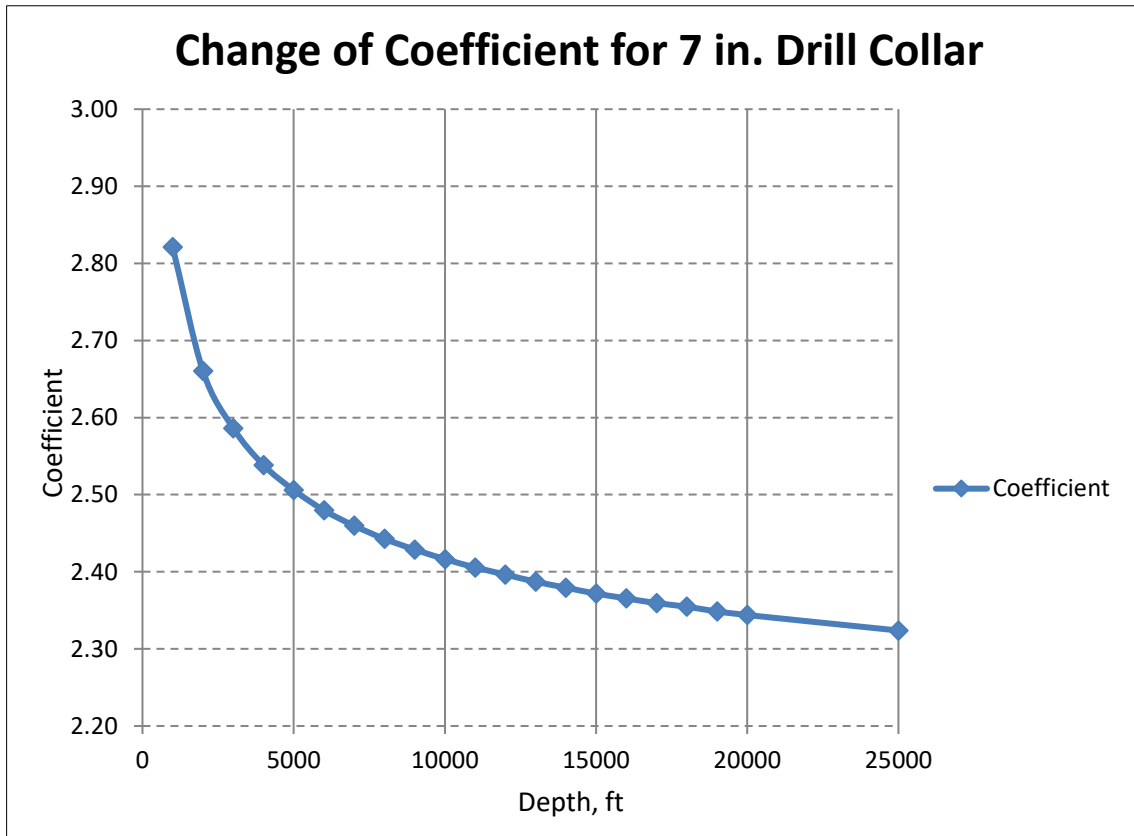


Figure A-3 Variable Coefficient for 7 in. Drill Collar

In Figure A-4, variable coefficients are calculated for 8.25 in. drill collar based on simulation data.

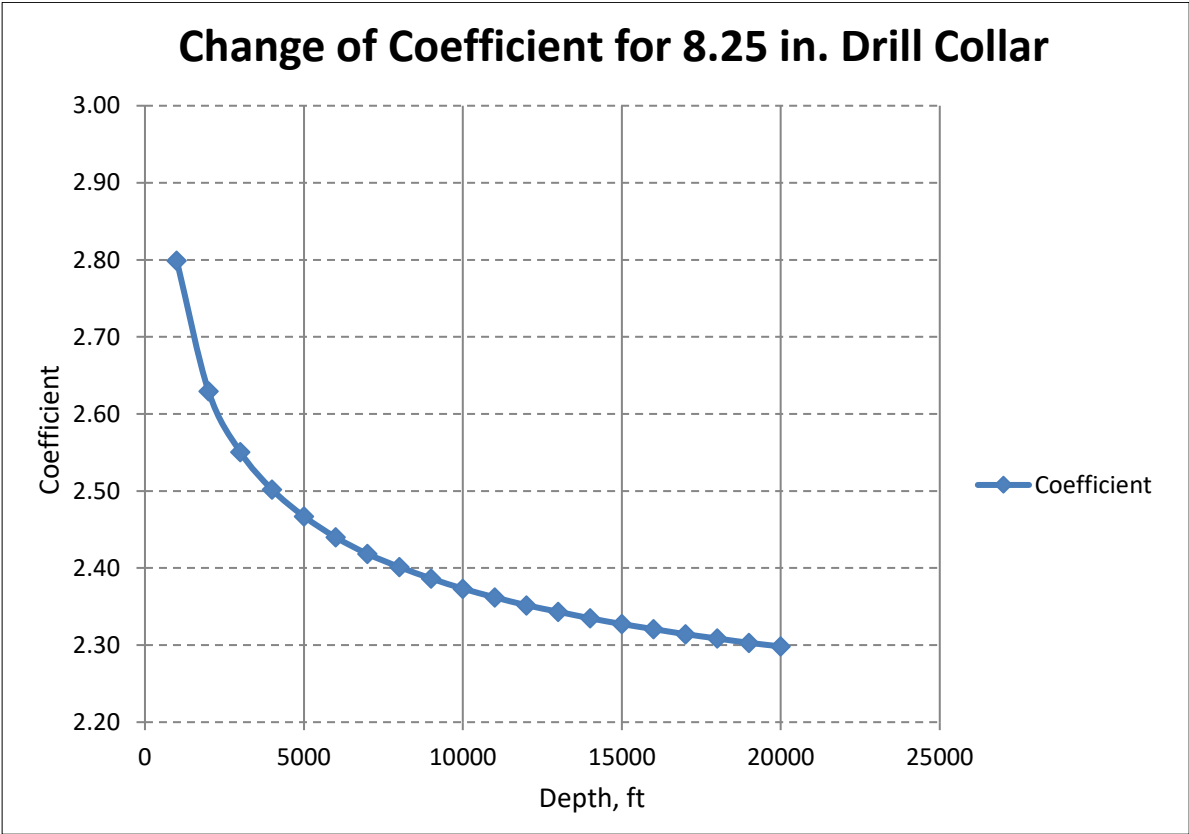


Figure A-4 Variable Coefficient for 8.25 in. Drill Collar

In Figure A-5, variable coefficients are calculated for 9.5 in. drill collar based on simulation data.

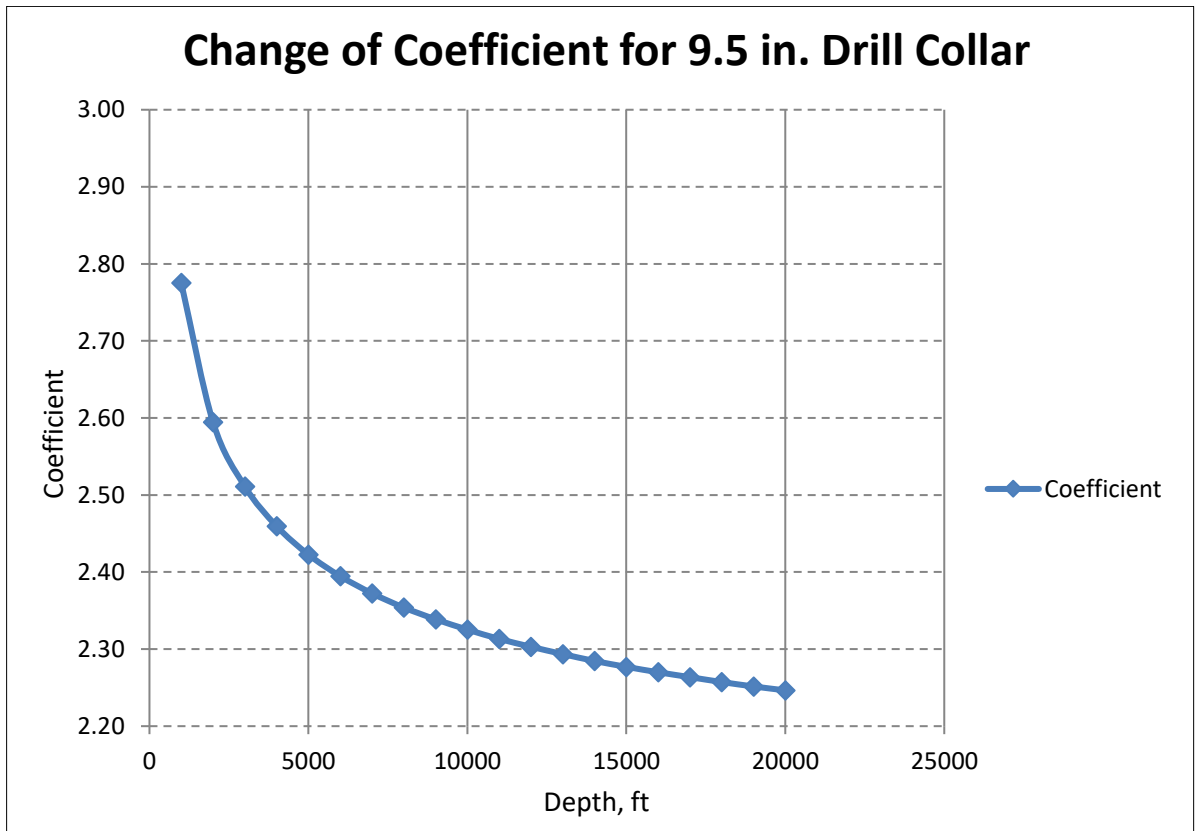


Figure A-5 Variable Coefficient for 9.5 in. Drill Collar

B-ANALYTICAL SOLUTIONS OF THE EQUATIONS

Lubinski's Solution:

Assumptions done during the derivations of the differential equation are:

1. Long drill string with no tool joint.
2. Drill string is centered completely to the wellbore.
3. Two ends of the drill string are hinged connections.
4. There is no rotation on drill string, and loading is "static loading".

The differential equation of the buckled drill string is found by Lubinski as follows:

$$EI \frac{d^3Y}{dX^3} + pX \frac{dY}{dX} + F_2 = 0 \quad \text{B.1}$$

where,

X: The axis of the hole,

Y: The axis transverse to the hole axis,

N: Neutral point of the drill string, shown in the Figure B-6.

p: Weight in mud per unit length of drill string lb/ft,

F₂: Lateral force at the bit, as shown in Figure 4-1.

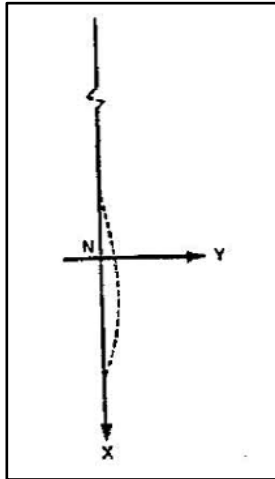


Figure B-1 Coordinate Axis of the Drilling String [16]

We have thus obtained the differential equation of the buckled drilling string. By properly choosing the unit of length, the equation may be put in a simpler form. Let:

$$X = mx \tag{B.2}$$

$$Y = my \tag{B.3}$$

where $m =$ a constant which will be chosen later.

Then:

$$\frac{dY}{dX} = \frac{dy}{dx} \tag{B.4}$$

$$\frac{d^2Y}{dX^2} = \frac{1}{m} \frac{d^2y}{dx^2} \tag{B.5}$$

$$\frac{d^3Y}{dX^3} = \frac{1}{m^2} \frac{d^3y}{dx^3} \tag{B.6}$$

Substituting Eqn. B2, B3, B4, B5, B6 in Eqn. B1,

$$\frac{d^3y}{dx^3} + \frac{p}{EI}x \frac{dY}{dX} + F_2 = 0 \quad \text{B.7}$$

The value “rn” should be chosen so that:

$$m^3 = \frac{EI}{p} \quad \text{B.8}$$

Let c be defined as follows:

$$c = \frac{F_2}{pm} \quad \text{B.9}$$

Substituting Eqn. B.8 and Eqn. B.9 in Eqn. B.7,

$$\frac{d^3y}{dx^3} + x \frac{dy}{dx} + c = 0 \quad \text{B.10}$$

Let,

$$z = \frac{dy}{dx} \quad \text{B.11}$$

Substituting Eqn. B.11 into Eqn. B.10,

$$\frac{d^2z}{dx^2} + xz + c = 0 \quad \text{B.12}$$

The variable “z” can be expressed in form of power series,

$$z = \sum_{n=0}^{n=\infty} a_n x^n \quad \text{B.13}$$

And substituting Eqn. B.13 into Eqn. B.12, we obtain,

$$\sum_{n=0}^{n=\infty} n(n-1)a_n x^{n-2} + \sum_{n=0}^{n=\infty} a_n x^{n+1} + c = 0 \quad \text{B.14}$$

This expression is a polynomial of powers of “x”. Expression Eqn. B.14 must be satisfied for any value of “x”, therefore, coefficients of x^0, x^1, x^2, x^3, x^4 , etc. must be all equal to zero. Thus, we obtain the following expressions:

$$\text{Coefficient of } x^0 = 2a_2 + c = 0 \quad \text{B.15}$$

$$\text{Coefficient of } x^1 = a_0 + 2(3a_3) = 0 \quad \text{B.16}$$

$$\text{Coefficient of } x^2 = a_1 + 3(4a_4) = 0 \quad \text{B.17}$$

$$\text{Coefficient of } x^3 = a_2 + 4(5a_5) = 0 \quad \text{B.18}$$

And so on. Substituting these equations in to Eqn. B.13, the general solution of the differential equation is,

$$\begin{aligned} z = & a_0 \left[1 - \frac{x^3}{2.3} + \frac{x^6}{2.3.5.6} - \frac{x^9}{2.3.5.6.8.9} + \dots \right] \\ & + a_1 x \left[1 - \frac{x^3}{3.4} + \frac{x^6}{3.4.6.7} - \frac{x^9}{3.4.6.7.9.10} + \dots \right] \\ & - \frac{c}{2} x^2 \left[1 - \frac{x^3}{4.5} + \frac{x^6}{4.5.7.8} - \frac{x^9}{4.5.7.8.10.11} + \dots \right] \end{aligned} \quad \text{B.19}$$

Putting in Eqn. B.19, $a_0 = a$, $a_1 = b$, and expressing $z = dy/dx$, following expressions are found,

$$y = aS(x) + bT(x) + cU(x) + g \quad \text{B.20}$$

$$\frac{dy}{dx} = aF(x) + bG(x) + cH(x) \quad \text{B.21}$$

$$\frac{d^2y}{dx^2} = aP(x) + bQ(x) + cR(x) \quad \text{B.22}$$

In Eqn. B.20, B.21 and B.22, the following designations are made. “ g ” is the integration constant.

$$S(x) = x \left[1 - \frac{x^3}{2.3.4} + \frac{x^6}{2.3.5.6.7} - \frac{x^9}{2.3.5.6.8.9.10} + \dots \right] \quad \text{B.23}$$

$$T(x) = x^2 \left[\frac{1}{2} - \frac{x^3}{3.4.5} + \frac{x^6}{3.4.6.7.8} - \frac{x^9}{3.4.6.7.9.10.11} + \dots \right] \quad \text{B.24}$$

$$U(x) = -\frac{x^3}{2} \left[\frac{1}{3} - \frac{x^3}{4.5.6} + \frac{x^6}{4.5.7.8.9} - \frac{x^9}{4.5.7.8.10.11.12} + \dots \right] \quad \text{B.25}$$

$$F(x) = 1 - \frac{x^3}{2.3} + \frac{x^6}{4.5.6} - \frac{x^9}{2.3.5.6.8.9} + \dots \quad \text{B.26}$$

$$G(x) = x \left[1 - \frac{x^3}{3.4} + \frac{x^6}{3.4.6.7} - \frac{x^9}{3.4.6.7.9.10} + \dots \right] \quad \text{B.27}$$

$$H(x) = -\frac{x^2}{2} \left[1 - \frac{x^3}{4.5} + \frac{x^6}{4.5.7.8} - \frac{x^9}{4.5.7.8.10.11} + \dots \right] \quad \text{B.28}$$

$$P(x) = -\frac{x^2}{2} \left[1 - \frac{x^3}{3.5} + \frac{x^6}{3.5.6.8} - \frac{x^9}{3.5.6.8.9.11} + \dots \right] \quad \text{B.29}$$

$$Q(x) = 1 - \frac{x^3}{3} + \frac{x^6}{3.4.6} - \frac{x^9}{3.4.6.7.9} + \dots \quad \text{B.30}$$

$$R(x) = -x \left[1 - \frac{x^3}{2.4} + \frac{x^6}{2.4.5.7} - \frac{x^9}{2.4.5.7.8.10} + \dots \right] \quad \text{B.31}$$

The functions $F(x)$, $G(x)$, $P(x)$, and $Q(x)$ may be expressed in the form of Bessel functions of fraction orders $1/3$, $-1/3$, and $-2/3$.

$$F(x) = \frac{1}{2}(3^{2/3}) \left[\Gamma\left(\frac{5}{3}\right) \right] x^{1/2} J_{-1/3} \left(\frac{2}{3} x^{3/2} \right) \quad \text{B.32}$$

$$G(x) = 3^{1/3} \left[\Gamma\left(\frac{4}{3}\right) \right] x^{1/2} J_{1/3} \left(\frac{2}{3} x^{3/2} \right) \quad \text{B.33}$$

$$P(x) = -\frac{1}{2}(3^{2/3}) \left[\Gamma\left(\frac{5}{3}\right) \right] x J_{2/3} \left(\frac{2}{3} x^{3/2} \right) \quad \text{B.34}$$

$$R(x) = 3^{1/3} \left[\Gamma\left(\frac{4}{3}\right) \right] x J_{-2/3} \left(\frac{2}{3} x^{3/2} \right) \quad \text{B.35}$$

Bessel function tables are available in the literature and for negative x values; the corresponding Bessel functions of the second kind must be used. Functions $S(x)$, $T(x)$, $U(x)$, $H(x)$, and $R(x)$ have been calculated by series, the convergence of which is fairly satisfactory.

Inasmuch as the differential equation, Eqn. B.10, is of third order, its general solution, Eqn. B.20 contains three integration constants, a , b , and g . In addition to integration constants, the parameter, c , is unknown because F_2 , (horizontal component of the reaction of the bottom hole on the bit) is also unknown. This parameter can be determined by imposing an additional boundary condition.

Let,

x_1 : Distance from neutral point to the top of the hole,

x_2 : Distance from neutral point to the bottom of the hole,

Let, P_1, Q_1, R_1, S_1 , etc. designate the values of the functions $P(x), Q(x), R(x), S(x)$, etc. for $x = x_1$, and P_2, Q_2, R_2, S_2 , etc. designate respectively the values of the same functions for $x = x_2$.

At both ends of the drilling string the bending moment is equal to zero (both bushings and the bit may be considered as hinged ends). Therefore, by using moment equation below,

$$M = pm^2 \frac{d^2 y}{dx^2} \quad \text{B.36}$$

And Eqn. B-22,

$$aP_1 + bQ_1 + cR_1 = 0 \quad \text{B.37}$$

$$aP_2 + bQ_2 + cR_2 = 0 \quad \text{B.38}$$

For both ends, $y = 0$; therefore, Eqn. B.20 gives,

$$aS_1 + bT_1 + cU_1 + g = 0 \quad \text{B.39}$$

$$aS_2 + bT_2 + cU_2 + g = 0 \quad \text{B.40}$$

By eliminating “ g ” between the two preceding equations and rewriting Eqn. B.37 and Eqn. B.38, we get the following set of 3 equations in which a, b, c are unknowns,

$$aP_1 + bQ_1 + cR_1 = 0 \quad \text{B.37}$$

$$aP_2 + bQ_2 + cR_2 = 0 \quad \text{B.38}$$

$$a(S_1 - S_2) + b(T_1 - T_2) + c(U_1 - U_2) = 0 \quad \text{B.41}$$

Since second members of all three equations of the set are equal to zero, the solution of the set has a physical meaning only if its determinant is equal to zero,

$$\begin{vmatrix} P_1 & Q_1 & R_1 \\ P_2 & Q_2 & R_2 \\ (S_1 - S_2) & (T_1 - T_2) & (U_1 - U_2) \end{vmatrix} = 0 \quad \text{B.42}$$

Eqn. B.42 is the relation between x_1 and x_2 which must be satisfied for the buckling to occur. By the trial-and-error method, it was found that Eqn. B.42 may be represented by a series of curves. Only the curve pertaining to the smallest value of x_2 corresponds to a stable equilibrium and has been drawn in Figure B-1.

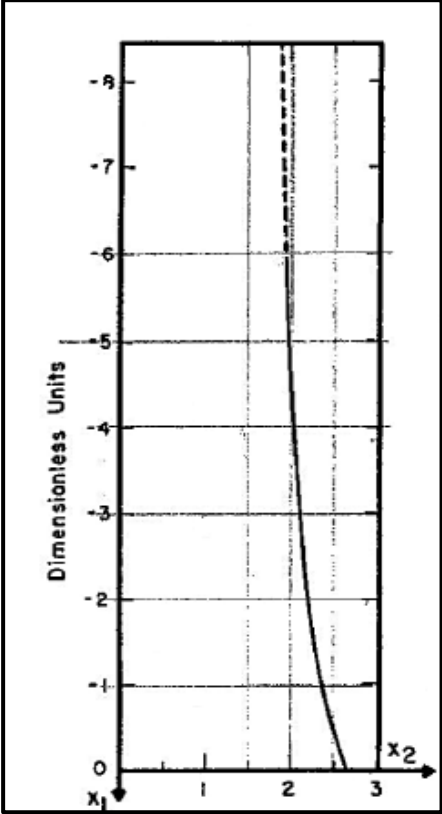


Figure B-2 Critical Conditions of the First Order [7]

Under actual drilling conditions x_1 is very large and x_2 is equal to its asymptotic limit. The Figure B-2 is calculated data between $x_1 = 0$ and $x_1 = -6$. Exploitation of the curve beyond $x_1 = -6$, shown as a dashed lines, seems to indicate that the asymptotic limit of “ x_2 ” is 1.88. On the other hand, $x_1 = -6$, x_2 is equal to 1.94. Consequently, we may assume with negligible error that $x_2 = 1.94$ is the critical condition for the first order.

$$F_{cri} = 1.94(EI)^{1/3}w^{2/3} \tag{B.43}$$

Wu`s Solution:

The axial load at the bottom of the pipe when the buckling occurs is found by Wu [4]:

$$F_{cri} = EI \left(\frac{n_{1/2}\pi}{L} \right)^2 + w_e \frac{L}{2} \quad \text{B.44}$$

Since, $\frac{\partial F_{cri}}{\partial n_{1/2}} > 0$, the value of $n_{1/2}$ has to be one (first order buckling) to yield the minimum buckling force at the bottom of the pipe. So, we have,

$$F_{cri} = EI \left(\frac{\pi}{L} \right)^2 + w_e \frac{L}{2} \quad \text{B.45}$$

Which is the same expression found to be as mentioned by Timoshenko [6] for a vertical bar hinged at the ends and submitted to the action of its own weight in addition to compressive load applied at the ends.

Then, by taking $\frac{\partial F_{cri}}{\partial L} = 0$, we obtain,

$$2EI \left(\frac{\pi}{L} \right) \left(-\frac{\pi}{L^2} \right) + w_e \frac{L}{2} = 0 \quad \text{B.46}$$

which results in,

$$L_{cri} = \left(\frac{4\pi^2 EI}{w_e} \right)^{1/3} \quad \text{B.47}$$

Substituting Eqn. B.47 into Eqn. B.45,

$$F_{cri} = \frac{w_e L_{cr}}{4} + w_e \frac{L_{cr}}{2} = \frac{3}{4} w_e L_{cr} \approx 2.55 (EI w_e^2)^{1/3} \quad \text{B.48}$$

Wang`s Solution:

The linearized form of the differential equation found by Wang [9] is,

$$\frac{d^2\phi}{dr^2} - r\phi = 0 \quad \text{B.49}$$

The general solution is in terms of Airy functions,

$$\phi = C_1 Ai(r) + C_2 Bi(r) \quad \text{B.49}$$

The boundary conditions are, at the top end at infinity, the beam is vertical,

$$\phi(\infty) = 0 \quad \text{B.50}$$

And zero moment at the bottom end,

$$\frac{d\phi}{dr}(-F) = 0 \quad \text{B.51}$$

Thus, for non-trivial solutions, we need,

$$\frac{dAi}{dr}(-F) = 0 \quad \text{B.52}$$

The smallest root is $F = 1.018793$. In other words,

$$F_{cri} = 1.018793(EIw_e^2)^{1/3} \quad \text{B.53}$$